A NEW FINITE DIFFERENCE APPROACH FOR MHD FLOW

A THESIS SUBMITTED TO
THE GRADUATE SCHOOL OF NATURAL AND APPLIED SCIENCES
OF
MIDDLE EAST TECHNICAL UNIVERSITY

BY

GAMZE ÖĞÜTCÜ

IN PARTIAL FULFILLMENT OF THE REQUIREMENTS
FOR
THE DEGREE OF MASTER OF SCIENCE
IN
MATHEMATICS

JULY 2023

Approval of the thesis:

A NEW FINITE DIFFERENCE APPROACH FOR MHD FLOW

submitted by **GAMZE ÖĞÜTCÜ** in partial fulfillment of the requirements for the degree of **Master of Science in Mathematics Department, Middle East Technical University** by,

Prof. Dr. Halil Kalıpçılar
Dean, Graduate School of **Natural and Applied Sciences** _____

Prof. Dr. Yıldıray Ozan
Head of Department, **Mathematics** _____

Prof. Dr. Canan Bozkaya
Supervisor, **Mathematics, METU** _____

Examining Committee Members:

Prof. Dr. Fatma Karakoç
Mathematics, Ankara University _____

Prof. Dr. Canan Bozkaya
Mathematics, METU _____

Assoc. Prof. Dr. Baver Okutmuştur
Mathematics, METU _____

Date: 25.07.2023

I hereby declare that all information in this document has been obtained and presented in accordance with academic rules and ethical conduct. I also declare that, as required by these rules and conduct, I have fully cited and referenced all material and results that are not original to this work.

Name, Surname: Gamze Öğütcü

Signature :

ABSTRACT

A NEW FINITE DIFFERENCE APPROACH FOR MHD FLOW

Öğütcü, Gamze
M.S., Department of Mathematics
Supervisor: Prof. Dr. Canan Bozkaya

July 2023, 113 pages

The magnetohydrodynamic (MHD) flow equations with mixed-type boundary conditions, which are presented in this thesis as modified Helmholtz equations, are numerically solved using the finite difference methods (FDM), precisely the standard and new (novel) finite difference approaches. A new finite difference (NFD) method is derived from the standard finite difference (SFD) approach by eliminating the error due to truncation in the finite difference formulas that approximate the derivatives. In light of the fact that the NFD method involves no truncation error, it is regarded as a numerically exact method. First, the NFD formulas are established for approximating first-order derivatives in mixed-type boundary conditions and second-order derivatives in one- and two-dimensional modified Helmholtz equations. Second, the reduced modified Helmholtz form of MHD flow equations and the related mixed boundary conditions are discretized using these formulas. In this regard, we focus primarily on the magnetohydrodynamic flow problems in parallel infinite plates and infinite channels with rectangular cross-sections. The one-dimensional MHD flow between parallel infinite plates, for which the analytical solution exists, is initially solved to build and validate the FDM codes and perform a quantitative comparison of

the standard and new finite difference approaches. The two-dimensional MHD flow problem in a rectangular duct is the next application to which we extend the usage of these finite difference approaches. In order to examine the combined impacts associated with the conductivity parameter and slip length on the velocity V and induced magnetic field B, numerical simulations with SFD and NFD methods are carried out for several cases in both problems using a variety of Hartmann numbers. The progressive numerical outcomes are conceptually presented as distributions of velocity and induced magnetic field across the entire computational interval in one dimension and along straight lines close to slippery or variably conducting duct walls in two dimensions. It has been observed that, even with a coarse mesh, the NFD method produces numerical results that are noticeably more precise when compared to the findings of the SFD methodology in each case. Additionally, a finer mesh is required in both NFD and SFD approaches to accurately capture the characteristics of the flow velocity and the induced magnetic field at high Hartmann numbers, and with slippery and variably conducting boundaries of the computational domain.

Keywords: new FDM, standard FDM, modified Helmholtz equation, Hartmann flow, MHD duct flow, slip velocity condition, variable conductivity

ÖZ

MHD AKIŞ İÇİN YENİ BİR SONLU FARKLAR YAKLAŞIMI

Öğütcü, Gamze
Yüksek Lisans, Matematik Bölümü
Tez Yöneticisi: Prof. Dr. Canan Bozkaya

Temmuz 2023 , 113 sayfa

Bu tezde; değiştirilmiş Helmholtz denklemleri olarak sunulan karışık tip sınır koşullarına sahip magnetohidrodinamik (MHD) akış denklemleri, sonlu farklar yöntemleri (SFM), standart ve yeni sonlu farklar (YSF) yaklaşımları kullanılarak sayısal olarak çözülmüştür. Yeni bir sonlu farklar yöntemi türevlere yaklaşan sonlu farklar formüllerindeki kesmeden kaynaklanan hatayı ortadan kaldırarak standart sonlu farklar (SSF) yaklaşımından türetilmiştir. YSF yöntemi herhangi bir kesme hatası içermemesi nedeniyle sayısal olarak kesin bir yöntem olarak kabul edilir. Bu tezde, ilk olarak, karma tip sınır koşullarında birinci mertebeden türevleri ve bir- ve iki-boyutlu değiştirilmiş Helmholtz denklemlerinde ikinci mertebeden türevleri tahmin etmek için YSF formülleri oluşturulmuştur. İkinci olarak, MHD akış denklemlerinin indirgenmiş değiştirilmiş Helmholtz formu ve ilgili karma sınır koşulları, bu formüller kullanılarak ayrıklaştırılmıştır. Bu bağlamda, öncelikle paralel sonsuz plakalar arasında ve dikdörtgen kesitli sonsuz kanallar boyunca akan manyetohidrodinamik akış problemlerine odaklanılmıştır. Analitik çözümün mevcut olduğu paralel sonsuz plakalar arasındaki tek-boyutlu MHD akışı, başlangıçta SFM kodlarını oluşturmak ve doğrulamak, ve standart ve yeni sonlu farklar yaklaşımlarının niceliksel bir karşılaştırmasını

yapmak için çözülmüştür. Dikdörtgen bir kanaldaki iki-boyutlu MHD akış problemi, bu sonlu farklar yaklaşımlarının kullanımını genişlettiğimiz bir sonraki uygulamadır. Geçirgenlik parametresi ve kayma uzunluğu ile ilişkili hız V ve indüklenmiş manyetik alan B üzerindeki birleşik etkileri incelemek için, çeşitli Hartmann sayıları kullanılarak her iki problem için de SSF ve YSF yöntemleri ile sayısal simülasyonlar gerçekleştirilmiştir. Progresif sayısal sonuçlar kavramsal olarak, tek boyutta tüm hesaplama aralığı boyunca ve iki boyutta kaygan veya değişken geçirgen kanal duvarlarına yakın düz çizgiler boyunca hız ve indüklenmiş manyetik alan dağılımları olarak sunulmuştur. Kaba bir ağ ile bile, YSF yönteminin, her durumda SSF metodolojisinin bulgularıyla karşılaştırıldığında belirgin şekilde daha kesin olan sayısal sonuçlar ürettiği gözlemlenmiştir. Ek olarak, hem YSF hem de SSF yaklaşımlarında, yüksek Hartmann sayılarında ve hesaplama alanının kaygan ve değişken geçirgen sınırlarında akış hızı özelliklerini ve indüklenmiş manyetik alan davranışlarını doğru bir şekilde yakalamak için daha ince bir ağ gerektiği gözlemlenmiştir.

Anahtar Kelimeler: yeni sonlu farklar yöntemi, standart sonlu farklar yöntemi, değiştirilmiş Helmholtz denklemi, Hartmann akışı, magnetohidrodinamik kanal akışı, kayma hızı koşulu, değişken geçirgenlik

To my mother Huriye, my father Cevdet,
my grandfather Mehmet Akyüz

ACKNOWLEDGMENTS

First of all, I want to sincerely thank my supervisor, Prof. Dr. Canan Bozkaya, for all of her help, patience, and contributions throughout the writing of this thesis. I consider it an honor to work with her.

I would also like to thank the members of my defense committee, Prof. Dr. Fatma Karakoç and Assoc. Prof. Dr. Baver Okutmuştur.

This process has been difficult at times, but I have been able to handle it thanks to my family's faith in me and their unwavering support. My mother and also my best friend, Huriye Öğütcü, and my father, Cevdet Öğütcü, deserve my deepest gratitude for their constant encouragement in every decision I make and their unwavering belief that I will finish any job I undertake.

TABLE OF CONTENTS

ABSTRACT v

ÖZ vii

ACKNOWLEDGMENTS x

TABLE OF CONTENTS xi

LIST OF TABLES xiv

LIST OF FIGURES xv

LIST OF ABBREVIATIONS xviii

CHAPTERS

1 INTRODUCTION 1

1.1 MHD Flow Equations 4

1.2 Transformation of the MHD Flow Equations into Modified Helmholtz Equations 7

1.3 Literature Survey 9

1.4 The Outline of the Thesis 14

2 FINITE DIFFERENCE METHODS 17

2.1 Standard Finite Difference Formulas 20

2.1.1 Finite difference formulas for the first-order partial derivatives 20

2.1.2 Central difference formulas for the second-order partial derivatives 22

2.2 New (Novel) Finite Difference Method 23

2.2.1 New finite difference method for one-dimensional Helmholtz equation 23

2.2.2 NFD method for the two-dimensional Helmholtz equation . . . 25

3 FINITE DIFFERENCE SOLUTIONS TO ONE-DIMENSIONAL MHD FLOW 29

3.1 Application of the SFD method to one-dimensional MHD Flow . . . 32

3.1.1 Case I: Insulated plates with no-slip velocity condition: $\alpha = c = 0$ 37

3.1.2 Case II: Variably conducting plates with no-slip velocity condition: $c \neq 0, \alpha = 0$ 38

3.1.3 Case III: Insulated plates with slip velocity condition: $c = 0$, $\alpha \neq 0$ 39

3.2 Application of the NFD method to one-dimensional MHD flow . . . 41

3.2.1 Derivation of NFD method for one-dimensional modified Helmholtz equation 41

3.2.2 Derivation of NFD formulas for the mixed-type boundary conditions 43

3.2.3 The matrix-vector form of the NFD equations under various boundary conditions 46

3.2.3.1 Case I: Insulated plates with no-slip velocity condition: $\alpha = c = 0$ 50

3.2.3.2 Case II: Variably conducting plates with no-slip velocity condition: $c \neq 0, \alpha = 0$ 51

3.2.3.3 Case III: Insulated plates with slip velocity condition: $c = 0, \alpha \neq 0$ 53

3.3 Numerical results for one-dimensional MHD flow problem 54

4 FINITE DIFFERENCE SOLUTIONS TO TWO-DIMENSIONAL MHD FLOW 67

4.1 Application of the SFD method to two-dimensional MHD duct flow . 69

4.1.1 Test problem I: no-slip and insulated walls: $c = \alpha = 0$ 72

4.2 Application of the NFD method to two-dimensional MHD duct flow . 74

4.2.1 Test problem I: no-slip and insulated walls: $c = \alpha = 0$ 80

4.2.2 Test problem II: Variably conducting side walls with no-slip velocity condition: $c \in (0, \infty)$ at $y \pm \ell$, $\alpha = 0$ 82

4.2.3 Test Problem III: Insulated duct with slippery side walls: $c = 0$, $\alpha \neq 0$ at $y = \pm\ell$ 88

4.3 Numerical results for two-dimensional MHD duct flow 92

4.3.1 Test Problem I: no-slip and insulated walls: $c = \alpha = 0$ 92

4.3.2 Test Problem II: Variably conducting side walls with no-slip velocity condition: $c \in (0, \infty)$ at $y = \pm 1$, $\alpha = 0$ 97

4.3.3 Test Problem III: Insulated duct with slippery side walls: $\alpha \neq 0$ at $y = \pm 1$, $c = 0$ 101

5 CONCLUSION 105

REFERENCES 109

LIST OF TABLES

TABLES

Table 3.1 Relative errors for SFD and NFD at $M = 100$ in Case I and Case IV 57

Table 3.2 Relative errors for SFD and NFD at $M = 500$ in Case I and Case IV 58

Table 4.1 Relative errors for SFD and NFD at $M = 100$ in Problem I 92

Table 4.2 Volumetric flow rate for Problem I 93

LIST OF FIGURES

FIGURES

Figure 1.1 (a) MHD channel flow and (b) rectangular cross-section of the channel. 4

Figure 2.1 Discrete grid points in domain $[a, b] \times [c, d]$. 18

Figure 3.1 Flow configuration of Hartmann flow. 29

Figure 3.2 Grid dependency test for Case I: $c = 0$, $\alpha = 0$. 55

Figure 3.3 Grid dependency test for Case IV: $c = 2$, $\alpha = 0.2$. 56

Figure 3.4 Case I: Comparison of NFD and SFD with the exact solution, $M = 100$, $c = 0$, $\alpha = 0$. 58

Figure 3.5 Case II: Comparison of NFD and SFD with the exact solution, $M = 100$, $c = 2$, $\alpha = 0$. 59

Figure 3.6 Case III: Comparison of NFD and SFD with the exact solution, $M = 100$, $c = 0$, $\alpha = 0.2$. 59

Figure 3.7 Case IV: Comparison of NFD and SFD with the exact solution, $M = 100$, $c = 2$, $\alpha = 0.2$. 60

Figure 3.8 Case I: Effect of M on the velocity and induced magnetic field, $c = 0$, $\alpha = 0$. 61

Figure 3.9 Case II: Effect of c on the velocity and induced magnetic field with NFD, $\alpha = 0$. 62

Figure 3.10 Case III: Effects of α and M on the velocity and induced magnetic field with NFD, $c = 0$. 63

Figure 3.11 Case IV: Effects of c and M on the velocity and induced magnetic field with NFD, $N = 650$, $\alpha = 0.2$. 64

Figure 3.12 Case IV: Effects of c and M on the velocity and induced magnetic field with SFD, $N = 2500$, $\alpha = 0.2$. 64

Figure 3.13 Case IV: Effects of α and M on the velocity and induced magnetic field with NFD, $N = 650$, $c = 2$. 65

Figure 3.14 Case IV: Effects of α and M on the velocity and induced magnetic field with SFD, $N = 2500$, $c = 2$. 65

Figure 4.1 Flow configuration and the boundary conditions for Problem I. . 80

Figure 4.2 Flow configuration and the boundary conditions for Problem II. . 83

Figure 4.3 Flow configuration and the boundary conditions for Problem III. 89

Figure 4.4 Grid dependency test for Problem I: $\alpha = c = 0$, $M = 100$ along $y = 0$. 94

Figure 4.5 Grid dependency test for Problem I: $\alpha = c = 0$, $M = 100$. . . . 94

Figure 4.6 Problem I: Comparison of the numerical solutions by SFD (solid) and NFD (solid) with exact solution (dotted) at $M = 10,\ 100$. 95

Figure 4.7 Problem I: Variations of the velocity and induced magnetic field along $y = 0$ at $M = 10$. 95

Figure 4.8 Problem I: Variations of the velocity and induced magnetic field along $y = 0$ at $M = 100$. 96

Figure 4.9 Problem I: Effect of M on V and B along $y = 0$ by using NFD scheme with $N = 80$ for $5 \leq M \leq 50$, and $N = 240$ for $M = 100$. . . . 97

Figure 4.10 Grid dependency test for Problem II: $\alpha = 0$, $c = 2$, $M = 35$ along $y = 0$. 97

Figure 4.11 Problem II: Effects of M and c on velocity and induced magnetic field, $N = 128$. 99

Figure 4.12 Problem II: Effects of c and M on the distributions of V and B along $y = 0$. 100

Figure 4.13 Problem II: Effects of c and M on the distributions of V and B along $y = 0.9844$. 100

Figure 4.14 Grid dependency test for Test Problem III: $M = 35$, $\alpha = 0.4$ along $y = 0$. 101

Figure 4.15 Problem III: Effects of M and α on velocity, $N = 128$. 102

Figure 4.16 Problem III: Effects of M and α on induced magnetic field, $N = 128$. 103

Figure 4.17 Problem III: Effects of α and M on the distributions of V and B along $y = 0$. 104

Figure 4.18 Problem III: Effects of α and M on the distributions of V and B along $y = 0.9844$. 104

LIST OF ABBREVIATIONS

FDM	Finite Difference Method
MHD	Magnetohydrodynamics
NFD	New Finite Difference
SFD	Standard Finite Difference
B	induced magnetic field
B_0	intensity of the external magnetic field
B^{exact}	analytical solution of the induced magnetic field
B^{mb}	mean bulk induced magnetic field
B^{nfd}	new finite difference solution of the induced magnetic field
B^{sfd}	standard finite difference solution of the induced magnetic field
c	conductivity parameter
h	step size in x-direction
I_0	modified Bessel function of the first kind of order zero
J_0	Bessel function of the first kind of order zero
k	wave number and step size in y-direction
ℓ	half length of the computational interval in one-dimension
ℓ_x	half length of the computational interval along x-axis
ℓ_y	half length of the computational interval along y-axis
L_0	characteristic length
M	Hartmann number
$\mathbf{M} = (M_x, M_y)$	external magnetic field with component M_x and M_y
N	number of subintervals in discretization
Q	volumetric flow rate
R_k	remainder (error) term in Taylor series expansion

V	velocity
V^{exact}	analytical solution of the velocity
V^{mb}	mean bulk velocity
V^{nfd}	new finite difference solution of the velocity
V^{sfd}	standard finite difference solution of the velocity
α	slip length
γ	inclination angle between the magnetic field and the positive y-axis
Δx	increment in the x-direction
Δy	increment in the y-direction
$\Gamma = \partial\Omega$	boundary of computational domain Ω
μ	viscosity coefficient
σ	electrical conductivity
Ω	computational domain

CHAPTER 1

INTRODUCTION

A boundary value problem is the term for the mathematical representation of engineering or physical problems, which is often provided by a variety of ordinary or partial differential equations with specified conditions on the boundary of the problem domain. There are three different types of boundary conditions (BC), each of which specifies one of the following on the boundary: the unknown itself (Dirichlet type BC), the unknown's normal derivative (Neumann type BC), or a linear combination of the unknown and its normal derivative (mixed (or Robin) type BC). The boundary value problems that are subject to the current thesis arise from the field of magnetohydrodynamics, a discipline that studies the dynamics of electrically conducting fluids and their interactions with magnetic fields. In magnetohydrodynamics, a magnetic field can produce currents in a flowing conducting fluid, which in turn causes the fluid to experience Lorentz force. The magnetic field can also be altered. Thus, it is necessary to take into account both the electromagnetic field equations as well as the equations for fluid mechanics at the same time. Because of this, it is challenging to examine most MHD problems both theoretically and experimentally.

Due to its significant applications in numerous areas, magnetohydrodynamics is a difficult subject to study. In the magnetosphere that surrounds the Earth, in the dynamo that creates the planet's magnetic field, and throughout astrophysics, it occurs by nature. In laboratory investigations on controlled thermonuclear fusion, magnetohydrodynamics plays a crucial role in the magnetic confinement of plasmas. The propulsion and flight control of rockets and hypersonic aerodynamic vehicles, the pumping of conducting liquids, and the production of magnetohydrodynamic power are all carried out using magnetohydrodynamic principles. In addition, the under-

standing of the flow of a conducting fluid down a duct with finitely conducting walls driven by a pressure gradient is necessary for the design of the various devices involving the MHD generators, flow meters, pumps, brakes, accelerators, and blood flow measurements.

The equations that describe magnetohydrodynamics are produced by incorporating the Navier-Stokes equations for fluid dynamics and the Maxwell equations for electromagnetism via Ohm's law. These equations construct a coupled system of differential equations in velocity and the induced magnetic field for which a simultaneous solution is required. Due to the nature of the connection of the MHD equations in velocity and induced magnetic field, analytical solutions are only available for a few simple geometries with simple boundary conditions [1, 2]. As a result, a number of numerical approaches, including the domain decomposition techniques, namely the finite difference method (FDM), finite element method (FEM), spectral methods, and boundary integration techniques such as boundary element method (BEM) and dual reciprocity BEM, have been employed to provide approximate solutions for the MHD flow problems.

The FDM is going to be used in the present thesis to solve MHD flow problems. Finite difference methods are based on estimating the derivative terms by using finite differences in order to discretize the differential equations of the problem under consideration. The Taylor series expansion can be utilized to derive these finite difference formulas. These algebraically constructed finite difference formulas connect the values at numerous adjacent grid nodes to the value of the unknown variable at a discrete point, which results from the partitioning of the physical problem domain into a node grid. In other words, the main objective of finite difference methods is to convert the differential equations subject to the specified boundary and/or initial conditions into a system of algebraic equations that may be solved numerically using matrix algebra algorithms. The main benefits of the FDM can be categorized as higher-order precision of spatial and/or temporal discretization and ease of obtaining high-order approximations. However, since FDM needs a structured grid and is unable to be conveniently applied to unstructured grids, it can only be used for simple geometries. Finite difference techniques come in a wide variety of forms. The standard finite difference (SFD) method and the new (novel) finite difference (NFD) method which is

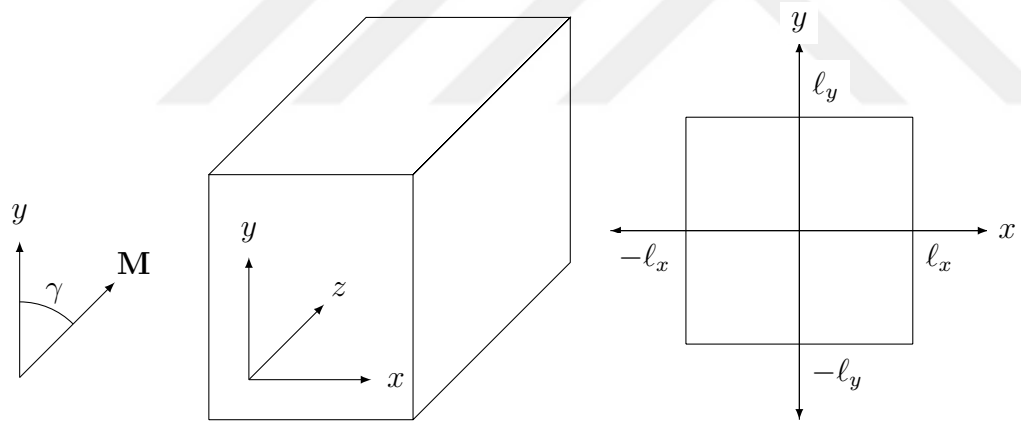
described in [3, 4], will be the two types of finite difference methods we are going to investigate in this thesis. In SFD, the derivative terms in the differential equations can be approximated by using various finite difference formulas involving truncation errors, namely backward, forward, and central differences which can be derived by using Taylor's series expansions around appropriate grid points (see Chapter 2, Section 2.1). However, the finite difference formulas for NFD can be created from those for SFD by eliminating the truncation errors. This is managed by substituting the weights in the standard finite difference formulas with optimal weights which are going to be derived in Section 2.2. As a result, the NFD is regarded as an exact numerical method since it preserves the simple structure of the discretized systems created by the standard finite difference methods while introducing no truncation error. NFD techniques thus perfectly resolve the governing continuous problem without using fine step sizes. Additionally, despite the fact that the linear systems produced by the new and standard finite difference techniques have identical structures, the new method yields more precise findings [3, 4].

The primary focus of the thesis is the use of the aforementioned finite difference methods, namely the standard and novel finite differences, to solve numerically the differential equations in the form of a modified Helmholtz equation. In this respect, the new finite difference formulas for the approximation of second-order derivatives in one and two-dimensional modified Helmholtz equations have been established for the first time to the best of the author's knowledge. The application problem is taken from the area of magnetohydrodynamics, which is an attractive and well-researched field of study as mentioned previously. Specifically, we consider the magnetohydrodynamic flow problems in parallel infinite plates and infinite channels with rectangular cross-sections. The governing equations describing these problems are basically convection-diffusion type equations that are coupled in velocity and the induced magnetic field. However, they can be transformed into two decoupled modified Helmholtz equations under suitable transformations, and hence the derived new finite difference formulas can be employed for the discretization of these equations. In order to develop and verify the FDM codes and to carry out a quantitative comparison of the standard and new finite difference approaches, the one-dimensional MHD flow between parallel infinite plates, for which the analytical solution is available, is first

solved. Next, we expand the uses of these finite difference techniques to the two-dimensional MHD flow problem in rectangular ducts subject to an externally applied uniform magnetic field.

1.1 MHD Flow Equations

It is common knowledge that Maxwell's equations of electromagnetism and the continuity-momentum equations of fluid dynamics are combined via Ohm's law to generate the governing equations for the MHD flow, which are coupled convection-diffusion type equations in velocity and induced magnetic field. The steady, laminar, fully developed flow of a viscous, incompressible, and electrically conducting fluid is considered in rectangular channels or pipes subject to an external, constant, and uniform inclined magnetic field. The electrically conducting fluid is driven through the sufficiently long pipe/channel in the z-direction by a constant pressure gradient and flows with unidirectional velocity in the pipe-axis direction (see Figure 1.1 (a)).



(a) MHD channel flow (b) Rectangular cross-section of the channel

Figure 1.1: (a) MHD channel flow and (b) rectangular cross-section of the channel.

The walls of the pipe on which the magnetic field has a normal component are called the *Hartmann walls*, while the walls tangential to the magnetic field are called the *side walls*. A fully developed flow in the cross-section of the pipe (see Figure 1.1 (b)) causes the flow to become two-dimensional. In light of the above assumptions, a

standard non-dimensional form of the governing MHD flow equations can be written as [1, 2, 5]

$$\begin{aligned} \nabla^2 V + M_x \frac{\partial B}{\partial x} + M_y \frac{\partial B}{\partial y} &= -1 \\ \nabla^2 B + M_x \frac{\partial V}{\partial x} + M_y \frac{\partial V}{\partial y} &= 0 \end{aligned} \qquad \text{in} \quad \Omega \tag{1.1}$$

where Ω is the rectangular cross-section of the pipe, $V(x, y)$ and $B(x, y)$ are the velocity and the induced magnetic field, respectively. The uniform magnetic field of intensity B_0 is $\mathbf{M} = (M_x, M_y)$ with the components $M_x = M \sin\gamma$ and $M_y = M \cos\gamma$. The magnitude of the magnetic field $\mathbf{M}$ is the Hartmann number M, which is defined by $M = B_0 L_0 \sqrt{\sigma}/\sqrt{\mu}$ (σ: electrical conductivity, μ: viscosity coefficient, L_0: characteristic length, and γ is the inclination angle between the magnetic field and the positive y-axis). The velocity $V(x, y)$ and the induced magnetic field $B(x, y)$ are parallel to the z-axis, which is the pipe-axis direction. The derivation of the MHD equations (1.1) can be found in the works of Dragoş [1], Shercliff [2], and Müller and Bühler [5].

In order to have a well-defined problem, the boundary conditions for the velocity and the induced magnetic field along the boundaries (walls) of the channel are determined according to the physical properties of the walls being slippery or no-slip and electrically conducting or insulated. In other words, the walls of the channel are said to be electrically insulated when $B = 0$, perfectly conducting when $\partial B/\partial n = 0$, and variably conducting when $c\frac{\partial B}{\partial n} + B = 0$ where $c \in (0, \infty)$ is the parameter of the electrical wall conductivity. The conductivity parameter $c \to \infty$ (symbolically $c = \infty$) represents the perfectly conducting walls, and $c = 0$ represents the insulated walls. On the other hand, the boundary condition for the velocity on the slipping channel walls is taken as $\alpha\frac{\partial V}{\partial n} + V = 0$, where α is the slip length of the slipping velocity. The slip length $\alpha = 0$, i.e. $V = 0$, represents the no-slip velocity condition along the walls. In this thesis, the MHD flow equations (1.1) are solved with the most general boundary conditions, that is the slipping and variably conducting walls,

$$\alpha\frac{\partial V}{\partial n} + V = 0, \qquad c\frac{\partial B}{\partial n} + B = 0 \qquad \text{on} \quad \Gamma = \partial\Omega \tag{1.2}$$

where $\Gamma = \partial\Omega$ is the boundary of the problem domain Ω. When the external magnetic field is applied horizontally (that is, $\gamma = \pi/2$) and vertically (that is, $\gamma = 0$), the MHD

flow equation (1.1) reduces to

$$\begin{aligned} \nabla^2 V + M\frac{\partial B}{\partial x} &= -1 \\ \nabla^2 B + M\frac{\partial V}{\partial x} &= 0 \end{aligned} \tag{1.3}$$

and

$$\begin{aligned} \nabla^2 V + M\frac{\partial B}{\partial y} &= -1 \\ \nabla^2 B + M\frac{\partial V}{\partial y} &= 0 \end{aligned} \tag{1.4}$$

respectively, for horizontally and vertically applied magnetic fields. The coupled MHD flow equations (1.3) and (1.4) remain applicable for both one-dimensional flow between parallel plates (when $V = V(x)$, $B = B(x)$ in the case of the horizontal magnetic field, and when $V = V(y)$, $B = B(y)$ in the case of vertical magnetic field), and two-dimensional MHD channel flow in rectangular channels (when $V = V(x, y)$, $B = B(x, y)$). That is, when the one-dimensional MHD flow in between two parallel plates subject to a horizontal magnetic field is considered, its governing equations become

$$\begin{aligned} \frac{d^2V}{dx^2} + M\frac{dB}{dx} &= -1 \\ \frac{d^2B}{dx^2} + M\frac{dV}{dx} &= 0 \end{aligned} \qquad \text{in} \quad -\ell_x < x < \ell_x \tag{1.5}$$

since the velocity and the induced magnetic field are functions of x only, and $2\ell_x$ is the length of the computational interval along the x-axis. The corresponding boundary conditions are as follows:

$$\pm\alpha\frac{dV}{dx} + V = 0, \qquad \pm c\frac{dB}{dx} + B = 0 \qquad \text{at} \quad x = \pm\ell_x \tag{1.6}$$

which are the reduced forms of the most general boundary conditions given in Equation (1.2). Similarly, in the presence of a vertically applied magnetic field, the one-dimensional MHD flow equations and the related boundary conditions can be written as

$$\begin{aligned} \frac{d^2V}{dy^2} + M\frac{dB}{dy} &= -1 \\ \frac{d^2B}{dy^2} + M\frac{dV}{dy} &= 0 \end{aligned} \qquad \text{in} \quad -\ell_y < y < \ell_y \tag{1.7}$$

and

$$\pm\alpha\frac{dV}{dy} + V = 0, \qquad \pm c\frac{dB}{dy} + B = 0 \qquad \text{at} \quad y = \pm\ell_y \tag{1.8}$$

since the velocity and the induced magnetic field are functions of y only, and $2\ell_y$ is the length of the computational interval along the y-axis.

1.2 Transformation of the MHD Flow Equations into Modified Helmholtz Equations

In the content of the present thesis, the standard and novel finite difference solutions are investigated for the problems of both one- and two-dimensional MHD flows subject to an external magnetic field applied horizontally in x-direction. We, therefore, focus on the one-dimensional MHD flow equations (1.5) with boundary conditions (1.6) in Chapter 3 and the two-dimensional MHD flow equations (1.3) with general boundary conditions (1.2) in Chapter 4. However, the MHD flow equations should be transformed into the modified Helmholtz equations to be able to apply the novel finite difference method to these equations. In this respect, the transformation processes for the two-dimensional MHD equation (1.3)

$$\begin{aligned} \nabla^2 V + M\frac{\partial B}{\partial x} &= -1 \\ &\qquad \text{in} \quad \Omega \\ \nabla^2 B + M\frac{\partial V}{\partial x} &= 0 \end{aligned} \tag{1.9}$$

and the boundary conditions (1.2)

$$\alpha\frac{\partial V}{\partial n} + V = 0, \qquad c\frac{\partial B}{\partial n} + B = 0 \qquad \text{on} \quad \Gamma = \partial\Omega \tag{1.10}$$

are given in this section.

Equation (1.9) is coupled in velocity and induced magnetic field which is decoupled into two non-homogeneous equations:

$$\begin{aligned} \nabla^2 U_1 + M\frac{\partial U_1}{\partial x} &= -1 \\ \nabla^2 U_2 - M\frac{\partial U_2}{\partial x} &= -1 \end{aligned} \tag{1.11}$$

by the use of change of variables

$$U_1 = V + B \qquad \text{and} \qquad U_2 = V - B. \tag{1.12}$$

Then, the boundary conditions (1.10) become

$$\alpha\frac{\partial(U_1 + U_2)}{\partial n} + U_1 + U_2 = 0, \qquad c\frac{\partial(U_1 - U_2)}{\partial n} + U_1 - U_2 = 0. \tag{1.13}$$

The homogeneous counterpart of Equation (1.11) is obtained with the change of variables

$$U_1 = W_1 - \frac{x}{M} \qquad \text{and} \qquad U_2 = W_2 + \frac{x}{M}. \tag{1.14}$$

That is, Equation (1.11) is reduced to

$$\begin{aligned} \nabla^2 W_1 + M\frac{\partial W_1}{\partial x} &= 0 \\ \nabla^2 W_2 - M\frac{\partial W_2}{\partial x} &= 0 \end{aligned} \tag{1.15}$$

with the boundary conditions

$$\begin{aligned} \alpha\frac{\partial(W_1+W_2)}{\partial n} + W_1 + W_2 &= 0, \\ c\frac{\partial(W_1-W_2)}{\partial n} + W_1 - W_2 - \frac{2}{M}\left(c\frac{\partial x}{\partial n} + x\right) &= 0. \end{aligned} \tag{1.16}$$

Then, by using the transformations

$$W_1 = u^1 e^{-kx} \qquad \text{and} \qquad W_2 = u^2 e^{kx} \tag{1.17}$$

with $M = 2k$, finally one can obtain

$$\begin{aligned} \nabla^2 u^1 - k^2 u^1 &= 0 \\ \nabla^2 u^2 - k^2 u^2 &= 0 \end{aligned} \tag{1.18}$$

which are modified Helmholtz equations in variables u^1 and u^2. The corresponding boundary conditions then become

$$\begin{aligned} \alpha\frac{\partial(u^1 e^{-kx} + u^2 e^{kx})}{\partial n} + u^1 e^{-kx} + u^2 e^{kx} &= 0, \\ c\frac{\partial(u^1 e^{-kx} - u^2 e^{kx})}{\partial n} + u^1 e^{-kx} - u^2 e^{kx} - \frac{1}{k}\left(c\frac{\partial x}{\partial n} - x\right) &= 0 \end{aligned} \tag{1.19}$$

which are coupled in terms of new variables u^1 and u^2 on the boundary $\partial\Omega$.

Once the modified Helmholtz equations (1.18) with boundary conditions (1.19) are solved for u^1 and u^2, the solution to MHD flow equations (1.9) in terms of original variables velocity V and the induced magnetic field B can be obtained by using the corresponding backward substitutions:

$$V = \frac{u^1 e^{-kx} + u^2 e^{kx}}{2} \qquad \text{and} \qquad B = \frac{u^1 e^{-kx} - u^2 e^{kx}}{2} - \frac{x}{M}. \tag{1.20}$$

The analogous of Equations (1.18) and (1.19) for the one-dimensional MHD flow equations (1.5) with the boundary conditions (1.6) can be written as

$$\begin{aligned} &\frac{d^2u^1}{dx^2} - k^2u^1 = 0 \\ &\qquad\qquad\qquad\qquad \text{in} \quad -\ell_x < x < \ell_x \\ &\frac{d^2u^2}{dx^2} - k^2u^2 = 0 \end{aligned} \tag{1.21}$$

and

$$\begin{aligned} \mp\alpha\frac{d(u^1e^{-kx} + u^2e^{kx})}{dx} + u^1e^{-kx} + u^2e^{kx} = 0 \quad \text{at} \quad x = \mp\ell_x \\ \mp c\frac{d(u^1e^{-kx} - u^2e^{kx})}{dx} + u^1e^{-kx} - u^2e^{kx} + \frac{1}{k}(\pm c - x) = 0 \quad \text{at} \quad x = \mp\ell_x. \end{aligned} \tag{1.22}$$

Similarly, by using the back substitutions in Equation (1.20), the solution for the one-dimensional MHD flow equations (1.5) is obtained in terms of V and B.

1.3 Literature Survey

Magnetohydrodynamics, which is the research field of electrically conducting fluids dynamics such as plasma and salt water subject to the magnetic field, is an attractive research field due to its wide range of aforementioned applications in engineering, industry, physics, and chemistry. Hence, there have been many researchers working on the solution of the MHD flow problems. However, due to the complexity of the equations governing the MHD flow, it is challenging to examine most MHD problems both theoretically and experimentally. The analytical solutions exist only for some specific problems defined on regular regions. Thus, it is important to obtain approximate solutions to MHD flow problems through effective numerical techniques. Shercliff [2] investigated the constant motion of an electrically conducting fluid in insulated square and circular pipes subject to a transverse magnetic field. He derived an analytical solution to the problem in certain circumstances, that is for the insulated and no-slip duct walls, and provided also a theoretical perspective to Hartmann layer formation as well as Dragos [1]. Smolentsev [6] analytically solved the fully developed MHD flow in an insulated square duct with slip condition at the Hartmann walls by expanding the velocity and the induced magnetic field as Fourier cosine series in the direction perpendicular to the applied magnetic field. He observed that the boundary layers along the Hartmann walls become noticeably thicker than the ones along

the side walls when the slip length is substantial. Later, Ligere et al. [7], derived an analytical solution, depending on integral transformations, to the MHD flow in a rectangular duct with perfectly conducting Hartmann walls and insulated side walls with slip boundary conditions. Ligere et al. [8] further obtained the analytical solution of the same problem by using the Fourier series expansions. According to their findings, the slip length enhances the velocity of the fluid in the duct, and larger Hartmann number values strengthen the slip impact on the flow. In Ligere et al. [9], the analytical solution found in [8], has been expanded for the MHD flow in a duct with perfectly conducted Hartmann walls and slippery side walls with finite conductivity. However, the analytical approach using the Fourier series suggested in the works [6, 8, 9] can not be applied to the MHD flow equations with slip on all walls as stated by Smolentsev [6]. As a result, the use of either numerical or asymptotic approaches is inevitable in order to approximate the solution to MHD flows in ducts with slippery and variably conducting walls. Thus, a variety of numerical methods such as FEM, BEM, dual reciprocity BEM (DRBEM), and spectral method have been widely used to solve MHD duct flow problems either with no-slip or slip velocity conditions. Singh and Lal [10, 11], Gardner and Gardner [12] and Tezer and Köksal [13] applied the finite element method for the solution of the MHD flow in ducts with walls of no-slip velocity and various types of conductivities for moderate values of Hartmann numbers ≤ 100, whereas the FEM solutions for higher values of Hartmann number were provided in the works [14, 15, 16, 17]. Due to the challenges of handling sizable systems and high computing costs resulting from domain discretization in FEM, BEM applications have been also used to solve MHD duct flow problems. There have been numerous studies on the BEM solutions of MHD flow issues in ducts with no-slip walls, and the work of Bozkaya [18] has a comprehensive compilation of these works that have been published in the literature. On the other hand, there are a few studies on the BEM solution of MHD duct flows when the slip effect is taken into account. Among these studies, Bozkaya [19] investigated the MHD flow in finite and semi-infinite rectangular ducts with variably conducting walls that exhibit slip by using a direct BEM approach, which discretized the MHD equations in their original coupled form. Senel and Tezer employed the dual reciprocity BEM, which is a variant to direct BEM, to solve the MHD duct flow in a circular duct with slippery and electrically conducting walls in their work [20], and in two ducts that are separated

by conducting Hartmann and slipping side walls in [21]. The DRBEM was utilized as well by Aydin and Tezer-Sezgin [22] to solve the Cauchy MHD duct flow with slipping perturbed boundaries. On the other hand, Bozkaya and Turk [23] recently used a Chebyshev spectral collocation approach to compute the MHD problem with slipping and electrically conducting walls in a rectangular duct.

On the other hand, the finite difference method, which is the approach implemented in the present thesis, is one of the most utilized numerical methods for solving differential equations. There are, however, very few studies on the FDM solution to the MHD flow problems. In very early studies by Singh and Lal [24, 25], the problem of MHD axial flow was solved along channels with triangular cross-sections by using FDM for only small values of Hartmann number. Further, in the work by Chutia and Deka [26], the FDM was also used to solve the two-dimensional MHD flow in a square duct subjected to a transverse magnetic field. They investigated the effect of the inclination angle on the distribution of the velocity and induced magnetic field at high Hartmann numbers. Later, Raslan and Ali [27] solved the general MHD flow in a rectangular electrically insulated duct subject to a transverse magnetic field by using the conventional central difference formulations in the discretization of the governing equations. Recently, Arslan [28], and Arslan and Tezer [29] solved analytically the one-dimensional MHD flow between infinitely long parallel plates which are electrically conducting and slippery. They also obtain numerical solutions for the same problem by using the FDM. Finally, Arslan and Tezer-Sezgin [30] extended their study for the two-dimensional MHD flow in a rectangular duct and solved it by using FDM to examine how the Hartmann number and slip length affect the distribution of the fluid flow and the induced magnetic field. It is important to highlight that the traditional (standard) finite difference method was used for the MHD flow equations in their original coupled convection-diffusion form in each of the studies mentioned above. That is, the well-known standard finite difference formulas provided in Section 2.1 were used to approximate either first-order or second-order derivatives in the MHD flow equations and in the given boundary conditions.

The application of FDM to address the MHD flow problems is the main topic of the current thesis, as was already noted. However, in addition to the standard FDM used in the studies mentioned above, a new FDM is intended to be used with the decou-

pled form of MHD flow equations, which are basically in the form of two modified Helmholtz equations. In other words, solving the MHD flow problem is transformed into solving the resulting two modified Helmholtz equations. To the best of the author's knowledge, there are no direct studies on the FDM solution of the modified Helmholtz equation. However, Britt et al. [31] solved the wave equation with variable speed of sound by using a high-order compact time and space finite difference scheme. They introduced a time-marching scheme that transformed the wave equation into a modified Helmholtz equation. Then, the resulting modified Helmholtz equation was solved on a Cartesian grid using the compact finite difference scheme given in [32]. The application of the compact time/space FDM used in [31] was expanded by Kahana et al. [33] for the two and three-dimensional wave equations with a damping layer in an unbounded region. On the other hand, there have been a quite number of works on the FDM solution of the Helmholtz equation. In these works, besides standard FDM some compact and higher-order accurate FDMs have been developed. Harari and Turkel [34] solved a time-harmonic acoustic problem which was modeled by the Helmholtz equation, by using high-order finite difference methods, where the order of accuracy of the resulting scheme was four on uniform grids and three in non-uniform grids. Singer and Turkel [32] created two fourth-order nine-point finite difference schemes for the one and two-dimensional Helmholtz equations subject to two types of boundary conditions, namely Dirichlet and/or Neumann boundary conditions. Singer and Turkel [35] further developed a nine-point sixth-order accurate finite difference scheme for the discretization of the two-dimensional Helmholtz equation. Sutmann [36] introduced a sixth-order compact finite-difference scheme to solve the Helmholtz equation and he applied this scheme to a set of different test cases only for Dirichlet-type boundary conditions. Finally, Nabavi et al. [37] solved the Helmholtz equation in one and two dimensions by using a new 9-point sixth-order accurate compact finite-difference method which was based on the sixth-order approximation for the derivatives in the Helmholtz equation and for the Neumann-type boundary condition. Even though these higher-order approaches produced reasonable solutions for the Helmholtz equation, the solution was extremely sensitive to the step size and it oscillated at high wavenumbers. In order to get overcome this problem, Lambe et al. [3] proposed a new finite difference method for the one, two, and three-dimensional Helmholtz equations by using symbolic compu-

tation. The new finite difference formulas were obtained from the standard central difference formulas by replacing the standard weights with weights that are optimal in the sense that the truncation error is avoided. By using the idea of Lambe et al. [3], later, Li and Yang [4] extended the new finite difference method for the radiation boundary conditions. Thus, they obtained a new finite difference method that produced solutions satisfying the Helmholtz equation exactly at both interior and boundary points. Since no truncation error is introduced, the new scheme results in an exact numerical solution at high wavenumbers even by using a coarse mesh. In the current thesis, the new finite difference method is going to be derived for the one and two-dimensional modified Helmholtz equations with the mixed-type boundary conditions in a similar manner introduced by Lambe et al. [3] and Li and Yang [4] for the Helmholtz equation.

In light of the above literature review, the position of the thesis subject within the related research field, as well as the contributions and novelties in the thesis can be summarized as follows:

- The one-dimensional Hartmann flow between parallel plates and the two-dimensional MHD flow problem in a rectangular duct with slip velocity and variable conductivity conditions are numerically solved in the presence of a horizontally applied external magnetic field by using finite difference methods.

- Specifically, the standard and new finite difference methods are employed for the MHD equations after decoupling them into two modified Helmholtz equations via suitable transformations.

- As was already indicated, although the works [28, 29, 30] focus on the SFD solution to MHD flow problems, in these studies SFD scheme is used to discretize the original coupled convection-diffusion form of MHD equations. Thus, it can be said that this thesis is the first to apply the SFD to the modified Helmholtz form of the MHD equations.

- The new finite difference formulas, which involve no truncation error, are derived for the approximation of the derivatives in the modified Helmholtz equation, which can be considered the main theoretical contribution of the thesis.

- Next, the newly developed NFD scheme, which is regarded as an exact numer-

ical approach due to no truncation error, is applied for the first time to solve the MHD flow problems. This is one of the main numerical contributions of the thesis.

- Numerical simulations with the SFD and NFD methods are carried out over numerous different cases in order to analyze the combined effects of the conductivity parameter and slip length on the velocity and induced magnetic field at different Hartmann numbers. The code, which is written by ourselves in MATLAB, validation and the accuracy of the obtained finite difference results are performed through benchmark MHD flow problems for which the analytical solutions exist.

1.4 The Outline of the Thesis

In Chapter 2, the well-known standard finite difference formulas are obtained by using the Taylor series expansions for the first- and second-order derivatives of a function with one and two variables. Then, a novel finite difference scheme for the one- and two-dimensional Helmholtz equations is presented. The NFD method is produced by constructing new finite difference formulas for the standard central difference formulas by substituting the standard weights with weights that are optimal in regards to the fact that the truncation error is eliminated. The optimization of the weights in the standard finite difference methods for the one-dimensional and two-dimensional Helmholtz equations is explained.

In Chapter 3, the finite difference solutions to one-dimensional MHD flow in between two parallel plates, which is called Hartmann flow, are given. Firstly, the one-dimensional MHD flow equations in the form of modified Helmholtz equations are discretized by using the standard finite difference method, and then by using the new finite difference scheme for different types of boundary conditions. The optimal weights in the new finite difference formulas for the modified Helmholtz equation and for the derivative boundary conditions are derived. Then, the numerical results obtained from SFD and NFD schemes are compared with the analytical solutions in terms of the variations of the velocity and induced magnetic field along the computa-

tional interval. Furthermore, the effects of various combinations of the slip length and the conductivity parameter on the velocity and induced magnetic field distributions are investigated at several values of the Hartmann number.

In Chapter 4, the steady, laminar, fully developed flow of a viscous, incompressible, and electrically conducting fluid in rectangular channels or pipes subject to an external, constant, and uniform magnetic field applied horizontally is solved by using finite difference schemes. First of all, the two-dimensional MHD flow equations are discretized by using the standard finite difference method only for the MHD flow in a rectangular duct with no-slip and insulated walls. Then, the NFD scheme is used for the numerical solution of MHD duct flow equations in the form of modified Helmholtz equations under different boundary conditions. To achieve this, first, the derivation of the new finite difference formulas with optimal weights are derived for the two-dimensional modified Helmholtz equations, and for the first-order derivatives in the boundary conditions. The validation of the numerical results obtained from SFD and NFD methods is performed by solving the MHD flow problem with no-slip and insulated duct walls for which the analytical solution is available. Then, the NFD solutions to two MHD duct flow problems subject to different boundary conditions are investigated to see the combined effects of the Hartmann number, slip length, and conductivity parameter on the velocity and the induced magnetic field.

CHAPTER 2

FINITE DIFFERENCE METHODS

One of the approximation techniques for solving differential equations that are hard or not possible to solve analytically is the finite difference method. Finite difference methods are numerical methods that approximate derivatives with finite differences to solve differential equations. We are given closed-form expressions by analytical solutions of partial differential equations that show the variation of the dependent variables in the domain. On the other hand, in the finite difference methods, the two-dimensional domain of the problem is discretized in x- and y- directions, and the resulting discrete points in the domain are called grid points. A domain of calculation in the xy-plane is shown in Figure 2.1 where $x \in [a, b]$ and $y \in [c, d]$. Suppose that the grid points in x and y-directions are evenly spaced and the increments in x and y-directions are indicated by $\Delta x = h$ and $\Delta y = k$, respectively.

In Figure 2.1, grid points are defined by an increasing index $m = 0, 1, ..., M$ where M is the number of subintervals in the positive x-direction and an increasing index $n = 0, 1, ..., N$ where N is the number of subintervals in the positive y-direction. If the index of point P in Figure 2.1 is (m, n) then the index of points directly to the right and left are $(m + 1, n)$ and $(m - 1, n)$, respectively. Similarly, the indices of points located right above and below to point P are $(m, n+1)$ and $(m, n-1)$, respectively. Thus, $x_m = a + m\Delta x$ and $y_n = c + n\Delta y$ give the x and y component of the grid point $P(x_m, y_n)$ if equally spaced points are employed. That is, the step sizes in x and y- directions are taken as $\Delta x = h = \dfrac{b-a}{M}$ and $\Delta y = k = \dfrac{d-c}{N}$. The value of u at the point $P(x_m, y_n)$ is $u(x_m, y_n)$ and its finite difference approximation is shown by $u_{m,n}$, where $u(x_m, y_n) \approx u_{m,n}$. The fundamental idea behind the finite difference methods is to use algebraic difference quotients in place of the derivatives of gov-

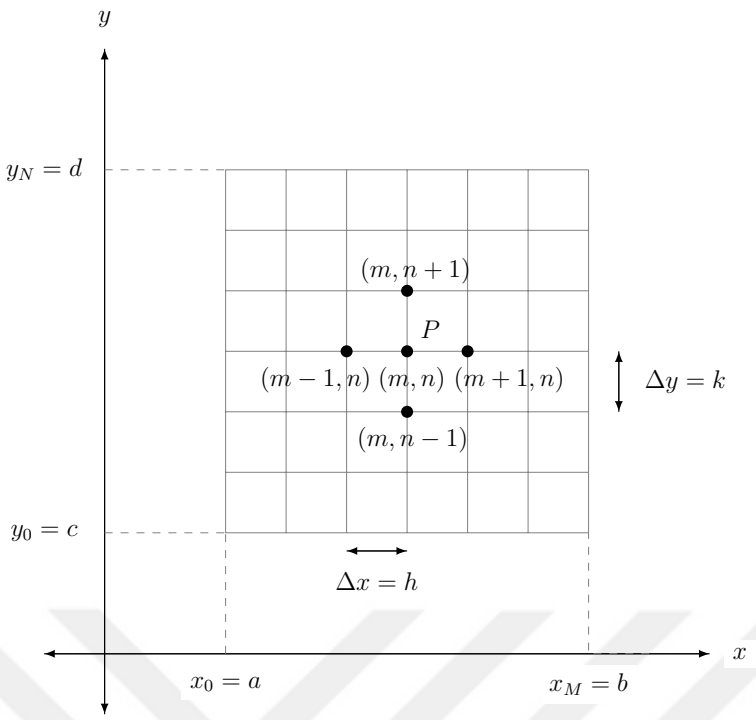


Figure 2.1: Discrete grid points in domain $[a, b] \times [c, d]$.

erning equations. As a consequence, a system of algebraic equations is generated, which may be easily solved on a computer for the dependent variables at the discrete grid points in the computational domain. Taylor series expansions are the source of these finite difference approximations for derivatives of a function. The Taylor series expansions in x-direction are

$$\begin{aligned} u(x_m + \Delta x, y_n) &= u(x_m, y_n) + \Delta x \frac{\partial u}{\partial x}(x_m, y_n) + \frac{(\Delta x)^2}{2!} \frac{\partial^2 u}{\partial x^2}(x_m, y_n) \\ &\quad + \frac{(\Delta x)^3}{3!} \frac{\partial^3 u}{\partial x^3}(x_m, y_n) + ... \\ &= \sum_{i=0}^{k} \frac{1}{i!} \left(\Delta x \frac{\partial}{\partial x} \right)^i u(x_m, y_n) + R_k \end{aligned} \tag{2.1}$$

$$\begin{aligned} u(x_m - \Delta x, y_n) &= u(x_m, y_n) - \Delta x \frac{\partial u}{\partial x}(x_m, y_n) + \frac{(\Delta x)^2}{2!} \frac{\partial^2 u}{\partial x^2}(x_m, y_n) \\ &\quad - \frac{(\Delta x)^3}{3!} \frac{\partial^3 u}{\partial x^3}(x_m, y_n) + ... \\ &= \sum_{i=0}^{k} \frac{(-1)^i}{i!} \left(\Delta x \frac{\partial}{\partial x} \right)^i u(x_m, y_n) + R_k \end{aligned} \tag{2.2}$$

and similarly in y-direction they become

$$\begin{aligned} u(x_m, y_n + \Delta y) &= u(x_m, y_n) + \Delta y \frac{\partial u}{\partial y}(x_m, y_n) + \frac{(\Delta y)^2}{2!}\frac{\partial^2 u}{\partial y^2}(x_m, y_n) \\ &\quad + \frac{(\Delta y)^3}{3!}\frac{\partial^3 u}{\partial y^3}(x_m, y_n) + ... \\ &= \sum_{i=0}^{k} \frac{1}{i!}\left(\Delta y \frac{\partial}{\partial y}\right)^i u(x_m, y_n) + R_k \end{aligned} \tag{2.3}$$

$$\begin{aligned} u(x_m, y_n - \Delta y) &= u(x_m, y_n) - \Delta y \frac{\partial u}{\partial y}(x_m, y_n) + \frac{(\Delta y)^2}{2!}\frac{\partial^2 u}{\partial y^2}(x_m, y_n) \\ &\quad - \frac{(\Delta y)^3}{3!}\frac{\partial^3 u}{\partial y^3}(x_m, y_n) + ... \\ &= \sum_{i=0}^{k} \frac{(-1)^i}{i!}\left(\Delta y \frac{\partial}{\partial y}\right)^i u(x_m, y_n) + R_k \end{aligned} \tag{2.4}$$

where R_k is the remainder (error) term in the series expansion which is given by

$$R_k(\Delta x, 0) = \frac{1}{(k+1)!}(\Delta x)^{k+1}\frac{\partial^{k+1}}{\partial x^{k+1}}u(x_m + \theta_1 \Delta x, y_n)$$

in x-direction and in y-direction it is as follows

$$R_k(0, \Delta y) = \frac{1}{(k+1)!}(\Delta y)^{k+1}\frac{\partial^{k+1}}{\partial y^{k+1}}u(x_m, y_n + \theta_2 \Delta y)$$

for $0 < \theta_1, \theta_2 < 1$. Assuming the series converges, Equations (2.1)-(2.4) provide an exact solution for $u(x_m, y_n)$. However, after a certain number of terms, the terms in Equations (2.1)-(2.4) can be neglected for any function $u(x, y)$ since every higher-order term of Δx (or Δy) is smaller than Δx (or Δy) as Δx (or Δy) is so small. The truncation error is indicated by these neglected higher-order terms. In other words, the difference between a function's analytical derivative and its derivative produced through numerical approximation is described as a truncation error. The rate at which a numerical approximation of a differential equation converges to the exact solution is defined as the order of accuracy and it is denoted by the notation $\mathcal{O}$, which also indicates the order of magnitude of the truncation error.

In Section 2.1, we first derive the standard finite difference (SFD) formulas approximating the first and second-order derivatives of a function $u(x, y)$ by using the Taylor series expansions given in Equations (2.1)-(2.4). Then, a new (novel) finite difference scheme (NFD), which was introduced in the works of Lambe et al. [3] and Wong and

Li [4] for the Helmholtz equation, is presented in Section 2.2. The NFD scheme is basically obtained from the SFD formulas by replacing the **standard weights** in the central difference formulas by **new weights** that are optimal in the sense that no truncation error is introduced in the NFD formulas.

2.1 Standard Finite Difference Formulas

The well-known standard finite difference formulas are derived by using the Taylor series expansions given in Equations (2.1)-(2.4) for the first-order derivatives of a function with two variables, $u(x, y)$, in Section 2.1.1 and for the second-order derivatives of $u(x, y)$ in Section 2.1.2.

2.1.1 Finite difference formulas for the first-order partial derivatives

The Taylor series expansions given in Equation (2.1) and Equation (2.2) can be written in the forms:

$$u(x_m + \Delta x, y_n) = u(x_m, y_n) + \Delta x \frac{\partial u}{\partial x}(x_m, y_n) + \mathcal{O}(\Delta x^2) \tag{2.5}$$

$$u(x_m - \Delta x, y_n) = u(x_m, y_n) - \Delta x \frac{\partial u}{\partial x}(x_m, y_n) + \mathcal{O}(\Delta x^2). \tag{2.6}$$

Then, the finite difference formulas for the first derivative $\dfrac{\partial u}{\partial x}(x_m, y_n)$ can be obtained by rearranging Equation (2.5) and Equation (2.6) as follows:

$$\begin{aligned} \frac{\partial u}{\partial x}(x_m, y_n) &= \frac{u(x_m + \Delta x, y_n) - u(x_m, y_n)}{\Delta x} + \mathcal{O}(\Delta x) \\ &\approx \frac{u_{m+1,n} - u_{m,n}}{\Delta x} \end{aligned} \tag{2.7}$$

and

$$\begin{aligned} \frac{\partial u}{\partial x}(x_m, y_n) &= \frac{u(x_m, y_n) - u(x_m - \Delta x, y_n)}{\Delta x} + \mathcal{O}(\Delta x) \\ &\approx \frac{u_{m,n} - u_{m-1,n}}{\Delta x} \end{aligned} \tag{2.8}$$

where $u_{m,n}$ denotes the finite difference approximation of $u(x, y)$ at the point (x_m, y_n). Equation (2.7) and Equation (2.8) are called **forward difference** and

backward difference formulas, respectively, for the first-order partial derivative of $u(x, y)$ with respect to x. In a similar manner, **the forward** and **backward difference** formulas for the first order y-derivative of $u(x, y)$ can be obtained, respectively, as:

$$\begin{aligned}\frac{\partial u}{\partial y}(x_m, y_n) &= \frac{u(x_m, y_n + \Delta y) - u(x_m, y_n)}{\Delta y} + \mathcal{O}(\Delta y) \\ &\approx \frac{u_{m,n+1} - u_{m,n}}{\Delta y}\end{aligned} \tag{2.9}$$

$$\begin{aligned}\frac{\partial u}{\partial y}(x_m, y_n) &= \frac{u(x_m, y_n) - u(x_m, y_n - \Delta y)}{\Delta y} + \mathcal{O}(\Delta y) \\ &\approx \frac{u_{m,n} - u_{m,n-1}}{\Delta y}.\end{aligned} \tag{2.10}$$

In these finite difference formulas, the error terms are $\mathcal{O}(\Delta x)$ or $\mathcal{O}(\Delta y)$, so these approximations are called first-order approximations.

On the other hand, the second-order finite difference formula for $\frac{\partial u}{\partial x}(x_m, y_n)$ can be obtained by subtracting Equation (2.2) from Equation (2.1) and rearranging accordingly. Thus, the following formula

$$\begin{aligned}\frac{\partial u}{\partial x}(x_m, y_n) &= \frac{u(x_m + \Delta x, y_n) - u(x_m - \Delta x, y_n)}{2\Delta x} + \mathcal{O}(\Delta x^2) \\ &\approx \frac{u_{m+1,n} - u_{m-1,n}}{2\Delta x}\end{aligned} \tag{2.11}$$

which is called the **central difference** formula for $\frac{\partial u}{\partial x}$ at the point (x_m, y_n), is obtained. Similarly, the central difference formula for the y-derivative of u at (x_m, y_n) becomes:

$$\begin{aligned}\frac{\partial u}{\partial y}(x_m, y_n) &= \frac{u(x_m, y_n + \Delta y) - u(x_m, y_n - \Delta y)}{2\Delta y} + \mathcal{O}(\Delta y^2) \\ &\approx \frac{u_{m,n+1} - u_{m,n-1}}{2\Delta y}.\end{aligned} \tag{2.12}$$

Here, the error terms are $\mathcal{O}(\Delta x^2)$ and $\mathcal{O}(\Delta y^2)$, so central difference approximations are of second-order.

On the other hand, for a one-variable function $u(x)$ the analogous forward, backward, and central difference formulas for the first-order ordinary derivative $\frac{du}{dx}$ are as follows:

- Forward difference:

$$\frac{du}{dx} \approx \frac{u(x_m + \Delta x) - u(x_m)}{\Delta x} = \frac{u_{m+1} - u_m}{\Delta x} \tag{2.13}$$

- Backward difference:

$$\frac{du}{dx} \approx \frac{u(x_m) - u(x_m - \Delta x)}{\Delta x} = \frac{u_m - u_{m-1}}{\Delta x} \tag{2.14}$$

- Central difference:

$$\frac{du}{dx} \approx \frac{u(x_m + \Delta x) - u(x_m - \Delta x)}{2\Delta x} = \frac{u_{m+1} - u_{m-1}}{2\Delta x} \tag{2.15}$$

where u_m denotes the finite difference approximation of $u(x)$ at $x = x_m$.

2.1.2 Central difference formulas for the second-order partial derivatives

The second-order finite difference formula, which is called the central difference formula, for the second-order partial derivative $\dfrac{\partial^2 u}{\partial x^2}$ at (x_m, y_n) is derived by adding the Taylor series expansions given in Equation (2.1) and (2.2). This addition yields,

$$u(x_m+\Delta x, y_n)+u(x_m-\Delta x, y_n) = 2u(x_m, y_n)+\Delta x^2 \frac{\partial^2 u}{\partial x^2}(x_m, y_n)+\mathcal{O}(\Delta x^4) \tag{2.16}$$

which can be written as

$$\begin{aligned} \frac{\partial^2 u}{\partial x^2}(x_m, y_n) &= \frac{u(x_m + \Delta x, y_n) - 2u(x_m, y_n) + u(x_m - \Delta x, y_n)}{\Delta x^2} + \mathcal{O}(\Delta x^2) \\ &\approx \frac{u_{m+1,n} - 2u_{m,n} + u_{m-1,n}}{\Delta x^2}. \end{aligned} \tag{2.17}$$

Similarly, the central difference formula for the derivative $\dfrac{\partial^2 u}{\partial y^2}$ at the point (x_m, y_n) is obtained as:

$$\begin{aligned} \frac{\partial^2 u}{\partial y^2}(x_m, y_n) &= \frac{u(x_m, y_n + \Delta y) - 2u(x_m, y_n) + u(x_m, y_n - \Delta y)}{\Delta y^2} + \mathcal{O}(\Delta y^2) \\ &\approx \frac{u_{m,n+1} - 2u_{m,n} + u_{m,n-1}}{\Delta y^2}. \end{aligned} \tag{2.18}$$

Finally, the analogous central difference formula for the second-order ordinary derivative d^2u/dx^2 for a one-variable function $u(x)$ becomes

$$\frac{d^2 u}{dx^2} \approx \frac{u(x_m + \Delta x) - 2u(x_m) + u(x_m - \Delta x)}{\Delta x^2} = \frac{u_{m+1} - 2u_m + u_{m-1}}{\Delta x^2}. \tag{2.19}$$

The higher-order finite difference formulas can be obtained in a similar way by the help of Taylor series expansions. However, in the content of the present thesis, the

basic first and second-order difference formulas (2.7)-(2.15) and (2.17)-(2.19) and their novel modifications, which are derived for the second-order difference formulas in Section 2.2, are employed for the discretization of the problems at hand.

2.2 New (Novel) Finite Difference Method

The present section is devoted presenting a novel finite difference scheme described in [3, 4]. The application of the method is performed by discretizing an equation of convection-reaction type, particularly the Helmholtz equation, as introduced in [3, 4]. The main objective of the NFD method is to produce an exact numerical solution for the governing equation and boundary conditions of the problem that involves no truncation error while maintaining the straightforward structure of the discretized systems generated by the standard finite difference schemes. In other words, the difference equations produced by the NFD formulas exactly solve the original continuous problem. The NFD method is based on constructing new finite difference formulas for the standard central difference formulas (2.17), (2.18) and (2.19), by substituting the standard weights with weights that are optimal in regards to the fact that the truncation error is eliminated. The optimization of the weights in the standard finite difference methods for the one-dimensional and two-dimensional Helmholtz equations is explained, respectively, in Section 2.2.1 and Section 2.2.2.

2.2.1 New finite difference method for one-dimensional Helmholtz equation

The one-dimensional Helmholtz equation

$$u'' + k^2 u = 0 \tag{2.20}$$

is considered for a function $u = u(x)$ with the wavenumber k. One can approximate the second order derivative $\left(u'' = \dfrac{d^2u}{dx^2}\right)$ by using the standard central finite difference formula (2.19) as:

$$u''(x) \approx \frac{u(x+h) - 2u(x) + u(x-h)}{h^2} \tag{2.21}$$

where $\Delta x = h$ is the step size in x-direction. In order to construct the novel finite difference formula described by [3], the coefficient two of $u(x)$ in the approximation

(2.21) is replaced with a new coefficient (weight) w that minimizes

$$\mid u''(x) - \frac{u(x+h) - wu(x) + u(x-h)}{h^2} \mid . \tag{2.22}$$

Equation (2.22) represents the truncation error in the approximation of the second-order derivative by using the new weighted finite difference formula. In other words, one chooses the weight w such that the truncation error (2.22) is optimized (or vanished). To obtain the weight w, consider the Taylor series expansion (which can be maintained by considering Equation (2.16) for a one-variable function $u = u(x)$):

$$u(x+h) + u(x-h) = 2\left(u(x) + \frac{h^2}{2!}u^{(2)}(x) + \frac{h^4}{4!}u^{(4)}(x) + ...\right) \tag{2.23}$$

where $u^{(2n)}(x) = \dfrac{d^{2n}u(x)}{dx^{2n}}$.

By rewriting the Helmholtz equation (2.20) as $u'' = -k^2u$ and differentiating it iteratively one can obtain the derivatives of $u(x)$ of order $2n$, $u^{(2n)}(x)$, as follows:

$$u^{(2n)}(x) = (-1)^n k^{2n} u(x), \quad n = 1, 2, ... \tag{2.24}$$

Substitution of these values in Equation (2.23) yields

$$\begin{aligned} u(x+h) + u(x-h) &= 2\left(1 - \frac{(hk)^2}{2!} + \frac{(hk)^4}{4!} - \frac{(hk)^6}{6!} + ...\right)u(x) \\ &= 2\cos(kh)u(x) \end{aligned} \tag{2.25}$$

by the Taylor's series of

$$\cos(x) = \sum_{k=0}^{\infty}(-1)^k \frac{x^{2k}}{(2k)!}$$

which converges for all x (with $x = kh$ here). Then, with the use of Equation (2.25), the Helmholtz equation becomes

$$-k^2u(x) = u''(x) = \frac{u(x+h) - wu(x) + u(x-h)}{h^2} = \frac{2\cos(kh) - w}{h^2}u(x). \tag{2.26}$$

Therefore, the NFD formula with the adjusted weight w given by

$$w = 2\cos(kh) + (kh)^2 \tag{2.27}$$

satisfies the equation exactly by producing no truncation error in the approximation of second-order derivative $u''(x)$. Consequently, the NFD scheme results in an exact numerical solution to the one-dimensional Helmholtz equation (2.20).

Finally, the NFD scheme for the one-dimensional Helmholtz equation $u'' + k^2 u = 0$ is given by

$$u(x+h) - 2\cos(kh)u(x) + u(x-h) = 0. \tag{2.28}$$

2.2.2 NFD method for the two-dimensional Helmholtz equation

The two-dimensional Helmholtz equation is given by

$$\nabla^2 u + k^2 u = 0 \tag{2.29}$$

with the Laplacian of u, $\nabla^2 u = u_{xx} + u_{yy} = \dfrac{\partial^2 u}{\partial x^2} + \dfrac{\partial^2 u}{\partial y^2}$.

The standard finite difference scheme for $u_{xx} + u_{yy}$ is given by

$$u_{xx} + u_{yy} \approx \frac{u(x+h,y) + u(x-h,y) - 4u(x,y) + u(x,y+h) + u(x,y-h)}{h^2} \tag{2.30}$$

by using the same step size h in x- and y-directions, that is $\Delta x = \Delta y = h$. As in the one-dimensional problem, we want to replace the coefficient 4 of $u(x,y)$ in Equation (2.30) with an optimal weight w which minimizes

$$\left| \nabla^2 u - \frac{u(x+h,y) + u(x-h,y) - wu(x,y) + u(x,y+h) + u(x,y-h)}{h^2} \right|. \tag{2.31}$$

The presence of cross-derivative terms prevents the solution approach for the one-dimensional problem from being directly expanded. However, Lambe et al. [3] suggested an inventive solution to overcome this problem by using the planar wave solutions of the two-dimensional Helmholtz equation given as

$$u(x,y) = e^{ik(x\cos\theta + y\sin\theta)} \tag{2.32}$$

where $i^2 = -1$ and $\theta \in [-\pi, \pi]$. The direct use of Equation (2.32) yields

$$\begin{aligned} u(x+h,y) + u(x-h,y) + u(x,y+h) + u(x,y-h) = \\ 2(\cos(kh\cos\theta) + \cos(kh\sin\theta))u(x,y). \end{aligned} \tag{2.33}$$

Then, when Equation (2.33) is substituted in Equation (2.31), we want to find w such that

$$\frac{2(\cos(kh\cos\theta) + \cos(kh\sin\theta))u(x,y) - wu(x,y)}{h^2} \approx -k^2 u(x,y) = u_{xx} + u_{yy}, \tag{2.34}$$

or, equivalently, one looks for an optimal weight w satisfying

$$2(\cos(kh\cos\theta)+\cos(kh\sin\theta))-(w-(kh)^2)\approx 0. \tag{2.35}$$

Equation (2.35) has no solution which is independent of angle θ, but as explained in the work of Lambe et al. [3] by minimizing the average over all angles as follows

$$\int_0^{2\pi}(2(\cos(kh\cos\theta)+\cos(kh\sin\theta))-(w-(kh)^2))d\theta=0 \tag{2.36}$$

one can obtain a solution

$$w=k^2h^2+\frac{1}{\pi}\int_0^{2\pi}(\cos(kh\cos\theta)+\cos(kh\sin\theta))d\theta. \tag{2.37}$$

It is known that the integral in Equation (2.37) has an analytic expression in terms of the Bessel function of the first kind of order zero which is denoted by $J_0(kh)$. That is,

$$4\pi J_0(kh)=\int_0^{2\pi}(\cos(kh\cos\theta)+\cos(kh\sin\theta))d\theta. \tag{2.38}$$

By Equations (2.37) and (2.38), the optimal weight w is obtained as

$$w=4J_0(kh)+(kh)^2. \tag{2.39}$$

Thus, the NFD scheme for the two-dimensional Helmholtz equation

$$u_{xx}+u_{yy}+k^2u=0$$

is given by

$$u(x+h,y)+u(x-h,y)-4J_0(kh)u(x,y)+u(x,y+h)+u(x,y-h)=0. \tag{2.40}$$

In conclusion, the NFD scheme, which is proposed first by Lambe et al. [3] for the one and two-dimensional Helmholtz equations, is provided here because that is the numerical scheme we will be using in this thesis to solve the magnetohydrodynamic flow problems. The governing equations for MHD flow are convection-diffusion type equations which are coupled in velocity and induced magnetic field. These equations can be decoupled into two modified Helmholtz equations (that is, $u''-k^2u=0$ in one-dimension, and $\nabla^2u-k^2u=0$ in two-dimension) providing appropriate transformations for the velocity and induced magnetic field (see Section 1.2). As can be noticed, the modified Helmholtz equation differs from the original Helmholtz equation in that the sign of the reaction term, k^2u, is negative. As a result, the optimal

weights required in the NFD formulas to discretize the resulting modified Helmholtz equations will be determined (in Chapter 3- Section 3.2 for one-dimensional MHD flow and in Chapter 4- Section 4.2 for two-dimensional MHD flow) similar to how it was carried out for the Helmholtz equation in this section.

CHAPTER 3

FINITE DIFFERENCE SOLUTIONS TO ONE-DIMENSIONAL MHD FLOW

The finite difference solutions to MHD flow in between two parallel plates, which is called Hartmann flow and described in the work of Müller and Bühler [5], is investigated in this chapter. The MHD flow is driven along z-axis, which is the channel axis direction, and in the gap between two infinite parallel plates subject to an external magnetic field applied perpendicular to the channel walls (see Figure 3.1).

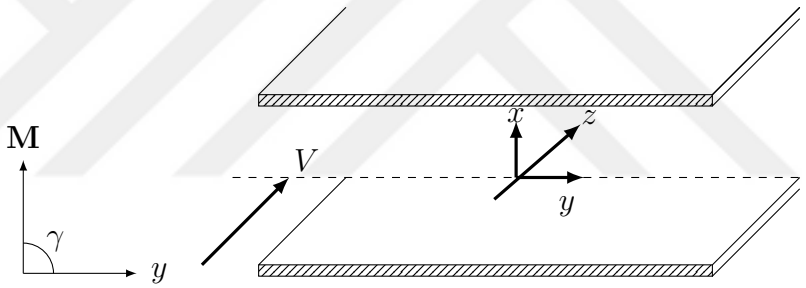


Figure 3.1: Flow configuration of Hartmann flow.

Thus, the velocity V and induced magnetic field B depend only on one coordinate x, that is $V = V(x)$ and $B = B(x)$. The governing equations describing Hartmann flow are represented by Equations (1.5) and (1.6) (see Section 1.1) and given as follows, [5]:

$$\begin{aligned} &\frac{d^2V}{dx^2} + M\frac{dB}{dx} = -1 \\ &\frac{d^2B}{dx^2} + M\frac{dV}{dx} = 0 \end{aligned} \qquad \text{in } -\ell < x < \ell \tag{3.1}$$

with the most general corresponding boundary conditions:

$$\pm\alpha\frac{dV}{dx} + V = 0, \quad \pm c\frac{dB}{dx} + B = 0 \quad \text{at } x = \pm\ell \tag{3.2}$$

where 2ℓ is the length of the computational interval along the x-axis, M is the Hartmann number, α is the slip length of slipping velocity and c is the conductivity parameter, respectively. As stated in Section 1.1, $\alpha = 0$ (i.e $V = 0$) corresponds to no-slip velocity boundary conditions, while $c = 0$ (i.e $B = 0$) implies electrically insulated walls, and $c = \infty$ represents electrically perfectly conducting walls. In computations, the interval half length ℓ is taken to be $\ell = 1$ since the analytical solution to Hartmann flow with $\ell = 1$ when $\alpha = 0$, $c \neq 0$ is available in [5]; and when $\alpha \neq 0$, $c \neq 0$ it was derived in [28]. Thus, the theoretical solution to MHD flow equation (3.1) with boundary condition (3.2) are given by [5, 28] as:

$$V(x) = -\overline{u}(\alpha M \sinh(M) + \cosh(M)) + \overline{u}\cosh(Mx) \tag{3.3}$$

$$B(x) = -\overline{u}\sinh(Mx) - \frac{x}{M} \tag{3.4}$$

with the characteristic velocity

$$\overline{u} = -\frac{1}{M}\frac{1+c}{cM\cosh(M) + \sinh(M)}\,. \tag{3.5}$$

In order to solve the MHD flow equations (3.1) and (3.2) by using the new finite difference scheme, the reduced form of these equations into modified Helmholtz equations (1.21) and (1.22) derived in Section 1.2 is going to be used. The MHD flow equations in modified Helmholtz equations are obtained as

$$\begin{aligned} &\frac{d^2u^1}{dx^2} - k^2u^1 = 0 \\ &\qquad\qquad\qquad\qquad \text{in } -\ell < x < \ell \\ &\frac{d^2u^2}{dx^2} - k^2u^2 = 0 \end{aligned} \tag{3.6}$$

with the corresponding reduced boundary conditions for velocity V

$$\begin{aligned} -\alpha\frac{du^1}{dx}e^{-kx} + (1+k\alpha)u^1e^{-kx} - \alpha\frac{du^2}{dx}e^{kx} + (1-k\alpha)u^2e^{kx} = 0, \quad &\text{at } x = -\ell \\ \alpha\frac{du^1}{dx}e^{-kx} + (1-k\alpha)u^1e^{-kx} + \alpha\frac{du^2}{dx}e^{kx} + (1+k\alpha)u^2e^{kx} = 0, \quad &\text{at } x = \ell \end{aligned} \tag{3.7}$$

and the corresponding reduced boundary conditions for the induced magnetic field B

$$\begin{aligned} -c\frac{du^1}{dx}e^{-kx} + (1+kc)u^1e^{-kx} + c\frac{du^2}{dx}e^{kx} + (-1+kc)u^2e^{kx} = \frac{x-c}{k}, \quad &\text{at } x = -\ell \\ c\frac{du^1}{dx}e^{-kx} + (1-kc)u^1e^{-kx} - c\frac{du^2}{dx}e^{kx} + (-1-kc)u^2e^{kx} = \frac{x+c}{k}, \quad &\text{at } x = \ell, \end{aligned} \tag{3.8}$$

respectively, by using the transformations

$$u^1 = e^{kx}\left(V + B + \frac{x}{M}\right) \qquad \text{and} \qquad u^2 = e^{-kx}\left(V - B - \frac{x}{M}\right) \tag{3.9}$$

with $M = 2k$ (see Section 1.2). Once the finite difference solution is obtained for Equation (3.6) with boundary conditions (3.7) and (3.8) in terms of u^1 and u^2, the original unknowns, the velocity V and the induced magnetic field B, are obtained by using the corresponding backward substitutions (see Equation 1.20):

$$V = \frac{u^1 e^{-kx} + u^2 e^{kx}}{2} \qquad \text{and} \qquad B = \frac{u^1 e^{-kx} - u^2 e^{kx}}{2} - \frac{x}{M}\,. \tag{3.10}$$

The MHD flow equations (3.6)-(3.8) are discretized by using the standard finite difference method in Section 3.1, and then by new finite difference scheme in Section 3.2, respectively, for different types of boundary conditions including four cases, namely:

Case I: Insulated plates with no-slip velocity boundary condition, that is $c = \alpha = 0$.

Case II: Variably conducting plates with no-slip velocity boundary condition, that is $c \neq 0$ and $\alpha = 0$.

Case III: Insulated plates with slip velocity boundary condition, that is $c = 0$, $\alpha \neq 0$.

Case IV: Variably conducting plates with slip velocity boundary condition, that is $c \neq 0$, $\alpha \neq 0$.

The derivation of the optimal weights in the new finite difference formulas for the modified Helmholtz equations (3.6) and for the first order derivatives in boundary conditions (3.2) are performed in Section 3.2 in details. The comparison of analytical solutions with the numerical results obtained by SFD and NFD schemes are visualized in Section 3.3 in terms of velocity and induced magnetic field variations along the computational interval $x \in [-\ell, \ell]$ with $\ell = 1$, and by indicating the accuracy between the solutions in terms of relative errors. Moreover, the effects of the Hartmann number on velocity and induced magnetic field are visualized under various combinations of slip length α and conductivity parameter c.

3.1 Application of the SFD method to one-dimensional MHD Flow

The modified Helmholtz form of MHD flow equations given in Equation (3.6) involves two second-order linear ordinary differential equations of the same form in u^1 and u^2 along $-\ell < x < \ell$, and hence their finite difference approximations are going to be the same as well. When the derivatives $(u^i)'' = d^2u^i/dx^2$, $i = 1, 2$, are replaced by the second order central difference formula (2.19) at node $x = x_m$, Equation (3.6) becomes

$$\frac{u^i_{m+1} - 2u^i_m + u^i_{m-1}}{h^2} - k^2 u^i_m = 0, \qquad m = 0, 1, ..., N, \quad i = 1, 2 \tag{3.11}$$

where $u^i_m \approx u^i(x_m)$, $x_m = x_0 + mh$ with $x_0 = -\ell$ and $x_N = \ell$, N represents the number of subintervals, and $h = \dfrac{2\ell}{N}$ is the step size. Equivalently, Equation (3.11) can be written as

$$u^i_{m+1} - (2 + (kh)^2)u^i_m + u^i_{m-1} = 0, \qquad m = 0, 1, ..., N, \quad i = 1, 2\,. \tag{3.12}$$

The corresponding boundary conditions in Equation (3.2) can also be discretized by using the central difference formula (2.15) for the derivative $\dfrac{dV}{dx}$ and $\dfrac{dB}{dx}$ at the boundary points $x_0 = -\ell$ and $x_N = \ell$. Then, the discretized boundary conditions for the velocity become

$$\begin{aligned} -\alpha\frac{V_1 - V_{-1}}{2h} + V_0 = 0, &\qquad \text{at } x = x_0 = -\ell \\ \alpha\frac{V_{N+1} - V_{N-1}}{2h} + V_N = 0, &\qquad \text{at } x = x_N = \ell \end{aligned} \tag{3.13}$$

and for the induced magnetic field they reduce to

$$\begin{aligned} -c\frac{B_1 - B_{-1}}{2h} + B_0 = 0, &\qquad \text{at } x = x_0 = -\ell \\ c\frac{B_{N+1} - B_{N-1}}{2h} + B_N = 0, &\qquad \text{at } x = x_N = \ell \end{aligned} \tag{3.14}$$

in which the truncation error is of $\mathcal{O}(h^2)$. Equivalently, they can be rewritten as

$$\begin{aligned} \alpha V_1 - 2hV_0 - \alpha V_{-1} = 0, &\qquad \text{at } x = x_0 = -\ell \\ \alpha V_{N+1} + 2hV_N - \alpha V_{N-1} = 0, &\qquad \text{at } x = x_N = \ell \end{aligned} \tag{3.15}$$

and

$$\begin{aligned} cB_1 - 2hB_0 - cB_{-1} = 0, &\qquad \text{at } x = x_0 = -\ell \\ cB_{N+1} + 2hB_N - cB_{N-1} = 0, &\qquad \text{at } x = x_N = \ell\,. \end{aligned} \tag{3.16}$$

Thus, to obtain finite difference schemes in terms of u^1 and u^2 we substitute the transformation (3.9) into Equations (3.15) and (3.16). Then, the standard central finite difference schemes for the velocity boundary conditions $\pm\alpha\dfrac{dV}{dx} + V = 0$ become

$$\begin{aligned}
&\alpha\frac{u_1^1 e^{-kx_1} + u_1^2 e^{kx_1}}{2} - 2h\frac{u_0^1 e^{-kx_0} + u_0^2 e^{kx_0}}{2} \\
&\qquad - \alpha\frac{u_{-1}^1 e^{-kx_{-1}} + u_{-1}^2 e^{kx_{-1}}}{2} = 0, \qquad \text{at } x = -\ell \\
&\alpha\frac{u_{N+1}^1 e^{-kx_{N+1}} + u_{N+1}^2 e^{kx_{N+1}}}{2} + 2h\frac{u_N^1 e^{-kx_N} + u_N^2 e^{kx_N}}{2} \\
&\qquad - \alpha\frac{u_{N-1}^1 e^{-kx_{N-1}} + u_{N-1}^2 e^{kx_{N-1}}}{2} = 0, \qquad \text{at } x = \ell
\end{aligned} \tag{3.17}$$

and for the induced magnetic field boundary conditions $\pm c\dfrac{dB}{dx} + B = 0$ they become

$$\begin{aligned}
&c\left(\frac{u_1^1 e^{-kx_1} - u_1^2 e^{kx_1}}{2} - \frac{x_1}{M}\right) - 2h\left(\frac{u_0^1 e^{-kx_0} - u_0^2 e^{kx_0}}{2} - \frac{x_0}{M}\right) \\
&- c\left(\frac{u_{-1}^1 e^{-kx_{-1}} - u_{-1}^2 e^{kx_{-1}}}{2} - \frac{x_{-1}}{M}\right) = 0, \qquad \text{at } x = -\ell \\
&c\left(\frac{u_{N+1}^1 e^{-kx_{N+1}} - u_{N+1}^2 e^{kx_{N+1}}}{2} - \frac{x_{N+1}}{M}\right) + 2h\left(\frac{u_N^1 e^{-kx_N} - u_N^2 e^{kx_N}}{2} - \frac{x_N}{M}\right) \\
&- c\left(\frac{u_{N-1}^1 e^{-kx_{N-1}} - u_{N-1}^2 e^{kx_{N-1}}}{2} - \frac{x_{N-1}}{M}\right) = 0, \qquad \text{at } x = \ell\,.
\end{aligned} \tag{3.18}$$

Since we use the standard central difference formula for the derivative boundary conditions, we have ghost points u_{-1}^i and u_{N+1}^i with $i = 1, 2$. To eliminate them in Equations (3.17) and (3.18), we use the standard finite difference formula (3.12) with $m = 0$ and $m = N$, which yield $u_{-1}^i = (2 + (kh)^2)u_0^i - u_1^i$ and $u_{N+1}^i = (2 + (kh)^2)u_N^i - u_{N-1}^i$ at $i = 1, 2$. Once they are substituted in Equations (3.17) and (3.18), the finite difference equations for the boundary conditions

with no ghost points can be written as:

$$
\begin{aligned}
&(-\alpha(2+(kh)^2)e^{-kx_{-1}} - 2he^{-kx_0})u_0^1 + \alpha(e^{-kx_{-1}} + e^{-kx_1})u_1^1 \\
&+ (-\alpha(2+(kh)^2)e^{kx_{-1}} - 2he^{kx_0})u_0^2 + \alpha(e^{kx_{-1}} + e^{kx_1})u_1^2 = 0, \quad \text{at } x = -\ell \\
&(\alpha(2+(kh)^2)e^{-kx_{N+1}} + 2he^{-kx_N})u_N^1 + \alpha(-e^{-kx_{N-1}} + e^{-kx_{N+1}})u_{N-1}^1 \\
&+ (\alpha(2+(kh)^2)e^{kx_{N+1}} + 2he^{kx_N})u_N^2 + \alpha(-e^{kx_{N-1}} - e^{kx_{N+1}})u_{N-1}^2 = 0, \quad \text{at } x = \ell
\end{aligned}
\tag{3.19}
$$

and

$$
\begin{aligned}
&(-c(2+(kh)^2)e^{-kx_{-1}} - 2he^{-kx_0})u_0^1 + c(e^{-kx_{-1}} + e^{-kx_1})u_1^1 \\
&+ (c(2+(kh)^2)e^{kx_{-1}} + 2he^{kx_0})u_0^2 + c(-e^{kx_{-1}} - e^{kx_1})u_1^2 \\
&= \frac{c}{k}(x_1 - \frac{2h}{c}x_0 - x_{-1}), \qquad \text{at } x = -\ell \\
&(c(2+(kh)^2)e^{-kx_{N+1}} + 2he^{-kx_N})u_N^1 + c(-e^{-kx_{N-1}} - e^{-kx_{N+1}})u_{N-1}^1 \\
&+ (-c(2+(kh)^2)e^{kx_{N+1}} - 2he^{kx_N})u_N^2 + c(e^{kx_{N-1}} + e^{kx_{N+1}})u_{N-1}^2 \\
&= \frac{c}{k}(x_{N+1} + \frac{2h}{c}x_N - x_{N-1}), \qquad \text{at } x = \ell\,.
\end{aligned}
\tag{3.20}
$$

Finally, the standard finite difference scheme (3.12) for interior points becomes

$$
u_{m+1}^i - (2+(kh)^2)u_m^i + u_{m-1}^i = 0, \qquad m = 1, 2, ..., N-1, \quad i = 1, 2\,. \tag{3.21}
$$

Insertion of the boundary conditions (3.19) and (3.20) into the difference equation (3.21) yields a linear system of equations of size $(2N+2) \times (2N+2)$ which can be written in the following matrix vector-form

$$
Au = b \tag{3.22}
$$

with the unknown vector u, which is ordered as:

$$
u = \begin{bmatrix} u_0^1 & u_1^1 & u_2^1 & \cdots & u_N^1 & | & u_0^2 & u_1^2 & u_2^2 & \cdots & u_N^2 \end{bmatrix}^T \tag{3.23}
$$

and the right-hand side vector of size $(2N+2)$ has the following form:

$$
b = \begin{bmatrix} b_1 & 0 & 0 & \cdots & 0 & b_{N+1} & | & 0 & \cdots & 0 \end{bmatrix}^T \tag{3.24}
$$

where $b_1 = \dfrac{cx_1}{k} - 2h\dfrac{x_0}{k} - \dfrac{cx_{-1}}{k}$ and $b_{N+1} = \dfrac{cx_{N+1}}{k} + 2h\dfrac{x_N}{k} - \dfrac{cx_{N-1}}{k}$.

The coefficient matrix can also be written as

$$A = \begin{bmatrix} A_1 & A_2 \\ A_3 & A_4 \end{bmatrix}$$

where A_i, $i = 1, 2, 3, 4$, are block matrices of the size $(N+1) \times (N+1)$ and they are given by:

$$A_1 = \begin{bmatrix} a^1_{1,1} & a^1_{1,2} & 0 & 0 & \cdots & 0 \\ 1 & -(2+(kh)^2) & 1 & 0 & \cdots & 0 \\ 0 & 1 & -(2+(kh)^2) & 1 & & \vdots \\ & & \ddots & \ddots & \ddots & 0 \\ \vdots & \ddots & & 1 & -(2+(kh)^2) & 1 \\ 0 & \cdots & & 0 & a^1_{N+1,N} & a^1_{N+1,N+1} \end{bmatrix}$$

with the components

$$\begin{aligned} a^1_{1,1} &= -c(2+(kh)^2)e^{-kx_{-1}} - 2he^{-kx_0}, & a^1_{1,2} &= c(e^{-kx_{-1}} + e^{-kx_1}), \\ a^1_{N+1,N+1} &= c(2+(kh)^2)e^{-kx_{N+1}} + 2he^{-kx_N}, & a^1_{N+1,N} &= c(-e^{-kx_{N-1}} - e^{-kx_{N+1}}), \end{aligned} \tag{3.25}$$

and

$$A_2 = \begin{bmatrix} a^2_{1,1} & a^2_{1,2} & 0 & \cdots & 0 & 0 & 0 \\ 0 & 0 & 0 & \cdots & 0 & 0 & 0 \\ \vdots & & & & & & \vdots \\ 0 & 0 & 0 & \cdots & 0 & 0 & 0 \\ 0 & 0 & 0 & \cdots & 0 & a^2_{N+1,N} & a^2_{N+1,N+1} \end{bmatrix}$$

with the components

$$\begin{aligned} a^2_{1,1} &= c(2+(kh)^2)e^{kx_{-1}} + 2he^{kx_0}, & a^2_{1,2} &= c(-e^{kx_{-1}} - e^{kx_1}), \\ a^2_{N+1,N+1} &= -c(2+(kh)^2)e^{kx_{N+1}} - 2he^{kx_N}, & a^2_{N+1,N} &= c(e^{kx_{N-1}} + e^{kx_{N+1}}) \,, \end{aligned} \tag{3.26}$$

and

$$A_3 = \begin{bmatrix} a^3_{1,1} & a^3_{1,2} & 0 & \cdots & 0 & 0 & 0 \\ 0 & 0 & 0 & \cdots & 0 & 0 & 0 \\ \vdots & & & & & & \vdots \\ 0 & 0 & 0 & \cdots & 0 & 0 & 0 \\ 0 & 0 & 0 & \cdots & 0 & a^3_{N+1,N} & a^3_{N+1,N+1} \end{bmatrix}$$

with the components

$$\begin{aligned} a^3_{1,1} &= -\alpha(2+(kh)^2)e^{-kx_{-1}} - 2he^{-kx_0}, & a^3_{1,2} &= \alpha(e^{-kx_{-1}} + e^{-kx_1}), \\ a^3_{N+1,N+1} &= \alpha(2+(kh)^2)e^{-kx_{N+1}} + 2he^{-kx_N}, & a^3_{N+1,N} &= \alpha(-e^{-kx_{N-1}} - e^{-kx_{N+1}}). \end{aligned} \tag{3.27}$$

Finally, the matrix A_4 is equal to

$$A_4 = \begin{bmatrix} a^4_{1,1} & a^4_{1,2} & 0 & 0 & \cdots & 0 \\ 1 & -(2+(kh)^2) & 1 & 0 & \cdots & 0 \\ 0 & 1 & -(2+(kh)^2) & 1 & & \vdots \\ & & \ddots & \ddots & \ddots & 0 \\ \vdots & \ddots & & 1 & -(2+(kh)^2) & 1 \\ 0 & \cdots & & 0 & a^4_{N+1,N} & a^4_{N+1,N+1} \end{bmatrix}$$

with the components

$$\begin{aligned} a^4_{1,1} &= -\alpha(2+(kh)^2)e^{kx_{-1}} - 2he^{kx_0}, & a^4_{1,2} &= \alpha(e^{kx_{-1}} + e^{kx_1}), \\ a^4_{N+1,N+1} &= \alpha(2+(kh)^2)e^{kx_{N+1}} + 2he^{kx_N}, & a^4_{N+1,N} &= \alpha(-e^{kx_{N-1}} - e^{kx_{N+1}}) \,. \end{aligned} \tag{3.28}$$

Once the system (3.22) is solved, u^1 and u^2 are obtained at nodes x_m, $m = 0, 1, ..., N$, and by using back substitutions in Equation (3.10), the velocity V and the induced magnetic field B are obtained.

It is important to note here that boundary conditions (3.19) and (3.20) are coupled in unknowns u^1 and u^2, which requires the simultaneous solution of the difference equation of the modified Helmholtz equations (3.6) for u^1 and u^2. Thus, the system (3.22) is of size $(2N+2) \times (2N+2)$ for the most general mixed-type boundary conditions (3.2) with $\alpha \neq 0$, $c \neq 0$ which corresponds to Case IV. The system of equations for other cases can be obtained from the system (3.22) by substituting $\alpha = c = 0$ for Case I, $\alpha = 0$ for Case II and $c = 0$ for Case III.

3.1.1 Case I: Insulated plates with no-slip velocity condition: $\alpha = c = 0$

Since $\alpha = c = 0$ implies $V = B = 0$ on the boundaries $x = \mp\ell$, the boundary conditions in terms of u^1 and u^2 are obtained by substituting $V = B = 0$ in Equation (3.9), that is, $u^1 = \dfrac{x}{2k}e^{kx}$ and $u^2 = -\dfrac{x}{2k}e^{-kx}$ at $x = \mp\ell$, which are decoupled as well as the modified Helmholtz equations (3.6). Thus, the system (3.22) can be decoupled and written separately in two systems of sizes $(N-1) \times (N-1)$ in unknowns u^1 and u^2.

The standard central finite difference equations for the modified Helmholtz equations (3.6) at the interior points are given in Equation (3.21) as

$$u^i_{m+1} - (2+(kh)^2)u^i_m + u^i_{m-1} = 0, \qquad m = 1, 2..., N-1, \qquad i = 1, 2 \tag{3.29}$$

with the boundary conditions

$$\begin{aligned} u^1_0 &= \frac{x_0}{2k}e^{kx_0}, \quad \text{at } x_0 = -\ell \quad \text{and} \quad u^1_N = \frac{x_N}{2k}e^{kx_N}, \quad \text{at } x_N = \ell \\ u^2_0 &= -\frac{x_0}{2k}e^{-kx_0}, \quad \text{at } x_0 = -\ell \quad \text{and} \quad u^2_N = -\frac{x_N}{2k}e^{-kx_N}, \quad \text{at } x_N = \ell \,. \end{aligned} \tag{3.30}$$

When these boundary conditions for u^1 and u^2 are substituted in Equation (3.29), one can obtain two separate systems in u^1 and u^2:

$$Au^1 = b_1 \qquad \text{and} \qquad Au^2 = b_2 \tag{3.31}$$

with the same coefficient matrix A of size $(N-1)\times(N-1)$ given by

$$A = \begin{bmatrix} -(2+(kh)^2) & 1 & 0 & 0 & \cdots & 0 \\ 1 & -(2+(kh)^2) & 1 & 0 & \cdots & 0 \\ 0 & 1 & -(2+(kh)^2) & 1 & & \vdots \\ & & \ddots & \ddots & \ddots & 0 \\ \vdots & \ddots & & 1 & -(2+(kh)^2) & 1 \\ 0 & \cdots & & 0 & 1 & -(2+(kh)^2) \end{bmatrix}.$$

The unknown vectors u^1 and u^2 are of the size $(N-1)$ and ordered as

$$u^1 = \begin{bmatrix} u_1^1 & u_2^1 & u_3^1 & \cdots & u_{N-1}^1 \end{bmatrix}^T \quad \text{and} \quad u^2 = \begin{bmatrix} u_1^2 & u_2^2 & u_3^2 & \cdots & u_{N-1}^2 \end{bmatrix}^T$$

where the right-hand side vectors b_1 and b_2 of size $(N-1)$ are

$$b_1 = \begin{bmatrix} -\frac{x_0}{2k}e^{kx_0} & 0 & \cdots & 0 & -\frac{x_N}{2k}e^{kx_N} \end{bmatrix}^T, \quad b_2 = \begin{bmatrix} \frac{x_0}{2k}e^{-kx_0} & 0 & \cdots & 0 & \frac{x_N}{2k}e^{-kx_N} \end{bmatrix}^T.$$

3.1.2 Case II: Variably conducting plates with no-slip velocity condition: $c \neq 0$, $\alpha = 0$

The discretized system for this case with boundary conditions $\mp c\frac{dB}{dx} + B = 0$ and $V = 0$ is obtained from the system (3.22)

$$Au = \begin{bmatrix} A_1 & A_2 \\ A_3 & A_4 \end{bmatrix} u = b \tag{3.32}$$

by substituting $\alpha = 0$ only in the components of the matrices A_i, $i = 3, 4$. That is, these components become

$$a^3_{1,1} = -2he^{-kx_0}, \quad a^3_{1,2} = 0, \quad a^3_{N+1,N} = 0 \quad \text{and} \quad a^3_{N+1,N+1} = 2he^{-kx_N} \tag{3.33}$$

and

$$a^4_{1,1} = -2he^{kx_0}, \quad a^4_{1,2} = 0, \quad a^4_{N+1,N} = 0, \quad \text{and} \quad a^4_{N+1,N+1} = 2he^{kx_N}\ . \quad (3.34)$$

Then, the matrices A_3 and A_4 reduce to

$$A_3 = \begin{bmatrix} e^{-kx_0} & 0 & 0 & \cdots & 0 & 0 & 0 \\ 0 & 0 & 0 & \cdots & 0 & 0 & 0 \\ \vdots & & & & & & \vdots \\ 0 & 0 & 0 & \cdots & 0 & 0 & 0 \\ 0 & 0 & 0 & \cdots & 0 & 0 & e^{-kx_N} \end{bmatrix}$$

and

$$A_4 = \begin{bmatrix} e^{kx_0} & 0 & 0 & 0 & \cdots & 0 \\ 1 & -(2+(kh)^2) & 1 & 0 & \cdots & 0 \\ 0 & 1 & -(2+(kh)^2) & 1 & & \vdots \\ & & \ddots & \ddots & \ddots & 0 \\ \vdots & \ddots & & 1 & -(2+(kh)^2) & 1 \\ 0 & \cdots & & 0 & 0 & e^{kx_N} \end{bmatrix}.$$

3.1.3 Case III: Insulated plates with slip velocity condition: $c = 0$, $\alpha \neq 0$

The system of equations for this case with the boundary conditions $\mp\alpha\dfrac{dV}{dx} + V = 0$, $B = 0$ is produced again from the system (3.22)

$$Au = \begin{bmatrix} A_1 & A_2 \\ A_3 & A_4 \end{bmatrix} u = b \quad (3.35)$$

by substituting $c = 0$ only in the components of A_i, $i = 1, 2$, given in Equations (3.25) and (3.26). In other words, the corresponding components become

$$a^1_{1,1} = -2he^{-kx_0}, \quad a^1_{1,2} = 0, \quad a^1_{N+1,N} = 0 \quad \text{and} \quad a^1_{N+1,N+1} = 2he^{-kx_N} \tag{3.36}$$

and

$$a^2_{1,1} = 2he^{kx_0}, \quad a^2_{1,2} = 0, \quad a^2_{N+1,N} = 0 \quad \text{and} \quad a^2_{N+1,N+1} = -2he^{kx_N}\,. \tag{3.37}$$

Hence, the matrices A_1 and A_2 are reduced to

$$A_1 = \begin{bmatrix} e^{-kx_0} & 0 & 0 & 0 & \cdots & 0 \\ 1 & -(2+(kh)^2) & 1 & 0 & \cdots & 0 \\ 0 & 1 & -(2+(kh)^2) & 1 & & \vdots \\ & & \ddots & \ddots & \ddots & 0 \\ \vdots & \ddots & & 1 & -(2+(kh)^2) & 1 \\ 0 & \cdots & & 0 & 0 & e^{-kx_N} \end{bmatrix}.$$

and

$$A_2 = \begin{bmatrix} -e^{kx_0} & 0 & 0 & \cdots & 0 & 0 & 0 \\ 0 & 0 & 0 & \cdots & 0 & 0 & 0 \\ \vdots & & & & & & \vdots \\ 0 & 0 & 0 & \cdots & 0 & 0 & 0 \\ 0 & 0 & 0 & \cdots & 0 & 0 & -e^{kx_N} \end{bmatrix}.$$

Finally, the right-hand side vector b is obtained by substituting $c = 0$ in Equation (3.24) and it becomes

$$b = \begin{bmatrix} b_1 & 0 & 0 & \cdots & 0 & b_{N+1} & | & 0 & \cdots & 0 \end{bmatrix}^T$$

with $b_1 = \dfrac{x_0}{k}$ and $b_{N+1} = \dfrac{x_N}{k}$.

3.2 Application of the NFD method to one-dimensional MHD flow

It is well-known that the MHD flow equations become convection-dominated at high Hartmann numbers $M = 2k$, making them challenging to solve. One needs to employ a fine mesh for the term $kh = Mh/2$ (or $k^2h = M^2h/4$) to be sufficiently small in standard finite difference schemes to have numerical results that are reasonably accurate at high Hartmann numbers. This generates a large system of equations that is costly to compute. Therefore, it is crucial to construct a numerical scheme whose precision is independent of the value of the step size h.

In this regard, the present section is devoted to developing a new finite difference scheme that, like the one described in Section 2.2.1 for the one-dimensional Helmholtz equation, [4], exactly satisfies the MHD flow in the modified Helmholtz equation form in Section 3.2.1. In addition, in Section 3.2.2, a new finite difference formula is also developed using the same notion to approximate the derivative-type boundary conditions for the velocity and the induced magnetic field with no truncation error. In other words, the new finite difference scheme is constructed in such a way that the solutions to the related finite difference equations exactly satisfy the solutions to the one-dimensional MHD flow at both interior and boundary points of the computational domain. These new finite difference formulas which correspond to standard central finite differences for the second and the first-order derivatives are *one of the main contributions of the present thesis* for the solution of the differential equations in modified Helmholtz type equations with mixed boundary conditions.

3.2.1 Derivation of NFD method for one-dimensional modified Helmholtz equation

The governing equations to one-dimensional MHD flow in the form of modified Helmholtz equations are given in Equation (3.6):

$$\frac{d^2u^i}{dx^2} - k^2u^i = 0, \quad i = 1, 2, \qquad -\ell < x < \ell\,. \tag{3.38}$$

The idea of deriving NFD scheme for the Helmholtz equation in Section 2.2.1, [4], is employed here in order to construct an exact numerical finite difference scheme

involving no truncation error in the discretization of the second-order derivative term, $(u^i)'' = d^2u^i/dx^2$, in modified Helmholtz equation (3.38) ($\frac{d^2u^i}{dx^2} = k^2u^i$).

The new weighted finite difference formula for the approximation of $(u^i)''$ is obtained by replacing the coefficient 'two' of u^i_m in the standard central difference equation (3.11) by a weight w which eliminates the truncation error:

$$\begin{aligned} & |\frac{d^2u^i(x)}{dx^2} - \frac{u^i(x+h) - wu^i(x) + u^i(x-h)}{h^2}| \\ = \quad & |k^2u^i(x) - \frac{u^i(x+h) - wu^i(x) + u^i(x-h)}{h^2}|, \qquad i = 1, 2\,. \end{aligned} \tag{3.39}$$

To find w, the Taylor series expansions of $u^i(x-h)$ and $u^i(x+h)$ around x are added, which yields

$$u^i(x-h)+u^i(x+h) = 2[u^i(x)+\frac{h^2}{2!}\frac{d^2u^i(x)}{dx^2}+\frac{h^4}{4!}\frac{d^4u^i(x)}{dx^4}+...+\frac{h^{2n}}{(2n)!}\frac{d^{2n}u^i(x)}{dx^{2n}}+...]. \tag{3.40}$$

By iterating the modified Helmholtz equation $\frac{d^2u^i}{dx^2} = k^2u^i$, one can obtain the relation

$$\frac{d^{2n}u^i}{dx^{2n}}(x) = k^{2n}u^i(x), \qquad n = 1, 2, \ldots \tag{3.41}$$

and by imposing this relation in Equation (3.40) we have

$$\begin{aligned} u^i(x-h) + u^i(x+h) \quad &= \quad 2u^i(x)\underbrace{[1 + \frac{(kh)^2}{2!} + \frac{(kh)^4}{4!} + \cdots + \frac{(kh)^{2n}}{(2n)!} + \cdots]}_{\cosh(kh)} \\ &= \quad 2\cosh(kh)u^i(x)\,. \end{aligned} \tag{3.42}$$

Then, by substituting Equation (3.42) in Equation (3.39), the truncation error in the modified Helmholtz equation becomes

$$|k^2u^i(x) - \frac{2\cosh(kh) - w}{h^2}u^i(x)|, \qquad i = 1, 2 \tag{3.43}$$

which is vanished with the optimal choice of the weight w as

$$w = 2\cosh(kh) - (kh)^2\,. \tag{3.44}$$

Thus, when the NFD scheme is employed for the approximation of the modified Helmholtz equation (3.38), we have

$$u^i(x+h) - 2\cosh(kh)u^i(x) + u^i(x+h) = 0, \quad i = 1, 2, \quad -\ell < x < \ell \tag{3.45}$$

for which the discretized form can be written as

$$u^i_{m+1} - 2\cosh(kh)u^i_m + u^i_{m-1} = 0, \quad m = 0, 1, 2, \ldots, N, \quad i = 1, 2 \tag{3.46}$$

by using N-equal length subintervals over $-\ell < x < \ell$ with step size $h = 2\ell/N$. The computational nodes are obtained from $x_m = x_0 + mh$ with $x_0 = -\ell$ and $x_N = \ell$, and u^i_m denotes the finite difference approximation to $u^i(x)$ at the node $x = x_m$.

3.2.2 Derivation of NFD formulas for the mixed-type boundary conditions

It is aimed to apply the NFD method for the solution of the one-dimensional MHD flow problem under the most general mixed-type boundary conditions, ($\pm\alpha\, dV/dx + V = 0$ and $\pm c\, dB/dx + B = 0$ at $x = \pm\ell$), given in Equation (3.2) for the velocity and the induced magnetic field, respectively. Thus, it is required to construct new finite difference schemes so that the solution of the finite difference equations satisfies the solution of the modified Helmholtz equation exactly not only at the interior nodes but also at the boundary nodes. The new finite difference formula corresponding to the standard central difference formula for the second-order derivatives is derived and applied to discretize the modified Helmholtz equation in Section 3.2.1. Thus, in this section, we focus on the derivation of a new finite difference approximation for the mixed-type boundary conditions of which the general form is

$$\pm a\frac{du}{dx} + u = 0, \qquad \text{at } x = \pm\ell \tag{3.47}$$

where a is a non-zero constant. In this regard, the same strategy used at the interior points in Section 3.2.1, is employed so that the new finite difference formula approximating the first order derivative du/dx does not produce truncation errors at the boundary nodes. The standard central difference formula for the first-order derivative is (see Equation (2.15))

$$\frac{du}{dx} = \frac{u(x+h) - u(x-h)}{2h} \tag{3.48}$$

with the step size h in x-direction. This formula is of $\mathcal{O}(h^2)$. The truncation error is eliminated by subtracting the Taylor series expansions of $u(x+h)$ around the point x from the one of $u(x-h)$. Hence, we have

$$u(x+h) - u(x-h) = 2h\left[\frac{du(x)}{dx} + \frac{h^2}{3!}\frac{d^3u(x)}{dx^3} + \frac{h^4}{5!}\frac{d^5u(x)}{dx^5} + \cdots\right]. \tag{3.49}$$

Then, by iterating the boundary condition (3.47), $\dfrac{du}{dx} = \mp\dfrac{1}{a}u$, one can obtain the following relation

$$\frac{d^{2n-1}u}{dx^{2n-1}} = \left(\frac{1}{a}\right)^{2n-2}\frac{du}{dx}, \quad n = 1, 2, \dots \ . \tag{3.50}$$

Substitution of relation (3.50) in Equation (3.49) and the use of the series representation of $\sinh(x)$ result in

$$\begin{aligned}\frac{u(x+h)-u(x-h)}{2h} =& (1 + \frac{1}{3!}\frac{h^2}{a^2} + \frac{1}{5!}\frac{h^4}{a^4} + \cdots)\frac{du(x)}{dx} \\ =& \frac{a}{h}\underbrace{(\frac{h}{a} + \frac{1}{3!}\frac{h^3}{a^3} + \frac{1}{5!}\frac{h^3}{a^3} + \cdots)}_{\sinh(h/a)}\frac{du(x)}{dx}\ .\end{aligned} \tag{3.51}$$

The new finite difference formula for du/dx, which eliminates the truncation error in the standard central difference formula, is obtained by rewriting Equation (3.51) as:

$$\frac{du(x)}{dx} = \frac{h}{a\sinh(h/a)}\frac{u(x+h)-u(x-h)}{2h}\ . \tag{3.52}$$

Then, when the computational domain is discretized by using N-equal length subintervals with $h = 2\ell/N$, and the nodes are taken as $x_m = x_0 + mh$, $m = 1, \dots, N$ where $x_0 = -\ell$ and $x_N = \ell$, the difference equation of the boundary condition $-a\dfrac{du}{dx} + u = 0$ at the node $x_0 = -\ell$ becomes

$$-a\frac{h}{a\sinh(h/a)}\frac{u(x_0+h)-u(x_0-h)}{2h} + u(x_0) = 0, \tag{3.53}$$

and the difference equation of the boundary condition $a\dfrac{du}{dx}+u = 0$ at the node $x_N = \ell$ results in

$$a\frac{h}{a\sinh(h/a)}\frac{u(x_N+h)-u(x_N-h)}{2h} + u(x_N) = 0\ . \tag{3.54}$$

Equivalently, Equation (3.53) and Equation (3.54), respectively, yield

$$u_1 - 2\sinh(h/a)u_0 - u_{-1} = 0, \qquad \text{at } x = x_0 = -\ell \tag{3.55}$$

and

$$u_{N+1} + 2\sinh(h/a)u_N - u_{N-1} = 0, \qquad \text{at } x = x_N = \ell\ . \tag{3.56}$$

Since the boundary conditions (3.2) of the one-dimensional MHD flow problem for the velocity $V(x)$ ($\pm\alpha dV/dx + V = 0$) and for the induced magnetic field $B(x)$

($\pm cdB/dx + B = 0$) are in the same form with Equation (3.47), their discretized forms are also same with Equations (3.55)-(3.56) for the velocity as:

$$\begin{aligned} &V_1 - 2\sinh(h/\alpha)V_0 - V_{-1} = 0, && \text{at } x = x_0 = -\ell \\ &V_{N+1} + 2\sinh(h/\alpha)V_N - V_{N-1} = 0, && \text{at } x = x_N = \ell \end{aligned} \tag{3.57}$$

and for the induced magnetic field

$$\begin{aligned} &B_1 - 2\sinh(h/c)B_0 - B_{-1} = 0, && \text{at } x = x_0 = -\ell \\ &B_{N+1} + 2\sinh(h/c)B_N - B_{N-1} = 0, && \text{at } x = x_N = \ell \end{aligned} \tag{3.58}$$

where $V_m \approx V(x_m)$ and $B_m \approx B(x_m)$ when $m = 0, N$.

Finally, by the use of backward substitutions (3.10) for V in Equation (3.57) and for B in Equation (3.58), the new finite difference equations in terms of new variables u^1 and u^2 at the boundaries $x = \pm\ell$ are obtained. Thus, the velocity boundary conditions become

$$\begin{aligned} &(u_1^1 e^{-kx_1} + u_1^2 e^{kx_1}) - 2\sinh(\frac{h}{\alpha})(u_0^1 e^{-kx_0} + u_0^2 e^{kx_0}) \\ &\qquad - (u_{-1}^1 e^{-kx_{-1}} + u_{-1}^2 e^{kx_{-1}}) = 0 \quad \text{at } x = x_0 = -\ell \\ &(u_{N+1}^1 e^{-kx_{N+1}} + u_{N+1}^2 e^{kx_{N+1}}) + 2\sinh(\frac{h}{\alpha})\left(u_N^1 e^{-kx_N} + u_N^2 e^{kx_N}\right) \\ &\qquad - (u_{N-1}^1 e^{-kx_{N-1}} + u_{N-1}^2 e^{kx_{N-1}}) = 0 \quad \text{at } x = x_N = \ell \end{aligned} \tag{3.59}$$

and for the induced magnetic field we have

$$\begin{aligned} &(u_1^1 e^{-kx_1} - u_1^2 e^{kx_1}) - 2\sinh(\frac{h}{c})\left(u_0^1 e^{-kx_0} - u_0^2 e^{kx_0} - \frac{x_0}{k}\right) \\ &- (u_{-1}^1 e^{-kx_{-1}} - u_{-1}^2 e^{kx_{-1}}) + \frac{1}{k}(x_{-1} - x_1) = 0 \quad \text{at } x = x_0 = -\ell \\ &(u_{N+1}^1 e^{-kx_{N+1}} - u_{N+1}^2 e^{kx_{N+1}}) + 2\sinh(\frac{h}{c})\left(u_N^1 e^{-kx_N} - u_N^2 e^{kx_N} - \frac{x_N}{k}\right) \\ &- (u_{N-1}^1 e^{-kx_{N-1}} - u_{N-1}^2 e^{kx_{N-1}}) + \frac{1}{k}(x_{N-1} - x_{N+1}) = 0 \quad \text{at } x = x_N = \ell. \end{aligned} \tag{3.60}$$

Since we use the new finite difference method derived from the standard central difference method for the derivative boundary conditions, we have ghost points u_{-1}^i and u_{N+1}^i with $i = 1, 2$. To eliminate them in Equations (3.59) and (3.60), we use the new finite difference formula (3.46) with $m = 0$ and $m = N$, that is $u_{-1}^i = 2\cosh(kh)u_0^i - u_1^i$ and $u_{N+1}^i = 2\cosh(kh)u_N^i - u_{N-1}^i$ at $i = 1, 2$. After

the substitution of these into Equations (3.59) and (3.60), the finite difference equations for the velocity become

$$\begin{aligned}
&(-2\cosh(kh)e^{-kx_{-1}} - 2\sinh(\frac{h}{\alpha})e^{-kx_0})u_0^1 + (e^{-kx_{-1}} + e^{-kx_1})u_1^1 \\
&+(-2\cosh(kh)e^{kx_{-1}} - 2\sinh(\frac{h}{\alpha})e^{kx_0})u_0^2 + (e^{kx_{-1}} + e^{kx_1})u_1^2 = 0, \quad \text{at } x = -\ell \\
&(2\cosh(kh)e^{-kx_{N+1}} + 2\sinh(\frac{h}{\alpha})e^{-kx_N})u_N^1 + (-e^{-kx_{N-1}} + e^{-kx_{N+1}})u_{N-1}^1 \\
&+(2\cosh(kh)e^{kx_{N+1}} + 2\sinh(\frac{h}{\alpha})e^{kx_N})u_N^2 \\
&\qquad + (-e^{kx_{N-1}} - e^{kx_{N+1}})u_{N-1}^2 = 0, \quad \text{at } x = \ell
\end{aligned} \tag{3.61}$$

and for the induced magnetic field, we have

$$\begin{aligned}
&(-2\cosh(kh)e^{-kx_{-1}} - 2\sinh(\frac{h}{c})e^{-kx_0})u_0^1 + (e^{-kx_{-1}} + e^{-kx_1})u_1^1 \\
&+(2\cosh(kh)e^{kx_{-1}} + 2\sinh(\frac{h}{c})e^{kx_0})u_0^2 + (-e^{kx_{-1}} - e^{kx_1})u_1^2 \\
&\qquad = \frac{1}{k}(x_1 - 2\sinh(\frac{h}{c})x_0 - x_{-1}), \qquad \text{at } x = -\ell \\
&(2\cosh(kh)e^{-kx_{N+1}} + 2\sinh(\frac{h}{c})e^{-kx_N})u_N^1 + (-e^{-kx_{N-1}} - e^{-kx_{N+1}})u_{N-1}^1 \\
&+(-2\cosh(kh)e^{kx_{N+1}} - 2\sinh(\frac{h}{c})e^{kx_N})u_N^2 + (e^{kx_{N-1}} + e^{kx_{N+1}})u_{N-1}^2 \\
&\qquad = \frac{1}{k}(x_{N+1} + 2\sinh(\frac{h}{c})x_N - x_{N-1}), \qquad \text{at } x = \ell\,.
\end{aligned} \tag{3.62}$$

Finally, the new finite difference scheme for interior points become

$$u_{m+1}^i - 2\cosh(kh)u_m^i + u_{m-1}^i = 0, \qquad m = 1, 2, ..., N-1, \quad i = 1, 2\,. \tag{3.63}$$

3.2.3 The matrix-vector form of the NFD equations under various boundary conditions

Once the conditions (3.61) and (3.62), which are coupled in u^1 and u^2 and corresponding to Case IV, are inserted in the difference equation (3.63), we end up with a system of linear equations

$$Cu = d\,. \tag{3.64}$$

Here, the unknown vector u of size $(2N+2)$ has the ordering as

$$u = \begin{bmatrix} u_0^1 & u_1^1 & u_2^1 & \cdots & u_N^1 & | & u_0^2 & u_1^2 & u_2^2 & \cdots & u_N^2 \end{bmatrix}^T \tag{3.65}$$

and the right hand side vector of size $(2N+2)$ is

$$d = \begin{bmatrix} d_1 & 0 & 0 & \cdots & 0 & d_{N+1} & | & 0 & \cdots & 0 \end{bmatrix}^T \tag{3.66}$$

where

$$d_1 = \frac{x_1}{k} - 2\sinh\left(\frac{h}{c}\right)\frac{x_0}{k} - \frac{x_{-1}}{k} \quad \text{and} \quad d_{N+1} = \frac{x_{N+1}}{k} + 2\sinh\left(\frac{h}{c}\right)\frac{x_N}{k} - \frac{x_{N-1}}{k}. \tag{3.67}$$

The coefficient matrix C of size $(2N+2)\times(2N+2)$ can be written in terms of block matrices C_i, $i = 1,2,3,4$ of sizes $(N+1)\times(N+1)$ as follows:

$$C = \begin{bmatrix} C_1 & C_2 \\ C_3 & C_4 \end{bmatrix}. \tag{3.68}$$

Here, C_1 is equal to

$$C_1 = \begin{bmatrix} c_{1,1}^1 & c_{1,2}^1 & 0 & 0 & \cdots & 0 \\ 1 & -2\cosh(hk) & 1 & 0 & \cdots & 0 \\ 0 & 1 & -2\cosh(hk) & 1 & & \vdots \\ & & \ddots & \ddots & \ddots & 0 \\ \vdots & \ddots & & 1 & -2\cosh(hk) & 1 \\ 0 & \cdots & & 0 & c_{N+1,N}^1 & c_{N+1,N+1}^1 \end{bmatrix} \tag{3.69}$$

with the components

$$\begin{aligned} &c_{1,1}^1 = -2\cosh(hk)e^{-kx_{-1}} - 2\sinh(\frac{h}{c})e^{-kx_0}, \qquad c_{1,2}^1 = e^{-kx_1} + e^{-kx_{-1}}, \\ &c_{N+1,N+1}^1 = 2\cosh(hk)e^{-kx_{N+1}} + 2\sinh(\frac{h}{c})e^{-kx_N}, \; c_{N+1,N}^1 = -e^{-kx_{N+1}} - e^{-kx_{N-1}}, \end{aligned} \tag{3.70}$$

and

$$C_2 = \begin{bmatrix} c^2_{1,1} & c^2_{1,2} & 0 & \cdots & 0 & 0 & 0 \\ 0 & 0 & 0 & \cdots & 0 & 0 & 0 \\ \vdots & & & & & & \vdots \\ 0 & 0 & 0 & \cdots & 0 & 0 & 0 \\ 0 & 0 & 0 & \cdots & 0 & c^2_{N+1,N} & c^2_{N+1,N+1} \end{bmatrix} \tag{3.71}$$

with the components

$$\begin{aligned} c^2_{1,1} &= 2\cosh(hk)e^{kx_{-1}} + 2\sinh(\frac{h}{c})e^{kx_0}, & c^2_{1,2} &= -e^{kx_1} - e^{kx_{-1}}, \\ c^2_{N+1,N+1} &= -2\cosh(hk)e^{kx_{N+1}} - 2\sinh(\frac{h}{c})e^{kx_N}, & c^2_{N+1,N} &= e^{kx_{N+1}} + e^{kx_{N-1}}, \end{aligned} \tag{3.72}$$

and

$$C_3 = \begin{bmatrix} c^3_{1,1} & c^3_{1,2} & 0 & \cdots & 0 & 0 & 0 \\ 0 & 0 & 0 & \cdots & 0 & 0 & 0 \\ \vdots & & & & & & \vdots \\ 0 & 0 & 0 & \cdots & 0 & 0 & 0 \\ 0 & 0 & 0 & \cdots & 0 & c^3_{N+1,N} & c^3_{N+1,N+1} \end{bmatrix} \tag{3.73}$$

with the entries

$$\begin{aligned} c^3_{1,1} &= -2\cosh(hk)e^{-kx_{-1}} - 2\sinh(\frac{h}{\alpha})e^{-kx_0}, & c^3_{1,2} &= e^{-kx_1} + e^{-kx_{-1}}, \\ c^3_{N+1,N+1} &= 2\cosh(hk)e^{-kx_{N+1}} + 2\sinh(\frac{h}{\alpha})e^{-kx_N}, & c^3_{N+1,N} &= -e^{-kx_{N+1}} - e^{-kx_{N-1}} \end{aligned} \tag{3.74}$$

and, finally,

$$C_4 = \begin{bmatrix} c^4_{1,1} & c^4_{1,2} & 0 & 0 & \cdots & 0 \\ 1 & -2\cosh(hk) & 1 & 0 & \cdots & 0 \\ 0 & 1 & -2\cosh(hk) & 1 & & \vdots \\ & & \ddots & \ddots & \ddots & 0 \\ \vdots & \ddots & & 1 & -2\cosh(hk) & 1 \\ 0 & \cdots & & 0 & c^4_{N+1,N} & c^4_{N+1,N+1} \end{bmatrix} \tag{3.75}$$

where

$$c^4_{1,1} = -2\cosh(hk)e^{kx_{-1}} - 2\sinh(\frac{h}{\alpha})e^{kx_0}, \qquad c^4_{1,2} = e^{kx_1} + e^{kx_{-1}},$$
$$c^4_{N+1,N+1} = 2\cosh(hk)e^{kx_{N+1}} + 2\sinh(\frac{h}{\alpha})e^{kx_N}, \quad c^4_{N+1,N} = -e^{kx_{N+1}} - e^{kx_{N-1}}\ . \tag{3.76}$$

The solution of system (3.64), which is associated to Case IV, results in the values of u^1 and u^2 at the nodes x_m, $m = 0, 1, ..., N$. By using the back substitutions in Equation (3.10), the velocity and the induced magnetic field are obtained at discretized points. On the other hand, the resulting NFD systems of linear equations corresponding to other cases, namely Case I, Case II, Case III, are going to be determined separately from the scratch by taking either $\alpha = 0$ or $c = 0$ or both in the original boundary conditions (3.2), while in SFD method they are derived from the system (3.22), $Au = b$ (corresponding to Case IV) by inserting $\alpha = 0$, or $c = 0$, or both (see Section 3.1). This is because, the NFD formula for the approximation of the first-order derivative in the boundary conditions contains $\sinh(h/\alpha)$ and $\sinh(h/c)$ which are undefined for $\alpha = 0$, $c = 0$. As a result, the finite difference equations (3.61) and (3.62) for the mixed-type boundary conditions when $\alpha \neq 0$, $c \neq 0$ in Case IV also involve the terms $\sinh(h/\alpha)$ and $\sinh(h/c)$, respectively. Thus, one can not use these equations to reduce the system of linear equations associated to Case IV into other cases. Instead, as mentioned above, the NFD equations for the boundary conditions in u^1 and u^2 are obtained by inserting $\alpha = 0$ and /or $c = 0$ in the original form of the

boundary conditions (3.2) given in terms of V and B. The systems of linear equations for Case I, Case II, and Case III are going to be given in the subsequent sections.

3.2.3.1 Case I: Insulated plates with no-slip velocity condition: $\alpha = c = 0$

As it is mentioned in the application of SFD method for Case I (see Section 3.1.1), the boundary conditions for $\alpha = c = 0$ are decoupled in u^1 and u^2, which enables one to write two decoupled systems of size $(N-1) \times (N-1)$ for the unknowns u^1 and u^2. That is, the new finite difference equations for the modified Helmholtz equations (3.6) at the interior points are given in Equation (3.63) as

$$u^i_{m+1} - 2\cosh(kh)u^i_m + u^i_{m-1} = 0, \qquad m = 1, 2, ..., N-1, \quad i = 1, 2 \tag{3.77}$$

with the boundary conditions

$$\begin{aligned} u^1_0 &= \frac{x_0}{2k}e^{kx_0}, \quad \text{at } x_0 = -\ell \quad \text{and} \quad u^1_N = \frac{x_N}{2k}e^{kx_N}, \quad \text{at } x_N = \ell \\ u^2_0 &= -\frac{x_0}{2k}e^{-kx_0}, \quad \text{at } x_0 = -\ell \quad \text{and} \quad u^2_N = -\frac{x_N}{2k}e^{-kx_N}, \quad \text{at } x_N = \ell\,. \end{aligned} \tag{3.78}$$

The insertion of these boundary conditions into Equation (3.77) results in the following systems of linear equations in u^1 and u^2:

$$Cu^1 = d_1 \quad \text{and} \quad Cu^2 = d_2 \tag{3.79}$$

with the coefficient matrix C of size $(N-1) \times (N-1)$ which is given by

$$C = \begin{bmatrix} -2\cosh(hk) & 1 & 0 & 0 & \cdots & 0 \\ 1 & -2\cosh(hk) & 1 & 0 & \cdots & 0 \\ 0 & 1 & -2\cosh(hk) & 1 & & \vdots \\ & & \ddots & \ddots & \ddots & 0 \\ \vdots & \ddots & & 1 & -2\cosh(hk) & 1 \\ 0 & \cdots & & 0 & 1 & -2\cosh(hk) \end{bmatrix}$$

when the unknowns u^1 and u^2 are ordered as

$$u^1 = \begin{bmatrix} u^1_1 & u^1_2 & u^1_3 & \cdots & u^1_{N-1} \end{bmatrix}^T \quad \text{and} \quad u^2 = \begin{bmatrix} u^2_1 & u^2_2 & u^2_3 & \cdots & u^2_{N-1} \end{bmatrix}^T . \tag{3.80}$$

In this case, the right-hand side vectors d_1 and d_2 of sizes $(N-1)$ are the same with the vectors b_1 and b_2 obtained from the application of SFD in Section 3.1.1. That is,

$$\mathrm{d}_1 = \left[-\frac{x_0}{2k}e^{kx_0} \quad 0 \quad \cdots \quad 0 \quad -\frac{x_N}{2k}e^{kx_N}\right]^T, \;\; d_2 = \left[\frac{x_0}{2k}e^{-kx_0} \quad 0 \quad \cdots \quad 0 \quad \frac{x_N}{2k}e^{-kx_N}\right]^T. \tag{3.81}$$

3.2.3.2 Case II: Variably conducting plates with no-slip velocity condition: $c \neq 0$, $\alpha = 0$

In this case, the boundary conditions for the velocity ($V = 0$ at $x = \pm\ell$) are

$$\begin{aligned} u_0^1 e^{-kx_0} + u_0^2 e^{kx_0} &= 0 \quad \text{at } x = x_0 = -\ell \\ u_N^1 e^{-kx_N} + u_N^2 e^{kx_N} &= 0 \quad \text{at } x = x_N = \ell \end{aligned} \tag{3.82}$$

and for the boundary conditions of the induced magnetic field ($\pm c\dfrac{dB}{dx} + B = 0$ at $x = \pm\ell$), the new finite difference equations are given in Equation (3.62) as

$$\begin{aligned} (-2\cosh(kh)e^{-kx_{-1}} - 2\sinh(\frac{h}{c})e^{-kx_0})u_0^1 + (e^{-kx_{-1}} + e^{-kx_1})u_1^1 \\ +(2\cosh(kh)e^{kx_{-1}} + 2\sinh(\frac{h}{c})u_0^2 + (-e^{kx_{-1}} - e^{kx_1})u_1^2 \\ = \frac{1}{k}(x_1 - 2\sinh(\frac{h}{c})x_0 - x_{-1}), \qquad \text{at } x = -\ell \end{aligned}$$

$$\begin{aligned} (2\cosh(kh)e^{-kx_{N+1}} + 2\sinh(\frac{h}{c})e^{-kx_N})u_N^1 + (-e^{-kx_{N-1}} - e^{-kx_{N+1}})u_{N-1}^1 \\ +(-2\cosh(kh)e^{kx_{N+1}} - 2\sinh(\frac{h}{c})e^{kx_N})u_N^2 + (e^{kx_{N-1}} + e^{kx_{N+1}})u_{N-1}^2 \\ = \frac{1}{k}(x_{N+1} + 2\sinh(\frac{h}{c})x_N - x_{N-1}), \qquad \text{at } x = \ell\,. \end{aligned} \tag{3.83}$$

The insertion of these boundary conditions in the NFD equation (3.63) results in a system of equations $Cu = d$ of size $(2N+2) \times (2N+2)$ which is similar to the system (3.64). That is, the resulting coefficient matrix

$$C = \begin{bmatrix} C_1 & C_2 \\ C_3 & C_4 \end{bmatrix} \tag{3.84}$$

is in the same form with the coefficient matrix C given in Equation (4.72) and the right-hand side vector d is the same with the one given in Equations (3.66) and (3.67).

Moreover, the block matrices C_1 and C_2 in Equation (3.84) are totally same with the ones given in (4.72), since the same boundary conditions for B used in Case IV are employed in Case II as well. However, since the boundary conditions for velocity are taken as, $V = 0$, in Case II, which is different from Case IV, the matrices C_3 and C_4 are modified in Case II when compared to Case IV. That is, the block matrix C_3 of the size $(N+1) \times (N+1)$ becomes

$$C_3 = \begin{bmatrix} e^{-kx_0} & 0 & 0 & \cdots & 0 & 0 & 0 \\ 0 & 0 & 0 & \cdots & 0 & 0 & 0 \\ \vdots & & & & & & \vdots \\ 0 & 0 & 0 & \cdots & 0 & 0 & 0 \\ 0 & 0 & 0 & \cdots & 0 & 0 & e^{-kx_N} \end{bmatrix}$$

and the matrix C_4 of size $(N+1) \times (N+1)$ reduces to

$$C_4 = \begin{bmatrix} e^{kx_0} & 0 & 0 & 0 & \cdots & 0 \\ 1 & -2\cosh(hk) & 1 & 0 & \cdots & 0 \\ 0 & 1 & -2\cosh(hk) & 1 & & \vdots \\ & & \ddots & \ddots & \ddots & 0 \\ \vdots & \ddots & & 1 & -2\cosh(hk) & 1 \\ 0 & \cdots & & 0 & 0 & e^{kx_N} \end{bmatrix}.$$

3.2.3.3 Case III: Insulated plates with slip velocity condition: $c = 0$, $\alpha \neq 0$

The system of equations for this case with boundary conditions $\pm\alpha\dfrac{dV}{dx} + V = 0$, $B = 0$, can be written as

$$Cu = \begin{bmatrix} C_1 & C_2 \\ C_3 & C_4 \end{bmatrix} u = d \tag{3.85}$$

which is in the same form with system (3.64). Actually, the difference in system (3.64) and system (3.85) is the block matrices C_1 and C_2, and the right-hand side vector d, due to the application of the insulated boundary conditions for B (i.e $B = 0$) in Case III instead of the full mixed boundary conditions for B (i.e $\pm c\dfrac{dB}{dx} + B = 0$) employed in Case IV. Hence, the modified block matrices C_1 and C_2, which are of size $(N+1) \times (N+1)$, become

$$C_1 = \begin{bmatrix} e^{-kx_0} & 0 & 0 & 0 & \cdots & 0 \\ 1 & -2\cosh(hk) & 1 & 0 & \cdots & 0 \\ 0 & 1 & -2\cosh(hk) & 1 & & \vdots \\ & & \ddots & \ddots & \ddots & 0 \\ \vdots & \ddots & & 1 & -2\cosh(hk) & 1 \\ 0 & \cdots & & 0 & 0 & e^{-kx_N} \end{bmatrix}$$

and

$$C_2 = \begin{bmatrix} -e^{kx_0} & 0 & 0 & \cdots & 0 & 0 & 0 \\ 0 & 0 & 0 & \cdots & 0 & 0 & 0 \\ \vdots & & & & & & \vdots \\ 0 & 0 & 0 & \cdots & 0 & 0 & 0 \\ 0 & 0 & 0 & \cdots & 0 & & -e^{kx_N} \end{bmatrix}.$$

Finally, the right-hand side vector d can be written as

$$d = \begin{bmatrix} d_1 & 0 & 0 & \cdots & 0 & d_{N+1} & | & 0 & \cdots & 0 \end{bmatrix}^T \tag{3.86}$$

in which the components are reduced to

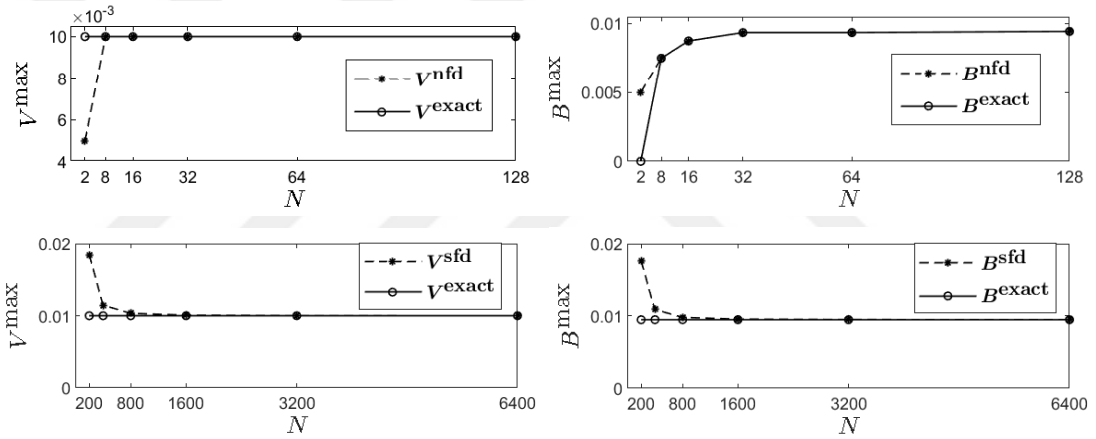
$$d_1 = \frac{x_0}{k} \quad \text{and} \quad d_{N+1} = \frac{x_N}{k} \, . \tag{3.87}$$

3.3 Numerical results for one-dimensional MHD flow problem

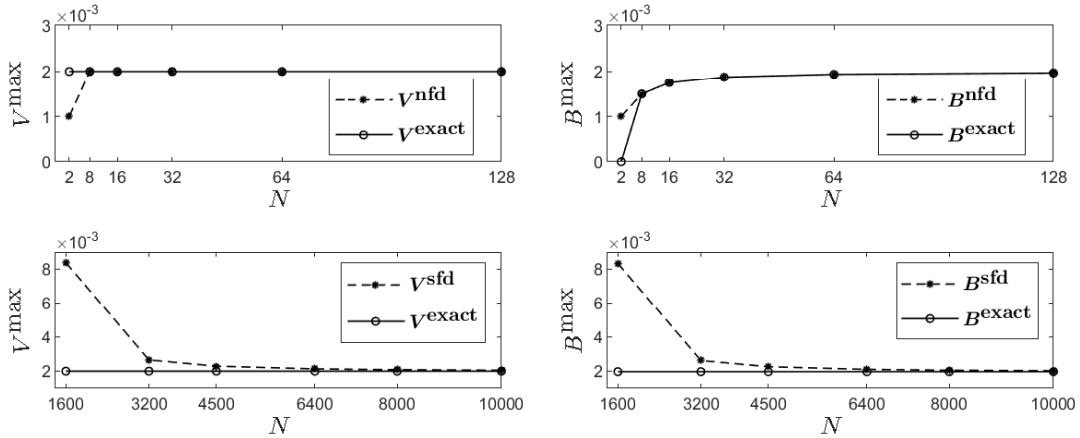
The one-dimensional MHD flow is investigated between infinitely long parallel plates with various types of boundary conditions including electrically insulated and variably conducting plates under no-slip or slip velocity conditions. The flow is driven by a constant pressure along the z-axis in the presence of a uniform constant magnetic field applied perpendicular to plates and parallel to the x-axis.

The numerical simulations with SFD and NFD are carried out from small to high values of the Hartmann number $5 \leq M = 2k \leq 500$ under various combinations of the plate conductivity c and slip length α in order to analyze their combined effects on the velocity and the induced magnetic field. Although the numerical solutions can be obtained for higher values of M up to $M = 700$, they are not visualized since the values of V and B get too small at high M which makes it hard to see the effects of the boundary conditions on the velocity and induced magnetic field distributions. The computational domain $(-\ell < x < \ell)$ is determined by taking $\ell = 1$ and it is discretized by an appropriate number of subintervals N. The choice of N is based on the grid independency tests performed by using different grid sizes for Case I: $\alpha = c = 0$ and Case IV: $\alpha = 0.2$, $c = 2$ at $M = 2k = 100$ and $M = 2k = 500$. The qualitative validation of the SFD and NFD results with the corresponding analytical ones obtained for different values of N are displayed, respectively, in Figure 3.2 for Case I and in Figure 3.3 for Case IV, in terms of the maximum velocity ($V^{\max}$) and the maximum induced magnetic field ($B^{\max}$) versus N. It is well-observed from Figure 3.2 that the accuracy of the NFD scheme, which admits no truncation error, does not depend on the grid size for any values of M in Case I. Thus, the choice of N is arbitrary so with even very small N, e.g. $N = 8$ which results in a large grid size h, one can get very accurate solutions. Case IV involves the most general

boundary conditions of mixed-type which must be discretized also by using finite differences. Thus, in this case, the NFD scheme needs a finer mesh compared to Case I as can be seen in Figure 3.3. That is, the NFD results agree with the exact ones only when $N \approx 650$ at $M = 100$ and $N \approx 1600$ at $M = 500$. On the other hand, the SFD scheme could generate a huge error, especially at high Hartmann number $M = 2k = 500$, when enough number of subintervals N is not taken in both Case I and Case IV. That is, the SFD scheme requires $N \approx 1600$ subintervals at $M = 100$ and a much finer mesh with $N > 6400$ subintervals at $M = 500$ in both Case I and Case IV. In fact, the SFD scheme is more sensitive to mesh size in Case IV at high $M = 500$ when compared to Case I. Thus, in the subsequent numerical computations with the NFD method, we use $N = 100$ subintervals in Case I, and for all the other cases involving mixed boundary conditions an adequate number of

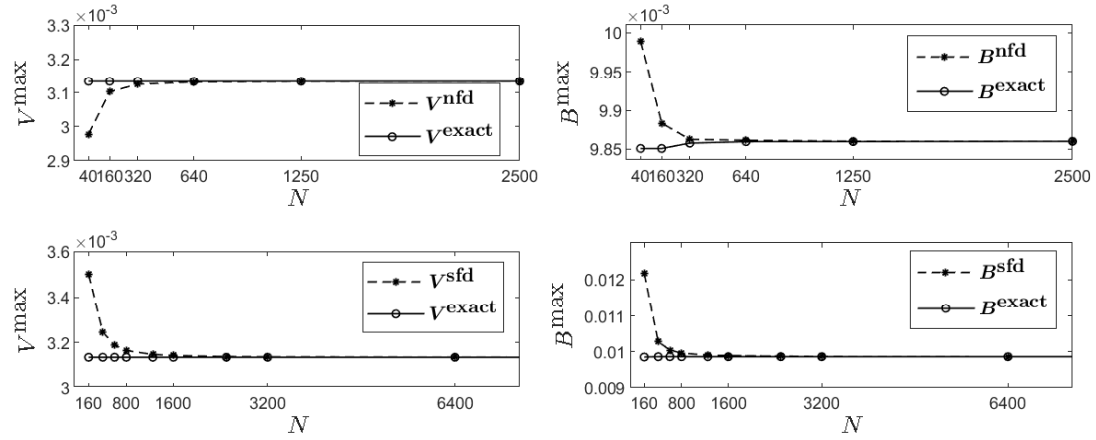


a) $M = 100$

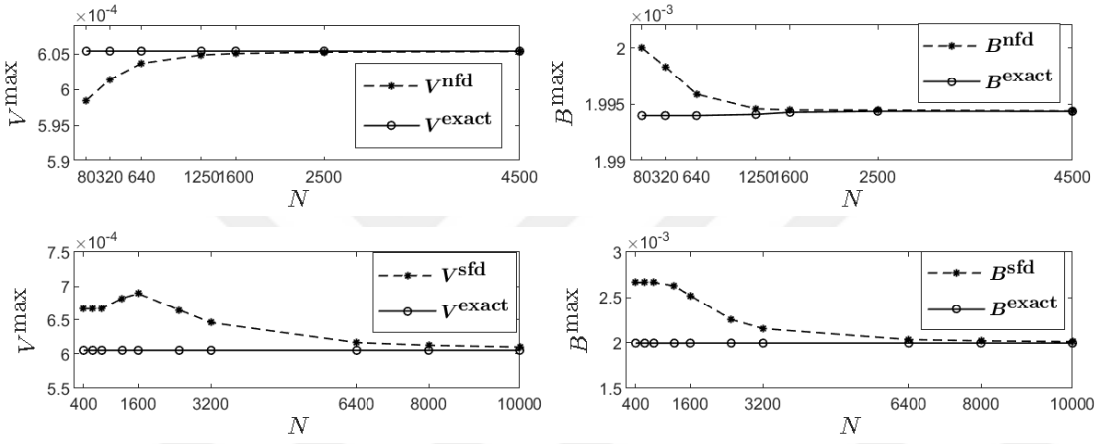


b) $M = 500$

Figure 3.2: Grid dependency test for Case I: $c = 0$, $\alpha = 0$.



a) $M = 100$



b) $M = 500$

Figure 3.3: Grid dependency test for Case IV: $c = 2$, $\alpha = 0.2$.

subintervals is used for increasing values of M ranging over $100 < M \leq 500$. In the SFD method, one can use also an adequate number of subintervals (e.g. $N \leq 1600$) for $M \leq 100$ in Case I, and for higher M and other cases, N is taken as accordingly in the range $1600 < N < 9000$. It is important to note here that for the case including only the slipping effect, namely Case III, one needs to use more number subintervals in both NFD and SFD schemes when compared to Case IV. This is due to the fact that the presence of both the slipping and conductive plates in Case IV results in a balance of their effects and the number of required subintervals is reduced which can be observed in the subsequent cases including Case III and Case IV.

On the other hand, a quantitative comparison of the finite difference results with the analytical solutions is performed by tabulating the relative errors in the velocity (e_V) and in the induced magnetic field (e_B) at various values of N in Table 3.1 when

$M = 100$ and in Table 3.2 when $M = 500$. The relative errors are defined by

$$e_{V^{\text{nfd}}} = \max_{1\le i\le N}\left|\frac{V_i^{\text{exact}} - V_i^{\text{nfd}}}{V_i^{\text{exact}}}\right| \quad \text{and} \quad e_{B^{\text{nfd}}} = \max_{1\le i\le N}\left|\frac{B_i^{\text{exact}} - B_i^{\text{nfd}}}{B_i^{\text{exact}}}\right|$$
$$e_{V^{\text{sfd}}} = \max_{1\le i\le N}\left|\frac{V_i^{\text{exact}} - V_i^{\text{sfd}}}{V_i^{\text{exact}}}\right| \quad \text{and} \quad e_{B^{\text{sfd}}} = \max_{1\le i\le N}\left|\frac{B_i^{\text{exact}} - B_i^{\text{sfd}}}{B_i^{\text{exact}}}\right| \tag{3.88}$$

where superscripts exact, nfd and sfd are the abbreviations for the analytical, new finite difference, and standard finite difference, respectively. These tables confirm the findings shown in Figures 3.2 and 3.3 that, regardless of the values M, a finer mesh is required to improve the SFD and NFD approximations in Case IV compared to Case I. Furthermore, it is noted that the NFD scheme achieves significantly more precise numerical results than the SFD scheme in each case. Actually, when the NFD approach is employed in Case I, the exact numerical solution is reached with no truncation error, meaning that even for coarse mesh $N = 100$, the relative error is around 10^{-15}. It is also observed that an increase in N at Case I yields an increase in relative errors in the NFD scheme although the NFD scheme remains no truncation error in finite difference approximations of the derivatives. This is because of the accumulation of round-off errors in the solution of the large-size systems resulting by the use of higher values of N. On the contrary, Case IV still performs pretty well, despite a drop in accuracy level in NFD scheme, with an error of approximately 10^{-4} for each M and $N = 1600$. The inclusion of derivative-type boundary conditions in Case IV, which must also be approximated by finite differences on the boundary points in addition to the discretization of the interior points, is the cause of this accuracy loss in Case IV. The SFD scheme, on the other hand, is sensitive to meshing and asks for higher resolutions than the NFD scheme in order to deliver reliable results with errors of around 10^{-2} in all cases.

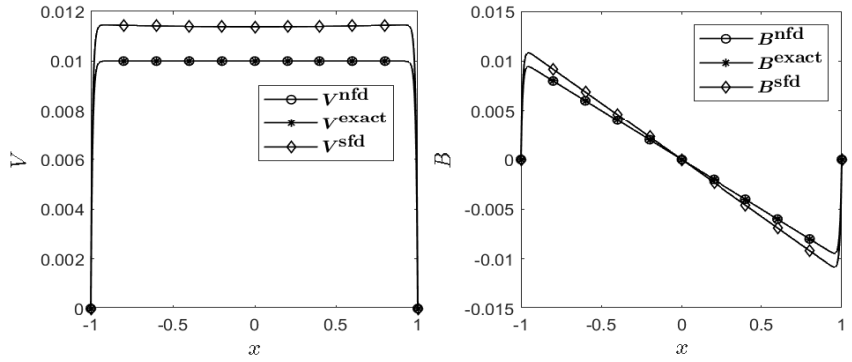
Table 3.1: Relative errors for SFD and NFD at $M = 100$ in Case I and Case IV

		Case I: $\alpha = c = 0$				Case IV: $\alpha = 0.2$, $c = 2$			
		SFD		NFD		SFD		NFD	
N	h	e_V	e_B	e_V	e_B	e_V	e_B	e_V	e_B
100	0.02	18.9969	20.0905	8.6736e-16	8.6581e-15	0.6651	0.3422	0.0208	0.0068
200	0.01	0.8496	0.8735	9.7145e-15	1.6368e-14	0.1120	0.1653	0.0068	0.0022
400	0.005	0.1461	0.1474	1.4287e-13	1.5107e-13	0.0367	0.0424	0.0018	6.0990e-04
800	0.0025	0.0335	0.0336	3.8389e-13	3.9385e-13	0.0096	0.0104	4.6573e-04	1.5577e-04
1600	0.0013	0.0082	0.0082	1.9446e-12	1.9934e-12	0.0024	0.0026	1.1703e-04	3.9153e-05
3200	6.25e-04	0.0020	0.0020	6.9094e-12	7.8150e-12	6.1004e-04	6.4991e-04	2.9295e-05	9.8015e-06
6400	3.125e-04	5.0884e-4	5.0863e-4	3.6451e-11	3.7344e-11	1.5265e-04	1.6167e-04	7.3262e-06	2.4512e-06

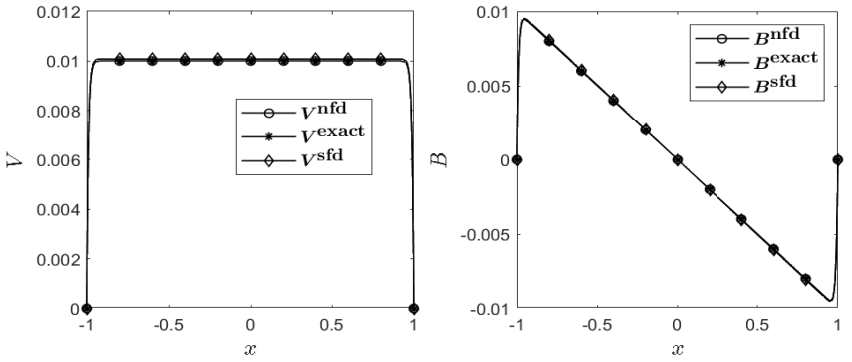
Table 3.2: Relative errors for SFD and NFD at $M = 500$ in Case I and Case IV

		Case I: $\alpha = c = 0$				Case IV: $\alpha = 0.2$, $c = 2$			
		SFD		NFD		SFD		NFD	
N	h	e_V	e_B	e_V	e_B	e_V	e_B	e_V	e_B
200	0.01	4.7668e+34	4.8480e+34	4.3368e-15	3.6167e-14	5.0027e+17	1.5188e+17	0.0087	0.0028
400	0.005	5.5572e+11	5.6450e+11	2.2226e-14	5.1212e-14	1.0000	0.3373	0.0053	0.0018
800	0.0025	1.1645e+03	1.1815e+03	1.1926e-14	4.0483e-14	0.9548	0.3373	0.0020	6.5986e-04
1600	0.0013	3.1941	3.2280	2.1749e-13	2.4829e-13	0.2622	0.2646	5.6065e-04	1.8694e-04
3200	6.25e-04	0.3289	0.3302	1.1130e-12	1.17370e-12	0.0675	0.0803	1.4486e-04	4.8318e-05
6400	3.125e-04	0.0677	0.0677	3.4547e-12	3.4806e-12	0.0187	0.0196	3.6521e-05	1.2182e-05
8000	2.5e-04	0.0423	0.0424	1.0597e-11	1.0677e-11	0.0121	0.0125	2.3397e-05	7.8047e-06
10000	2.0e-04	0.0267	0.0267	8.5392e-12	8.5918e-12	0.0078	0.0079	1.4984e-05	4.9983e-06

The velocity and induced magnetic field profiles are drawn along the computational interval ($-1 \leq x \leq 1$) in Figures 3.4 to 3.7 for $M = 100$ to validate the numerical results obtained by the standard and new finite differences against the analytical

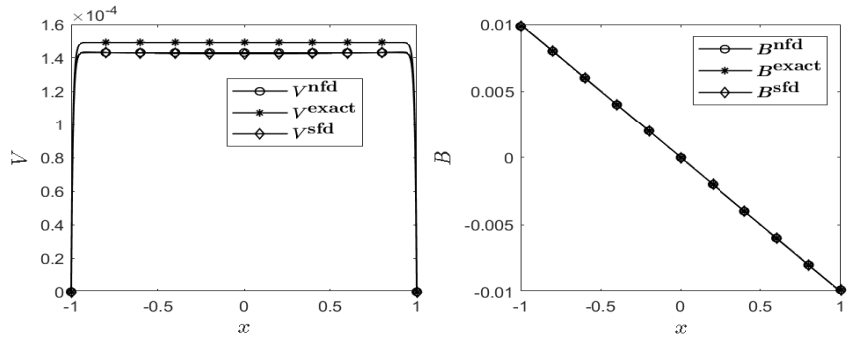


$a) N = 400$

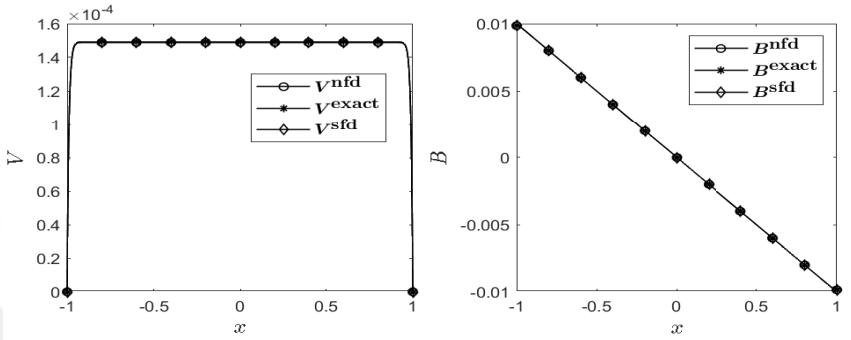


$b) N = 1600$

Figure 3.4: Case I: Comparison of NFD and SFD with the exact solution, $M = 100$, $c = 0$, $\alpha = 0$.

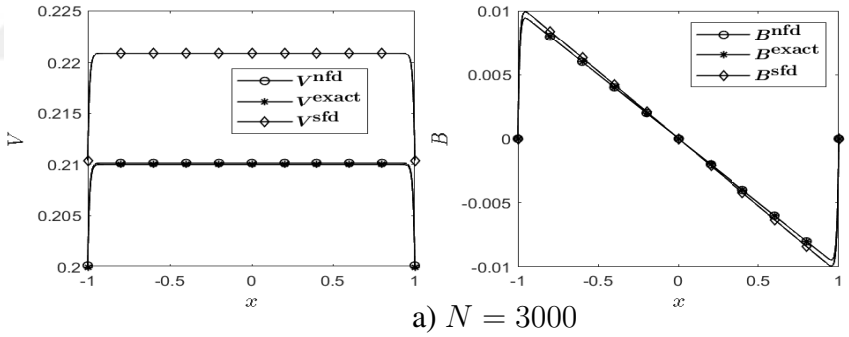


$a) N = 400$

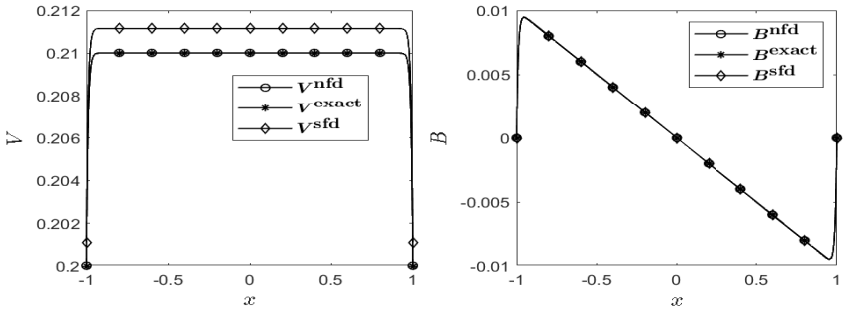


$b) N = 1600$

Figure 3.5: Case II: Comparison of NFD and SFD with the exact solution, $M = 100$, $c = 2$, $\alpha = 0$.

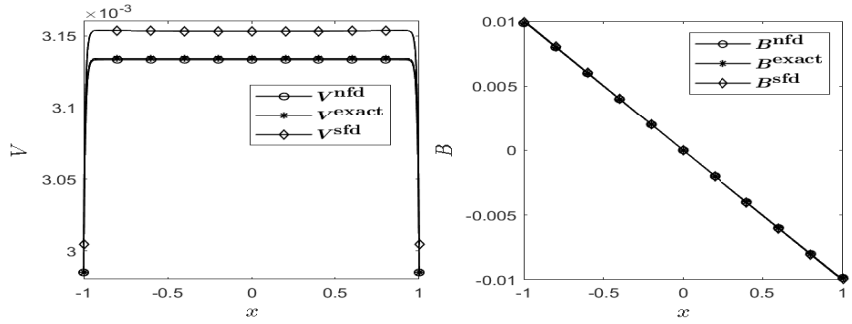


a) $N = 3000$

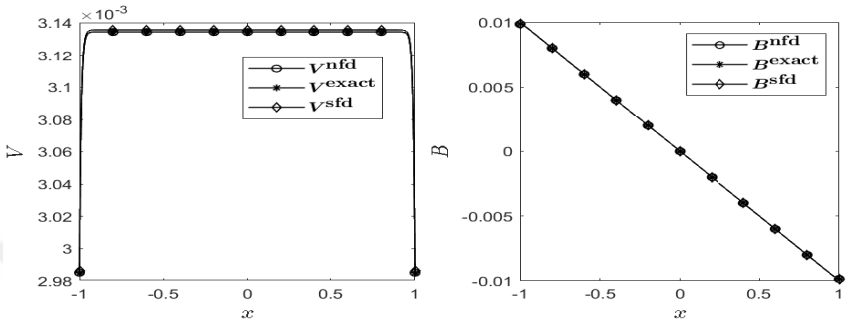


b) $N = 9000$

Figure 3.6: Case III: Comparison of NFD and SFD with the exact solution, $M = 100$, $c = 0$, $\alpha = 0.2$.



a) $N = 1000$



b) $N = 4000$

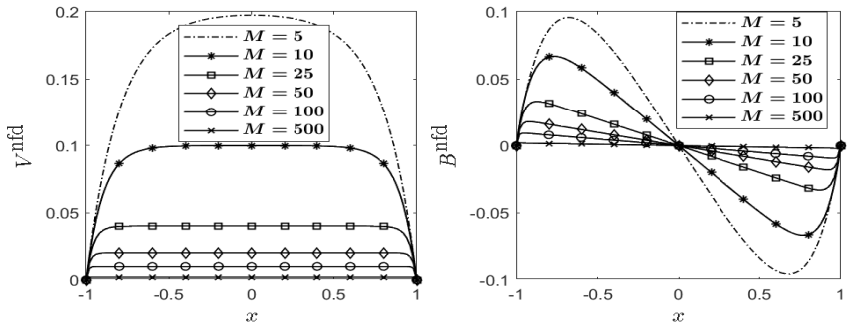
Figure 3.7: Case IV: Comparison of NFD and SFD with the exact solution, $M = 100$, $c = 2$, $\alpha = 0.2$.

solutions (3.3) and (3.4) of the Hartmann flow in each case. Even with a coarse mesh, the NFD solutions consistently agree with the analytical solutions far more than the SFD solutions. As seen in Figure 3.6, a finer mesh with a greater N must be used in SFD when the plates are slippery ($\alpha \neq 0$). In addition, the slipping velocity conditions require more subintervals (N) than the variably conducting boundary conditions, as observed in Figures 3.5 and 3.6. On the other hand, when the plates are both slippery and electrically conducting ($\alpha \neq 0$, $c \neq 0$), the required number of subintervals decreases because both conditions balance their effects on the MHD flow, as can be seen in Figure 3.7.

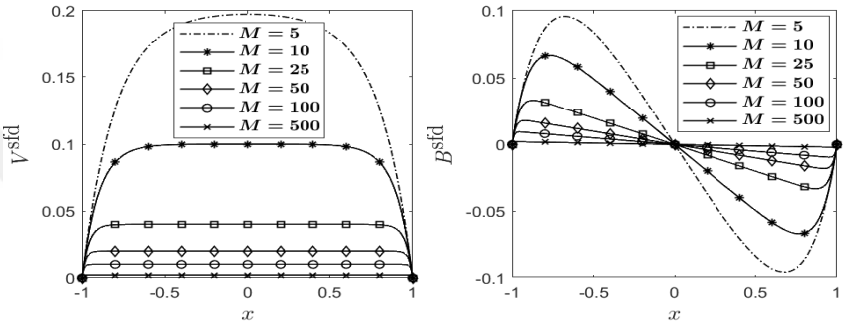
- **Case I:** $\alpha = c = 0$; no-slip and electrically insulated plates

Figure 3.8 displays the variations of the velocity and the induced magnetic field obtained by the NFD and the SFD schemes for increasing values of M ($5 \leq M \leq 500$). An increase in M results in a decrease in the magnitude of both the velocity and the induced magnetic. This is the well-known flattening tendency of the MHD flow that occurs when the intensity of the externally applied magnetic field is increased by larger values of M. As previously indicated, a finer mesh ($N = 1600$ for $5 \leq M \leq 100$ and

$N = 8000$ when $M = 500$) is utilized in the SFD approach to provide fairly precise approximations for V and B, whereas a relatively coarse mesh with $N = 100$ is used in the NFD scheme.



a) NFD, $N = 100$

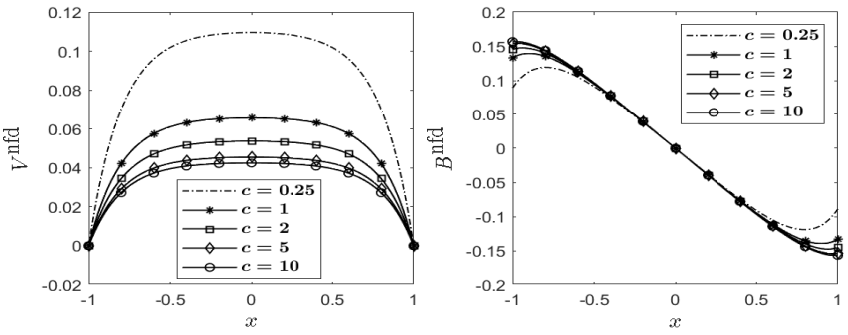


b) SFD, $N = 1600$ for $0 \leq M \leq 100$, and $N = 8000$ for $M = 500$

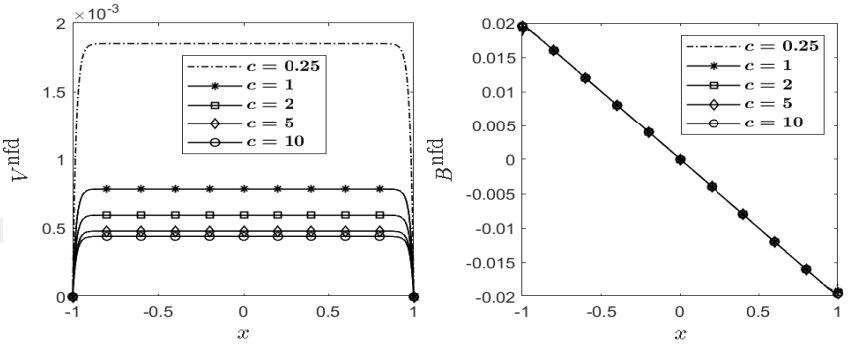
Figure 3.8: Case I: Effect of M on the velocity and induced magnetic field, $c = 0$, $\alpha = 0$.

- **Case II:** $\alpha = 0$, $c = 0.25 - 10$; no-slip and variably conducting plates

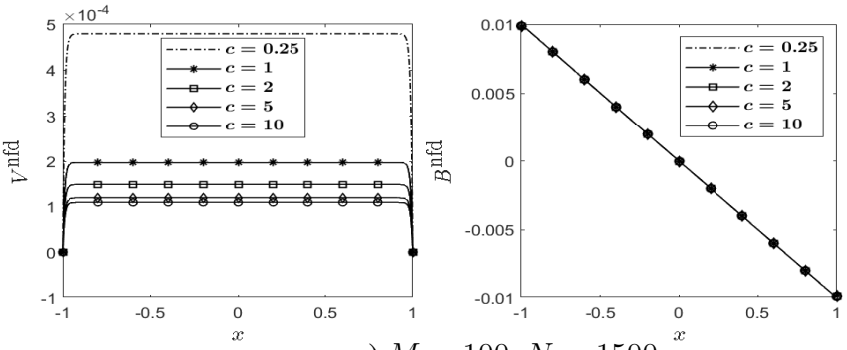
Figure 3.9 illustrates the influence of the conductivity parameter ($0.25 \leq c \leq 10$, which lies between being insulated and perfectly conducting) on the fluctuation of the velocity and the induced magnetic field along $-1 \leq x \leq 1$ for $M = 5$, 50, 100, and 500. We only display the NFD solutions in this case because, even for coarse mesh, the NFD scheme provides more accurate results than those obtained by the SFD method. Regardless of the values of M, the flow velocity decreases as c rises, and the rate of decrease becomes more noticeable at the center of the computational interval. As M ascends from 5 to 500, the magnetic field's retarding impact on the fluid velocity as in Case I is clearly seen. On the other hand, for small $M = 5$, the induced magnetic field grows with rising c at the endpoints $x = \pm 1$, but at larger values of M, the intensity of the magnetic field dampens the influence of the conductivity parameter c after a reduction in the magnitude of B.



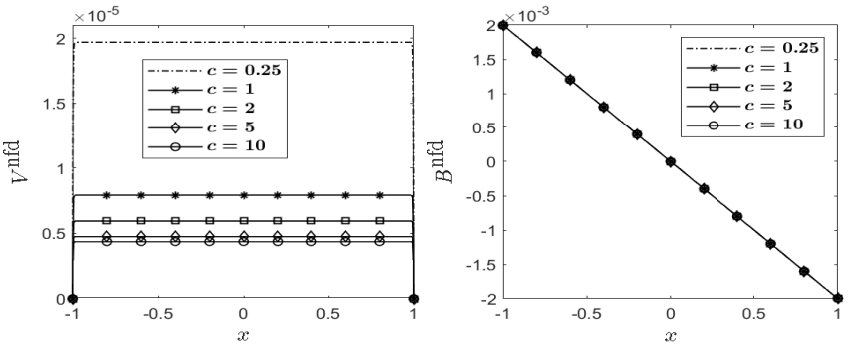
a) $M = 5$, $N = 100$



b) $M = 50$, $N = 1000$



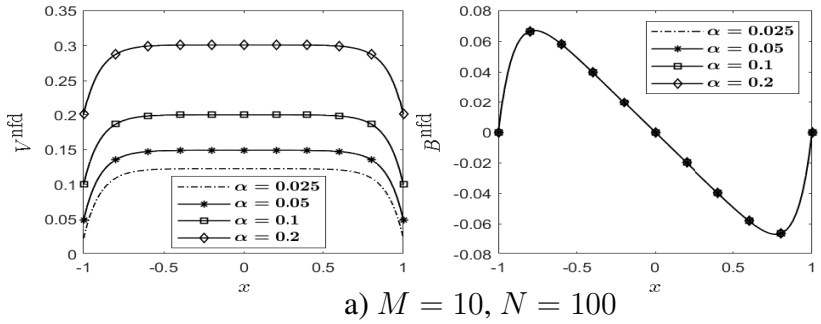
c) $M = 100$, $N = 1500$



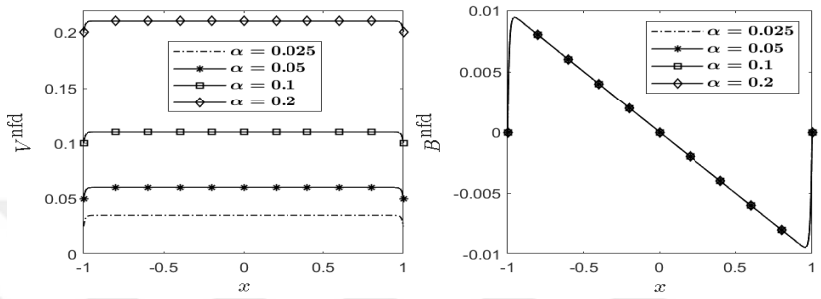
d) $M = 500$, $N = 4500$

Figure 3.9: Case II: Effect of c on the velocity and induced magnetic field with NFD, $\alpha = 0$.

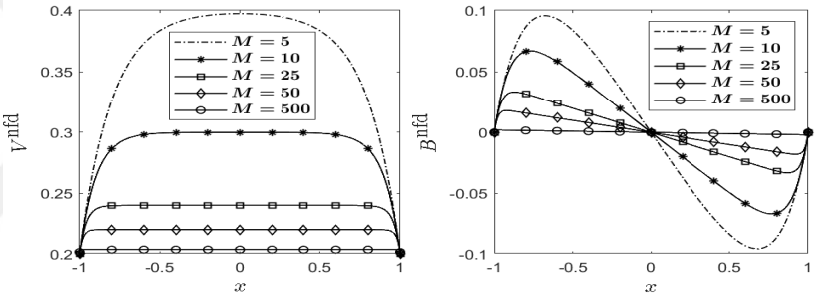
- **Case III:** $\alpha = 0.025 - 0.2$, $c = 0$; the slip velocity and insulated plates



a) $M = 10$, $N = 100$



b) $M = 100$, $N = 1500$

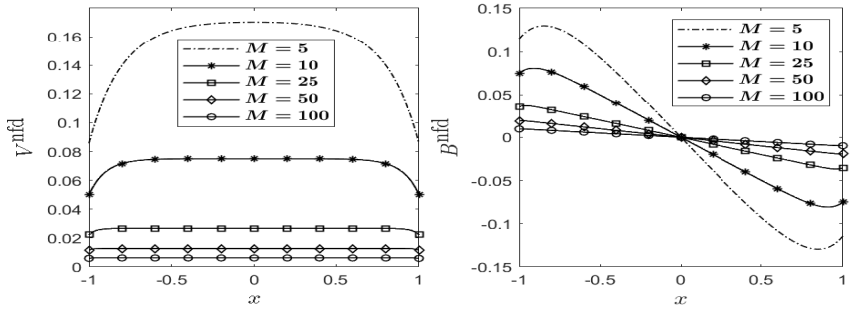


c) $\alpha = 0.2$, $N = 4500$ when $5 \leq M \leq 50$ and $N = 4500$ when $M = 500$

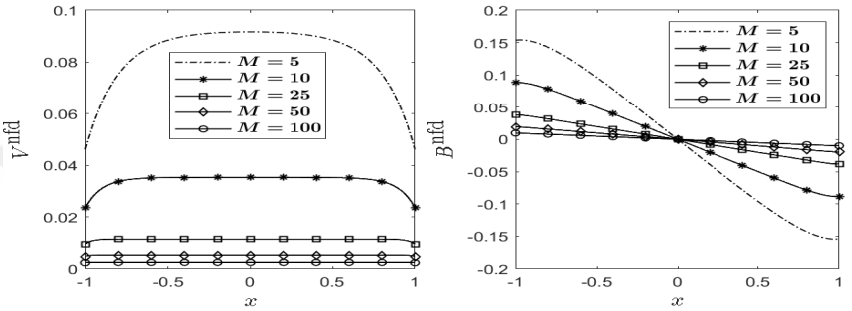
Figure 3.10: Case III: Effects of α and M on the velocity and induced magnetic field with NFD, $c = 0$.

The current case is taken into consideration to observe the pure impact of the slip length α on the NFD findings for V and B at various Hartmann number values. In Figure 3.10 (a)-(b), the alterations of V and B along , $-1 \leq x \leq 1$, are depicted at $\alpha = 0.25$, 0.05, 0.1, and 0.2 when the endpoints $x = \pm 1$ are maintained as an insulator by $c = 0$. While there is no significant change in the induced magnetic field, a rise in α enhances the velocity at each $M = 10,\ 100$. The higher magnetic field, however, at high values of M suppresses the impact of α on the velocity. Additionally, Figure 3.10 (c) for a fixed $\alpha = 0.2$ also confirms once again the tendency for magnitudes of V and B to flatten out at high M values. Additionally, when discretizing the computational interval at high values of α and M, more grid points are required in the case of slip velocity than in the cases with no-slip velocity (i.e., Case I and Case II).

- **Case IV:** $\alpha = 0.025, 0.2$, $c = 0.5, 2, 5$; the slip velocity and variably conducting plates

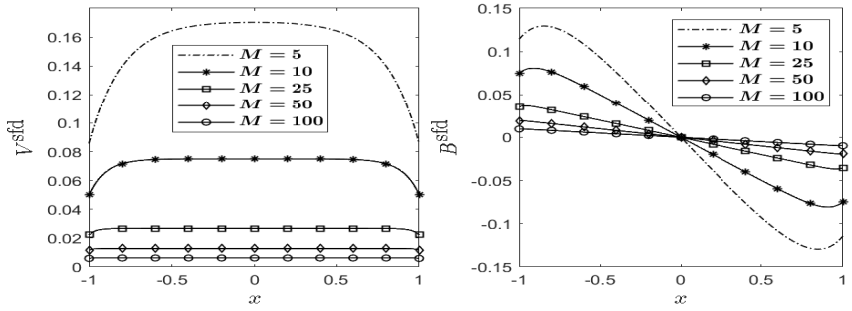


a) $c = 0.5$

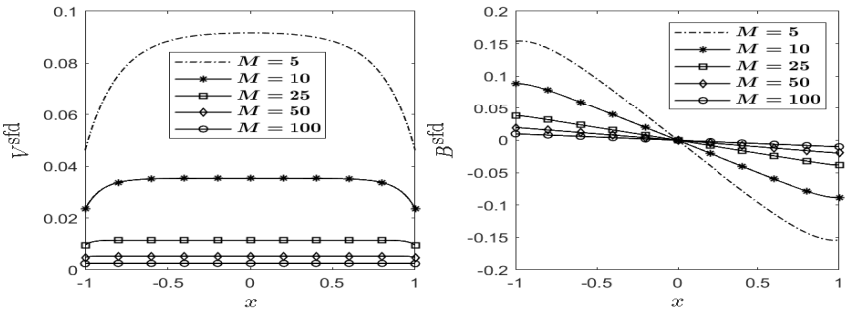


b) $c = 5$

Figure 3.11: Case IV: Effects of c and M on the velocity and induced magnetic field with NFD, $N = 650$, $\alpha = 0.2$.

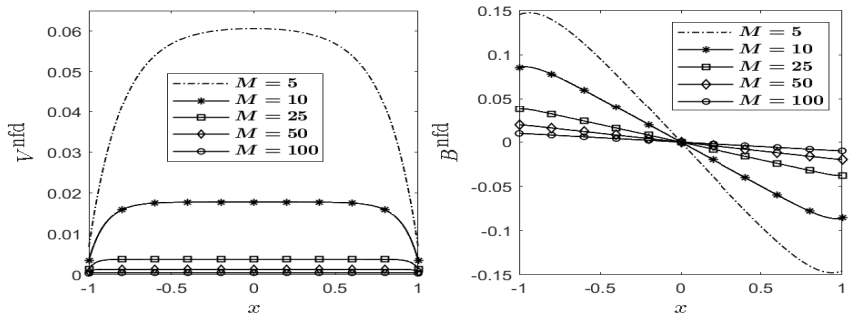


a) $c = 0.5$

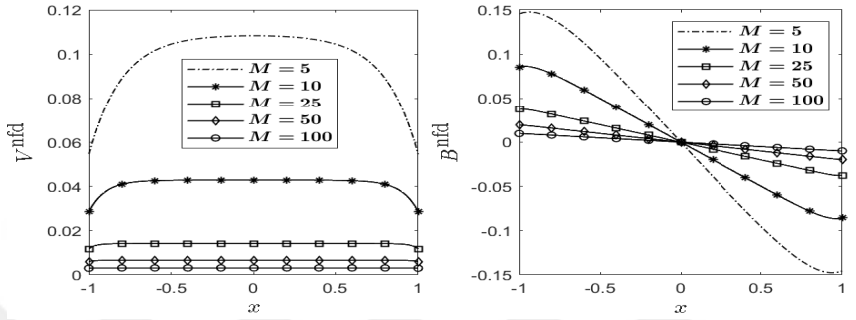


b) $c = 5$

Figure 3.12: Case IV: Effects of c and M on the velocity and induced magnetic field with SFD, $N = 2500$, $\alpha = 0.2$.

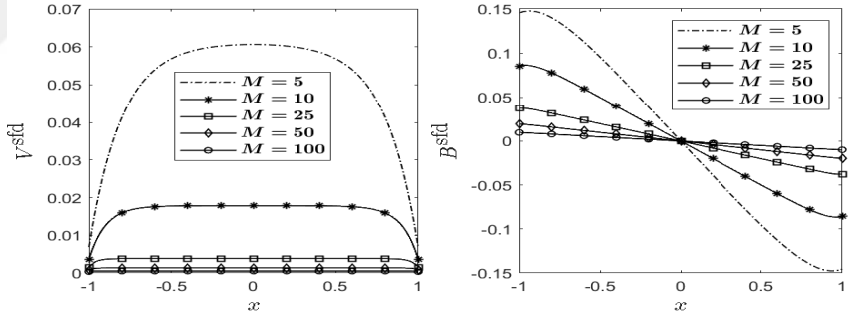


a) $\alpha = 0.025$

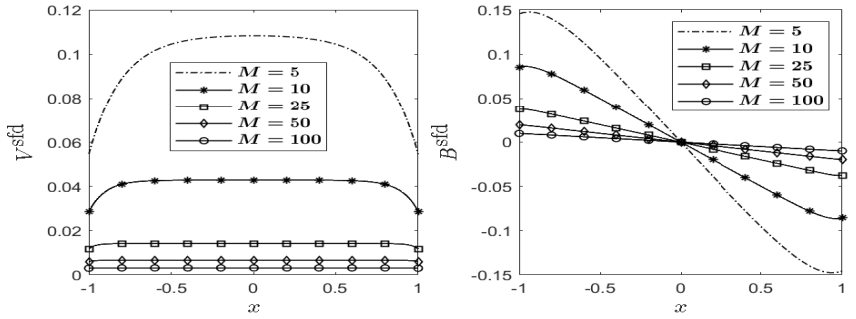


b) $\alpha = 0.2$

Figure 3.13: Case IV: Effects of α and M on the velocity and induced magnetic field with NFD, $N = 650$, $c = 2$.



a) $\alpha = 0.025$



b) $\alpha = 0.2$

Figure 3.14: Case IV: Effects of α and M on the velocity and induced magnetic field with SFD, $N = 2500$, $c = 2$.

In this case, the combined effects of the conductivity parameter and the slip length on the velocity and the induced magnetic field at different M are examined by using both the SFD and the NFD schemes with a finer mesh in SFD. The magnitude of the flow velocity decreases as the conductivity parameter increases while the magnitude of the induced magnetic field increases at small values of $M = 5,\ 10$ according to Figures 3.11 and 3.12, while there is no apparent change in the magnitude of B for higher values of $M = 25$, 50, and 100. These results support the findings of Case II as well. Also, when c increases, the magnetic field at the endpoints becomes perpendicular, indicating practically perfectly conducting plates at high c values.

Figures 3.13 and 3.14, on the other hand, indicate that for small M values, an increase in slip length at a fixed c improves the magnitude of flow velocity, whereas this magnitude enhancement diminishes for larger values of M as in Case III when $c = 0$.

CHAPTER 4

FINITE DIFFERENCE SOLUTIONS TO TWO-DIMENSIONAL MHD FLOW

The steady, laminar, fully developed flow of a viscous, incompressible, and electrically conducting fluid in rectangular channels or pipes subject to an external, constant, and uniform magnetic field applied horizontally is investigated in this chapter by using the standard and new finite difference schemes. The electrically conducting fluid is driven along a sufficiently long channel with a rectangular cross-section (as shown in Figure 1.1) with a constant pressure gradient. The fluid flows along the z-axis, which is the direction of the channel-axis, and becomes two-dimensional for a fully developed flow in the rectangular cross-section of the channel.

The governing equations of MHD flow are obtained by combining the Navier-Stokes equations for fluid dynamics and Maxwell equations for electromagnetism via Ohm's law. The MHD flow equations are thus provided in their non-dimensional form as [1, 2]:

$$\begin{aligned} \nabla^2 V + M\frac{\partial B}{\partial x} &= -1 \\ \nabla^2 B + M\frac{\partial V}{\partial x} &= 0 \end{aligned} \qquad \text{in} \quad \Omega \tag{4.1}$$

as given in Equations (1.2) and (1.3) (see Section 1.1), and with the most general corresponding boundary conditions:

$$\alpha\frac{\partial V}{\partial n} + V = 0, \qquad c\frac{\partial B}{\partial n} + B = 0 \qquad \text{on} \quad \Gamma = \partial\Omega\,. \tag{4.2}$$

Here, $V(x, y)$ is the velocity, $B(x, y)$ is the induced magnetic field, M is the Hartmann number, $\Omega = \{-\ell_x \leq x \leq \ell_x, -\ell_y \leq y \leq \ell_y\}$, $2\ell_x$ is the side length of the rectangle along the x-axis and $2\ell_y$ is the side length of the rectangle along the y-axis, α is the slip length and c is the conductivity parameter, respectively. As stated in

Section 1.1, the velocity boundary conditions through the slipping walls is given by ($\alpha\dfrac{\partial V}{\partial n} + V = 0$), and $\alpha = 0$ (i.e $V = 0$) corresponds to no-slip velocity boundary conditions, while $c = 0$ (i.e $B = 0$) implies electrically insulated walls, $c = \infty$ represents electrically perfectly conducting walls, and $c \in (0, \infty)$ in $c\dfrac{\partial B}{\partial n} + B = 0$ corresponds to variably conducting duct walls.

As in Chapter 3, to employ the new finite difference scheme to MHD flow equations (4.1) and (4.2), the modified Helmholtz form of these equations (1.18) and (1.19) derived in Section 1.2 and given as

$$\begin{aligned} \nabla^2 u^1 - k^2 u^1 &= 0 \\ \nabla^2 u^2 - k^2 u^2 &= 0, \end{aligned} \tag{4.3}$$

are utilized with the corresponding reduced boundary conditions (see Equation (1.19) in Section 1.2)

$$\begin{aligned} \alpha\frac{\partial(u^1 e^{-kx} + u^2 e^{kx})}{\partial n} + u^1 e^{-kx} + u^2 e^{kx} &= 0, \\ c\frac{\partial(u^1 e^{-kx} - u^2 e^{kx})}{\partial n} + u^1 e^{-kx} - u^2 e^{kx} - \frac{1}{k}\left(c\frac{\partial x}{\partial n} - x\right) &= 0 \end{aligned} \tag{4.4}$$

by using the transformations

$$u^1 = e^{kx}\left(V + B + \frac{x}{M}\right) \qquad \text{and} \qquad u^2 = e^{-kx}\left(V - B - \frac{x}{M}\right) \tag{4.5}$$

with $M = 2k$. Once the finite difference solution for Equation (4.3) with boundary conditions (4.4) is found in terms of u^1 and u^2, the original unknowns, the velocity V and the induced magnetic field B, are calculated by applying the appropriate backward substitutions (see Equation 1.20):

$$V = \frac{u^1 e^{-kx} + u^2 e^{kx}}{2} \qquad \text{and} \qquad B = \frac{u^1 e^{-kx} - u^2 e^{kx}}{2} - \frac{x}{M}\,. \tag{4.6}$$

The structure of this chapter is as follows. The standard finite difference scheme is applied to the MHD flow in a rectangular duct with no-slip and insulated walls under the influence of an external horizontal magnetic field in Section 4.1. The new finite difference technique is then presented in Section 4.2 by establishing the optimal weight, which prevents the error caused by truncation in the approximation of the Laplacian term in the modified Helmholtz equation. In order to examine the effects of the Hartmann number and various types of boundary conditions on the flow velocity and the induced magnetic field, the numerical results of SFD and NFD schemes for three test problems are provided in Section 4.3.

4.1 Application of the SFD method to two-dimensional MHD duct flow

The standard finite difference equations for the MHD flow equations given in Equation (4.3) are obtained by using the second-order central difference formulas (2.17) and (2.18) at the point (x_m, y_n) in the approximations of the derivatives $u^i_{xx} = \partial^2 u^i/\partial x^2$ and $u^i_{yy} = \partial^2 u^i/\partial y^2$, $i = 1, 2$. Thus, Equation (4.3) reduces to

$$\begin{aligned} \frac{u^i_{m+1,n} - 2u^i_{m,n} + u^i_{m-1,n}}{h^2} + \frac{u^i_{m,n+1} - 2u^i_{m,n} + u^i_{m,n-1}}{h^2} - k^2 u^i_{m,n} = 0 \\ m, n = 0, 1, ..., N, \quad i = 1, 2 \end{aligned} \tag{4.7}$$

when the computational cross-section is taken as a square with $\ell_x = \ell_y = \ell$, and by using equal step sizes in x- and y-directions, that is $\Delta x = \Delta y = h = \dfrac{2\ell}{N}$. In Equation (4.7), $u^i_{m,n} \approx u^i(x_m, y_n)$, $x_m = x_0 + mh$ and $y_n = y_0 + nh$ with $x_0 = y_0 = -\ell$ and $x_N = y_N = \ell$, N represents the number of subintervals taken along the horizontal and vertical sides of the square cross-section. Equivalently, Equation (4.7) can be written as

$$\begin{aligned} u^i_{m+1,n} + u^i_{m-1,n} - (4 + (kh)^2)u^i_{m,n} + u^i_{m,n+1} + u^i_{m,n-1} = 0 \\ m, n = 0, 1, 2, \ldots, N, \quad i = 1, 2. \end{aligned} \tag{4.8}$$

The corresponding boundary conditions in Equation (4.2) can also be discretized by using the central difference formula (2.11) for the derivatives $\dfrac{\partial V}{\partial x}$ and $\dfrac{\partial B}{\partial x}$ and (2.12) for the derivatives $\dfrac{\partial V}{\partial y}$ and $\dfrac{\partial B}{\partial y}$ at the boundary points $x_0 = y_0 = -\ell$ and $x_N = y_N = \ell$, where $\dfrac{\partial V}{\partial n} = \pm\dfrac{\partial V}{\partial x}$, $\dfrac{\partial B}{\partial n} = \pm\dfrac{\partial B}{\partial x}$ at $x = \pm\ell$ and $\dfrac{\partial V}{\partial n} = \pm\dfrac{\partial V}{\partial y}$, $\dfrac{\partial B}{\partial n} = \pm\dfrac{\partial B}{\partial y}$ at $y = \pm\ell$. Then, the discretized boundary conditions for the velocity become

$$\begin{aligned} -\alpha\frac{V_{1,n} - V_{-1,n}}{2h} + V_{0,n} = 0, \qquad & \text{at } x = x_0 = -\ell, \quad n = 0, 1, .., N \\ \alpha\frac{V_{N+1,n} - V_{N-1,n}}{2h} + V_{N,n} = 0, \qquad & \text{at } x = x_N = \ell, \quad n = 0, 1, .., N \end{aligned} \tag{4.9}$$

and

$$\begin{aligned} -\alpha\frac{V_{m,1} - V_{m,-1}}{2h} + V_{m,0} = 0, \qquad & \text{at } y = y_0 = -\ell, \quad m = 0, 1, .., N \\ \alpha\frac{V_{m,N+1} - V_{m,N-1}}{2h} + V_{m,N} = 0, \qquad & \text{at } y = y_N = \ell, \quad m = 0, 1, .., N \end{aligned} \tag{4.10}$$

and for the induced magnetic field they reduce to

$$\begin{aligned} -c\frac{B_{1,n}-B_{-1,n}}{2h}+B_{0,n}=0, \qquad & \text{at } x=x_0=-\ell, \quad n=0,1,..,N \\ c\frac{B_{N+1,n}-B_{N-1,n}}{2h}+B_{N,n}=0, \qquad & \text{at } x=x_N=\ell, \quad n=0,1,..,N \end{aligned} \tag{4.11}$$

and

$$\begin{aligned} -c\frac{B_{m,1}-B_{m,-1}}{2h}+B_{m,0}=0, \qquad & \text{at } y=y_0=-\ell, \quad m=0,1,..,N \\ c\frac{B_{m,N+1}-B_{m,N-1}}{2h}+B_{m,N}=0, \qquad & \text{at } y=y_N=\ell, \quad m=0,1,..,N\,. \end{aligned} \tag{4.12}$$

They can be further written as

$$\begin{aligned} \alpha V_{1,n}-2hV_{0,n}-\alpha V_{-1,n}=0, \qquad & \text{at } x=x_0=-\ell, \quad n=0,1,..,N \\ \alpha V_{N+1,n}+2hV_{N,n}-\alpha V_{N-1,n}=0, \qquad & \text{at } x=x_N=\ell, \quad n=0,1,..,N \end{aligned} \tag{4.13}$$

$$\begin{aligned} \alpha V_{m,1}-2hV_{m,0}-\alpha V_{m,-1}=0, \qquad & \text{at } y=y_0=-\ell, \quad m=0,1,..,N \\ \alpha V_{m,N+1}+2hV_{m,N}-\alpha V_{m,N-1}=0, \qquad & \text{at } y=y_N=\ell, \quad m=0,1,..,N \end{aligned} \tag{4.14}$$

and

$$\begin{aligned} cB_{1,n}-2hB_{0,n}-cB_{-1,n}=0, \qquad & \text{at } x=x_0=-\ell, \quad n=0,1,..,N \\ cB_{N+1,n}+2hB_{N,n}-cB_{N-1,n}=0, \qquad & \text{at } x=x_N=\ell, \quad n=0,1,..,N \end{aligned} \tag{4.15}$$

$$\begin{aligned} cB_{m,1}-2hB_{m,0}-cB_{m,-1}=0, \qquad & \text{at } y=y_0=-\ell, \quad m=0,1,..,N \\ cB_{m,N+1}+2hB_{m,N}-cB_{m,N-1}=0, \qquad & \text{at } y=y_N=\ell, \quad m=0,1,..,N. \end{aligned} \tag{4.16}$$

Finally, the use of the transformations in Equation (4.5) in Equations (4.13)-(4.16) gives the standard central finite difference schemes to the boundary conditions in terms of u^1 and u^2 for the velocity as:

$$\begin{aligned} &\alpha\frac{u^1_{1,n}e^{-kx_1}+u^2_{1,n}e^{kx_1}}{2}-2h\frac{u^1_{0,n}e^{-kx_0}+u^2_{0,n}e^{kx_0}}{2} \\ &-\alpha\frac{u^1_{-1,n}e^{-kx_{-1}}+u^2_{-1,n}e^{kx_{-1}}}{2}=0, \qquad \text{at } x=-\ell, \quad n=0,1,..,N \\ &\alpha\frac{u^1_{N+1,n}e^{-kx_{N+1}}+u^2_{N+1,n}e^{kx_{N+1}}}{2}+2h\frac{u^1_{N,n}e^{-kx_N}+u^2_{N,n}e^{kx_N}}{2} \\ &-\alpha\frac{u^1_{N-1,n}e^{-kx_{N-1}}+u^2_{N-1,n}e^{kx_{N-1}}}{2}=0, \qquad \text{at } x=\ell, \quad n=0,1,..,N \end{aligned} \tag{4.17}$$

$$
\begin{aligned}
&\alpha\frac{u^1_{m,1}e^{-kx_m}+u^2_{m,1}e^{kx_m}}{2}-2h\frac{u^1_{m,0}e^{-kx_m}+u^2_{m,0}e^{kx_m}}{2}\\
&-\alpha\frac{u^1_{m,-1}e^{-kx_m}+u^2_{m,-1}e^{kx_m}}{2}=0, \qquad \text{at } y=-\ell, \quad m=0,1,..,N\\
&\alpha\frac{u^1_{m,N+1}e^{-kx_m}+u^2_{m,N+1}e^{kx_m}}{2}+2h\frac{u^1_{m,N}e^{-kx_m}+u^2_{m,N}e^{kx_m}}{2}\\
&-\alpha\frac{u^1_{m,N-1}e^{-kx_m}+u^2_{m,N-1}e^{kx_m}}{2}=0, \qquad \text{at } y=\ell, \quad m=0,1,..,N
\end{aligned}
\tag{4.18}
$$

and for the induced magnetic field they become

$$
\begin{aligned}
&c\left(\frac{u^1_{1,n}e^{-kx_1}-u^2_{1,n}e^{kx_1}}{2}-\frac{x_1}{M}\right)-2h\left(\frac{u^1_{0,n}e^{-kx_0}-u^2_{0,n}e^{kx_0}}{2}-\frac{x_0}{M}\right)\\
&-c\left(\frac{u^1_{-1,n}e^{-kx_{-1}}-u^2_{-1,n}e^{kx_{-1}}}{2}-\frac{x_{-1}}{M}\right)=0, \qquad \text{at } x=-\ell, \quad n=0,1,..,N\\
&c\left(\frac{u^1_{N+1,n}e^{-kx_{N+1}}-u^2_{N+1,n}e^{kx_{N+1}}}{2}-\frac{x_{N+1}}{M}\right)+2h\left(\frac{u^1_{N,n}e^{-kx_N}-u^2_{N,n}e^{kx_N}}{2}-\frac{x_N}{M}\right)\\
&-c\left(\frac{u^1_{N-1,n}e^{-kx_{N-1}}-u^2_{N-1,n}e^{kx_{N-1}}}{2}-\frac{x_{N-1}}{M}\right)=0, \qquad \text{at } x=\ell, \quad n=0,1,..,N
\end{aligned}
\tag{4.19}
$$

$$
\begin{aligned}
&c\left(\frac{u^1_{m,1}e^{-kx_m}-u^2_{m,1}e^{kx_m}}{2}-\frac{x_m}{M}\right)-2h\left(\frac{u^1_{m,0}e^{-kx_m}-u^2_{m,0}e^{kx_m}}{2}-\frac{x_m}{M}\right)\\
&-c\left(\frac{u^1_{m,-1}e^{-kx_m}-u^2_{m,-1}e^{kx_m}}{2}-\frac{x_m}{M}\right)=0, \qquad \text{at } y=-\ell, \quad m=0,1,..,N\\
&c\left(\frac{u^1_{m,N+1}e^{-kx_m}-u^2_{m,N+1}e^{kx_m}}{2}-\frac{x_m}{M}\right)+2h\left(\frac{u^1_{m,N}e^{-kx_m}-u^2_{m,N}e^{kx_m}}{2}-\frac{x_m}{M}\right)\\
&-c\left(\frac{u^1_{m,N-1}e^{-kx_m}-u^2_{m,N-1}e^{kx_m}}{2}-\frac{x_m}{M}\right)=0, \qquad \text{at } y=\ell, \quad m=0,1,..,N\,.
\end{aligned}
\tag{4.20}
$$

Although the SFD equations to approximate the MHD flow equations are provided for the most general type of boundary conditions for the velocity and induced magnetic field, in the present section we will only concentrate on the matrix-vector form for the case when $V = B = 0$. This is due to the fact that, as we already mentioned in

Chapter 3, the NFD scheme produces more accurate results than the SFD scheme. As a result, the SFD formulation for the MHD duct flow with $V = B = 0$ on the walls is covered in the section that follows.

4.1.1 Test problem I: no-slip and insulated walls: $c = \alpha = 0$

In this case, the homogeneous boundary conditions $V = B = 0$ in Equation (4.5) yield decoupled boundary conditions in u^1 and u^2, that is, $u^1 = \dfrac{x}{2k}e^{kx}$ and $u^2 = -\dfrac{x}{2k}e^{-kx}$ at $x = y = \mp\ell$. Hence, we end up with a decoupled problem in u^1 and u^2, which can be written in two separate linear systems of equations of sizes $(N-1)^2 \times (N-1)^2$ for the unknowns u^1 and u^2. Then, the standard central finite difference equations for the modified Helmholtz equations (4.3) as given in Equation (4.8), can be written at the interior points as

$$\begin{gathered} u^i_{m+1,n} + u^i_{m-1,n} - (4 + (kh)^2)u^i_{m,n} + u^i_{m,n+1} + u^i_{m,n-1} = 0 \\ m, n = 1, 2, \ldots, N-1, \quad i = 1, 2 \end{gathered} \tag{4.21}$$

and the corresponding boundary conditions are

$$\begin{aligned} u^1_{0,n} &= \frac{x_0}{2k}e^{kx_0}, \quad \text{at } x_0 = -\ell \quad \text{and} \quad u^1_{N,n} = \frac{x_N}{2k}e^{kx_N}, \quad \text{at } x_N = \ell \\ u^1_{m,0} &= \frac{x_m}{2k}e^{kx_m}, \quad \text{at } y_0 = -\ell \quad \text{and} \quad u^1_{m,N} = \frac{x_m}{2k}e^{kx_m}, \quad \text{at } y_N = \ell \\ u^2_{0,n} &= -\frac{x_0}{2k}e^{-kx_0}, \quad \text{at } x_0 = -\ell \quad \text{and} \quad u^2_{N,n} = -\frac{x_N}{2k}e^{-kx_N}, \quad \text{at } x_N = \ell \\ u^2_{m,0} &= -\frac{x_m}{2k}e^{-kx_m}, \quad \text{at } y_0 = -\ell \quad \text{and} \quad u^2_{m,N} = -\frac{x_m}{2k}e^{-kx_m}, \quad \text{at } y_N = \ell \end{aligned} \tag{4.22}$$

for $m, n = 1, 2, ..., N-1$. Thus, when these boundary conditions for u^1 and u^2 are substituted in Equation (4.21), one can obtain two separate systems in u^1 and u^2 as:

$$Au^1 = b_1 \qquad \text{and} \qquad Au^2 = b_2 \tag{4.23}$$

with the block tridiagonal matrix A of size $(N-1)^2 \times (N-1)^2$ given by

$$A = \begin{bmatrix} A_1 & I & & & & \\ I & A_1 & I & & 0 & \\ & I & A_1 & I & & \\ & & \ddots & \ddots & \ddots & \\ & 0 & & I & A_1 & I \\ & & & & I & A_1 \end{bmatrix}$$

where I is the identity matrix of size $(N-1) \times (N-1)$, and A_1 is the tridiagonal matrix of size $(N-1) \times (N-1)$ given by

$$A_1 = \begin{bmatrix} -(4+(kh)^2) & 1 & 0 & 0 & \cdots & 0 \\ 1 & -(4+(kh)^2) & 1 & 0 & \cdots & 0 \\ 0 & 1 & -(4+(kh)^2) & 1 & & \\ & & \ddots & \ddots & \ddots & \\ \vdots & & & 1 & -(4+(kh)^2) & 1 \\ 0 & \cdots & & 0 & 1 & -(4+(kh)^2) \end{bmatrix}.$$

The unknown vectors u^1 and u^2 are of size $(N-1)^2$ and ordered as

$$\begin{aligned} u^1 &= \begin{bmatrix} u^1_{1,1} & u^1_{2,1} & \cdots & u^1_{N-1,1} & | & u^1_{1,2} & u^1_{2,2} & \cdots & u^1_{N-1,2} & | & \cdots & | & u^1_{1,N-1} & u^1_{2,N-1} & \cdots & u^1_{N-1,N-1} \end{bmatrix}^T \\ u^2 &= \begin{bmatrix} u^2_{1,1} & u^2_{2,1} & \cdots & u^2_{N-1,1} & | & u^2_{1,2} & u^2_{2,2} & \cdots & u^2_{N-1,2} & | & \cdots & | & u^2_{1,N-1} & u^2_{2,N-1} & \cdots & u^2_{N-1,N-1} \end{bmatrix}^T. \end{aligned} \tag{4.24}$$

The right-hand side vectors b_1 and b_2 of size $(N-1)^2$ are

$$\begin{aligned} b_1 &= \begin{bmatrix} b_{1,1} & | & b_{1,2} & | & b_{1,2} & | & \cdots & | & b_{1,2} & | & b_{1,2} & | & b_{1,1} \end{bmatrix}^T, \\ b_2 &= \begin{bmatrix} b_{2,1} & | & b_{2,2} & | & b_{2,2} & | & \cdots & | & b_{2,2} & | & b_{2,2} & | & b_{2,1} \end{bmatrix}^T, \end{aligned} \tag{4.25}$$

where $b_{i,j}$, $i = 1, 2$, $j = 1, 2$ are the subvectors of sizes $(N-1)$ with

$$b_{1,1} = \left[(-\frac{x_0}{2k}e^{kx_0} - \frac{x_1}{2k}e^{kx_1}) \quad -\frac{x_2}{2k}e^{kx_2} \quad \cdots \quad -\frac{x_{N-2}}{2k}e^{kx_{N-2}} \quad (-\frac{x_{N-1}}{2k}e^{kx_{N-1}} - \frac{x_N}{2k}e^{kx_N})\right]^T$$
$$b_{1,2} = \left[-\frac{x_0}{2k}e^{kx_0} \quad 0 \quad \cdots \quad 0 \quad -\frac{x_N}{2k}e^{kx_N}\right]^T$$

and

$$b_{2,1} = \left[(\frac{x_0}{2k}e^{-kx_0} + \frac{x_1}{2k}e^{-kx_1}) \quad \frac{x_2}{2k}e^{-kx_2} \quad \cdots \quad \frac{x_{N-2}}{2k}e^{-kx_{N-2}} \quad (\frac{x_{N-1}}{2k}e^{-kx_{N-1}} + \frac{x_N}{2k}e^{-kx_N})\right]^T$$
$$b_{2,2} = \left[\frac{x_0}{2k}e^{-kx_0} \quad 0 \quad \cdots \quad 0 \quad \frac{x_N}{2k}e^{-kx_N}\right]^T .$$

Once the systems (4.23) are solved, u^1 and u^2 are obtained at nodes (x_m, y_n), $m, n = 1, 2..., N-1$, and by using back substitutions in Equation (4.6), the velocity V and the induced magnetic field B are obtained.

4.2 Application of the NFD method to two-dimensional MHD duct flow

The governing equations to two-dimensional MHD flow in the form of modified Helmholtz equations are given in Equation (4.3):

$$\nabla^2 u^i - k^2 u^i = 0, \quad i = 1, 2, \quad -\ell < x, y < \ell. \tag{4.26}$$

Here, an exact numerical finite difference scheme is developed with no truncation error in the discretization of the Laplacian term, $\nabla^2 u^i = u^i_{xx} + u^i_{yy}$, $i = 1, 2$, in Equation (4.26) by employing the concept of deriving NFD scheme for the Helmholtz equation in Section 2.2.2.

The standard finite difference scheme for $u^i_{xx} + u^i_{yy}$ is given by

$$u^i_{xx} + u^i_{yy} \approx \frac{u^i(x+h, y) + u^i(x-h, y) - 4u^i(x, y) + u^i(x, y+h) + u^i(x, y-h)}{h^2} \tag{4.27}$$

by using the same step size h in x- and y-directions for $i = 1, 2$. As in the one-dimensional problem, we want to replace the coefficient 4 of $u^i(x, y)$ in Equation (4.27) with an optimal weight w which eliminates the truncation error

$$\left|\nabla^2 u^i - \frac{u^i(x+h, y) + u^i(x-h, y) - wu^i(x, y) + u^i(x, y+h) + u^i(x, y-h)}{h^2}\right|. \tag{4.28}$$

It is crucial to highlight here that, to the author's knowledge, the literature does not contain the derivation of such an optimal weight for the NFD discretization of the two-dimensional modified Helmholtz equation. Thus, the development of this novel finite difference approach is another main contribution made by this section of the current thesis. Due to the cross-derivative terms, it is not possible to simply apply the method used in the derivation of the optimal weight for the one-dimensional modified Helmholtz equation (established in Section 3.2.1) to the two-dimensional case. However, this difficulty is avoided by implementing the planar wave solution of the two-dimensional modified Helmholtz equation which is given by [38]

$$u^i(x,y) = e^{k(x\cos\theta + y\sin\theta)} \tag{4.29}$$

as in the innovative way proposed by Lambe et al. [3] for the Helmholtz equation (see Section 2.2.2) with $\theta \in [-\pi, \pi]$. The planar wave solution (4.29) satisfies the differential equation (4.26), and the direct use of it gives

$$\begin{aligned} u^i(x+h,y) + u^i(x-h,y) + u^i(x,y+h) + u^i(x,y-h) = \\ 2(\cosh(kh\cos\theta) + \cosh(kh\sin\theta))u^i(x,y)\,. \end{aligned} \tag{4.30}$$

Thus, by substituting Equation (4.30) in Equation (4.28), we want to find w such that

$$\frac{2(\cosh(kh\cos\theta) + \cosh(kh\sin\theta))u^i(x,y) - wu^i(x,y)}{h^2} \approx k^2 u^i(x,y) = u^i_{xx} + u^i_{yy} \tag{4.31}$$

or, equivalently, one wants to find a weight that is optimal and satisfies the following equation

$$2(\cosh(kh\cos\theta) + \cosh(kh\sin\theta)) - (w + (kh)^2) \approx 0. \tag{4.32}$$

Equation (4.32) has no solution which is independent of angle θ, but as explained in the work of Lambe et al. [3] by minimizing the average over all angles as follows

$$\frac{1}{2\pi}\int_0^{2\pi} [2(\cosh(kh\cos\theta) + \cosh(kh\sin\theta)) - (w + (kh)^2)]d\theta = 0\,, \tag{4.33}$$

we can obtain

$$2\pi w = -2\pi(kh)^2 + \int_0^{2\pi} 2(\cosh(kh\cos\theta) + \cosh(kh\sin\theta))d\theta\,. \tag{4.34}$$

Thus, the weight w becomes

$$\begin{aligned} w =& -(kh)^2 + \frac{1}{\pi}\int_0^{2\pi} (\cosh(kh\cos\theta) + \cosh(kh\sin\theta))d\theta \\ =& -(kh)^2 + \frac{1}{\pi}\int_0^{\pi} (\cosh(kh\cos\theta) + \cosh(kh\sin\theta))d\theta \\ &+ \frac{1}{\pi}\int_{\pi}^{2\pi} (\cosh(kh\cos\theta) + \cosh(kh\sin\theta))d\theta \,. \end{aligned} \tag{4.35}$$

The second integral in Equation (4.35)

$$I = \int_{\pi}^{2\pi} (\cosh(kh\cos\theta) + \cosh(kh\sin\theta))d\theta \tag{4.36}$$

can be converted into an integral over $(0, \pi)$ by using the change of variable $u = \theta - \pi$. Then, I becomes

$$\begin{aligned} I &= \int_0^{\pi} (\cosh(kh\cos(u+\pi)) + \cosh(kh\sin(u+\pi)))du \\ &= \int_0^{\pi} (\cosh(kh\cos(\theta+\pi)) + \cosh(kh\sin(\theta+\pi)))d\theta \end{aligned} \tag{4.37}$$

where

$$\begin{aligned} \cosh(kh\cos(\theta+\pi)) &= \cosh(kh(-\cos\theta)) = \cosh(kh\cos\theta)\,, \\ \cosh(kh\sin(\theta+\pi)) &= \cosh(kh(-\sin\theta)) = \cosh(kh\sin\theta)\,. \end{aligned} \tag{4.38}$$

Now, Equation (4.37) becomes

$$I = \int_0^{\pi} (\cosh(kh\cos\theta) + \cosh(kh\sin\theta))d\theta \tag{4.39}$$

and when it is substituted in Equation (4.35), we have

$$w = -(kh)^2 + \frac{2}{\pi}\int_0^{\pi} (\cosh(kh\cos\theta) + \cosh(kh\sin\theta))d\theta \tag{4.40}$$

or, equivalently,

$$w = 2\left[\underbrace{\frac{1}{\pi}\int_0^{\pi} \cosh(kh\cos\theta)d\theta}_{A} + \underbrace{\frac{1}{\pi}\int_0^{\pi} \cosh(kh\sin\theta)d\theta}_{B}\right] - (kh)^2 \tag{4.41}$$

where the integral A is equal to the modified Bessel function of the first kind and order zero $I_0(kh)$ (see Equation (9.6.16) in the work of Abramowitz and Stegun [39]), that is:

$$A = \frac{1}{\pi}\int_0^{\pi} \cosh(kh\cos\theta)d\theta = I_0(kh). \tag{4.42}$$

On the other hand, the integral B can be written in terms of the Bessel function of the first kind of order zero, $J_0(ikh)$, as follows, (see Equation (9.1.18) in [39]),

$$\begin{aligned} B &= \frac{1}{\pi}\int_0^{\pi} \cosh(kh\sin\theta)d\theta = \frac{1}{\pi}\int_0^{\pi} \cosh\left(i\frac{kh\sin\theta}{i}\right)d\theta \\ &= \frac{1}{\pi}\int_0^{\pi} \cos\left(\frac{kh\sin\theta}{i}\right)d\theta = \frac{1}{\pi}\int_0^{\pi} \cos(-ikh\sin\theta)d\theta \\ &= \frac{1}{\pi}\int_0^{\pi} \cos(ikh\sin\theta)d\theta = J_0(ikh). \end{aligned} \tag{4.43}$$

Then, by using the identity $I_0(z) = J_0(iz)$ with $i^2 = -1$, (see Equation (9.6.3) in [39]), the integral B can be written as

$$B = J_0(ikh) = I_0(kh) = A. \tag{4.44}$$

Finally, the optimal weight w given in Equation (4.41) becomes

$$w = 2[A + B] - (kh)^2 = 4I_0(kh) - (kh)^2\,. \tag{4.45}$$

Thus, the NFD scheme for the two-dimensional modified Helmholtz equation

$$u^i_{xx} + u^i_{yy} - k^2u^i = 0, \quad i = 1, 2$$

is given by

$$\begin{aligned} u^i(x+h,y) + u^i(x-h,y) - 4I_0(kh)u^i(x,y) + u^i(x,y+h) + u^i(x,y-h) = 0 \\ i = 1, 2, \qquad -\ell < x, y < \ell \end{aligned} \tag{4.46}$$

for which the discretized form can be written as

$$\begin{aligned} u^i_{m+1,n} + u^i_{m-1,n} - 4I_0(kh)u^i_{m,n} + u^i_{m,n+1} + u^i_{m,n-1} = 0 \\ m, n = 0, 1, 2, \ldots, N, \quad i = 1, 2 \end{aligned} \tag{4.47}$$

by using N-equal length subintervals over $-\ell \le x, y \le \ell$ with the step size $h = \frac{2\ell}{N}$. The computational nodes are obtained from $x_m = x_0 + mh$ and $y_n = y_0 + nh$ with $x_0 = y_0 = -\ell$ and $x_N = y_N = \ell$, and $u^i_{m,n}$ denotes the finite difference approximation to $u^i(x, y)$ at the point (x_m, y_n).

Boundary conditions (4.2) are in the general form $a\dfrac{\partial u}{\partial n} + u = 0$ where $\dfrac{\partial u}{\partial n} = \pm\dfrac{\partial u}{\partial x}$ at $x = \pm\ell$ and $\dfrac{\partial u}{\partial n} = \pm\dfrac{\partial u}{\partial y}$ at $y = \pm\ell$, so in this case the boundary conditions (4.2)

can be rewritten as

$$\begin{aligned} \pm\alpha\frac{\partial V}{\partial x} + V = 0, \quad \pm c\frac{\partial B}{\partial x} + B = 0 \quad \text{at} \quad x = \pm\ell \\ \pm\alpha\frac{\partial V}{\partial y} + V = 0, \quad \pm c\frac{\partial B}{\partial y} + B = 0 \quad \text{at} \quad y = \pm\ell\,. \end{aligned} \tag{4.48}$$

These are mixed-type boundary conditions which are in the same form given in Section 3.2.2, thus we can apply the same formulas which were derived there for the approximation of the velocity and the induced magnetic field boundary conditions. Thus, the NFD scheme for the boundary conditions (4.48) can be written by using the new finite difference formulas for the first-order derivatives given in Section 3.2.2 for the velocity as:

$$\begin{aligned} &V_{1,n} - 2\sinh(h/\alpha)V_{0,n} - V_{-1,n} = 0, && \text{at } x = x_0 = -\ell \\ &V_{N+1,n} + 2\sinh(h/\alpha)V_{N,n} - V_{N-1,n} = 0, && \text{at } x = x_N = \ell, \end{aligned} \tag{4.49}$$

$$\begin{aligned} &V_{m,1} - 2\sinh(h/\alpha)V_{m,0} - V_{m,-1} = 0, && \text{at } y = y_0 = -\ell \\ &V_{m,N+1} + 2\sinh(h/\alpha)V_{m,N} - V_{m,N-1} = 0, && \text{at } y = y_N = \ell, \end{aligned} \tag{4.50}$$

and for the induced magnetic field

$$\begin{aligned} &B_{1,n} - 2\sinh(h/c)B_{0,n} - B_{-1,n} = 0, && \text{at } x = x_0 = -\ell \\ &B_{N+1,n} + 2\sinh(h/c)B_{N,n} - B_{N-1,n} = 0, && \text{at } x = x_N = \ell, \end{aligned} \tag{4.51}$$

$$\begin{aligned} &B_{m,1} - 2\sinh(h/c)B_{m,0} - B_{m,-1} = 0, && \text{at } y = y_0 = -\ell \\ &B_{m,N+1} + 2\sinh(h/c)B_{m,N} - B_{m,N-1} = 0, && \text{at } y = y_N = \ell, \end{aligned} \tag{4.52}$$

where $V_{m,n} \approx V(x_m, y_n)$ and $B_{m,n} \approx B(x_m, y_n)$ when $m, n = 0, 1, .., N$.

Then, by the use of backward substitutions (4.6) for V in Equations (4.49) and (4.50) and for B in Equations (4.51) and (4.52), the new finite difference equations in terms of new variables u^1 and u^2 at the boundaries $x, y = \pm\ell$ are obtained. Thus, the velocity boundary conditions become

$$\begin{aligned} &(u^1_{1,n}e^{-kx_1} + u^2_{1,n}e^{kx_1}) - 2\sinh(\frac{h}{\alpha})(u^1_{0,n}e^{-kx_0} + u^2_{0,n}e^{kx_0}) \\ &\qquad - (u^1_{-1,n}e^{-kx_{-1}} + u^2_{-1,n}e^{kx_{-1}}) = 0 \quad \text{at } x = x_0 = -\ell \\ &(u^1_{N+1,n}e^{-kx_{N+1}} + u^2_{N+1,n}e^{kx_{N+1}}) + 2\sinh(\frac{h}{\alpha})\left(u^1_{N,n}e^{-kx_N} + u^2_{N,n}e^{kx_N}\right) \\ &\qquad - (u^1_{N-1,n}e^{-kx_{N-1}} + u^2_{N-1,n}e^{kx_{N-1}}) = 0 \quad \text{at } x = x_N = \ell, \end{aligned} \tag{4.53}$$

$$
\begin{aligned}
&(u^1_{m,1}e^{-kx_m} + u^2_{m,1}e^{kx_m}) - 2\sinh(\frac{h}{\alpha})(u^1_{m,0}e^{-kx_m} + u^2_{m,0}e^{kx_m}) \\
&\qquad - (u^1_{m,-1}e^{-kx_m} + u^2_{m,-1}e^{kx_m}) = 0 \quad \text{at } y = y_0 = -\ell \\
&(u^1_{m,N+1}e^{-kx_m} + u^2_{m,N+1}e^{kx_m}) + 2\sinh(\frac{h}{\alpha})\left(u^1_{m,N}e^{-kx_m} + u^2_{m,N}e^{kx_m}\right) \\
&\qquad - (u^1_{m,N-1}e^{-kx_m} + u^2_{m,N-1}e^{kx_m}) = 0 \quad \text{at } y = y_N = \ell,
\end{aligned}
\tag{4.54}
$$

and for the induced magnetic field we have

$$
\begin{aligned}
&(u^1_{1,n}e^{-kx_1} - u^2_{1,n}e^{kx_1}) - 2\sinh(\frac{h}{c})\left(u^1_{0,n}e^{-kx_0} - u^2_{0,n}e^{kx_0} - \frac{x_0}{k}\right) \\
&- (u^1_{-1,n}e^{-kx_{-1}} - u^2_{-1,n}e^{kx_{-1}}) + \frac{1}{k}(x_{-1} - x_1) = 0 \quad \text{at } x = x_0 = -\ell \\
&(u^1_{N+1,n}e^{-kx_{N+1}} - u^2_{N+1,n}e^{kx_{N+1}}) + 2\sinh(\frac{h}{c})\left(u^1_{N,n}e^{-kx_N} - u^2_{N,n}e^{kx_N} - \frac{x_N}{k}\right) \\
&- (u^1_{N-1,n}e^{-kx_{N-1}} - u^2_{N-1,n}e^{kx_{N-1}}) + \frac{1}{k}(x_{N-1} - x_{N+1}) = 0 \quad \text{at } x = x_N = \ell,
\end{aligned}
\tag{4.55}
$$

$$
\begin{aligned}
&(u^1_{m,1}e^{-kx_m} - u^2_{m,1}e^{kx_m}) - 2\sinh(\frac{h}{c})\left(u^1_{m,0}e^{-kx_m} - u^2_{m,0}e^{kx_m} - \frac{x_m}{k}\right) \\
&\qquad - (u^1_{m,-1}e^{-kx_m} - u^2_{m,-1}e^{kx_m}) = 0 \quad \text{at } y = y_0 = -\ell \\
&(u^1_{m,N+1}e^{-kx_m} - u^2_{m,N+1}e^{kx_m}) + 2\sinh(\frac{h}{c})\left(u^1_{m,N}e^{-kx_m} - u^2_{m,N}e^{kx_m} - \frac{x_m}{k}\right) \\
&\qquad - (u^1_{m,N-1}e^{-kx_m} - u^2_{m,N-1}e^{kx_m}) = 0 \quad \text{at } y = y_N = \ell
\end{aligned}
\tag{4.56}
$$

where $m, n = 0, 1, ..., N$ in Equations (4.53)-(4.56).

To conclude the NFD equations for the modified Helmholtz equation subject to mixed-type boundary conditions are obtained by using:

i.) the optimal weight $w = 4I_0(kh) - (kh)^2$ for the approximation of the Laplacian term in Equation (4.26), which yields the NFD equation (4.47) for the modified Helmholtz equations, and

ii.) the discretized form of boundary conditions derived in Section 3.2.2 yielding the NFD equations (4.53)-(4.56) for V and B.

In the subsequent sections the matrix-vector forms of the NFD scheme equations corresponding to different boundary conditions, which produces specifically three test problems, are going to be given.

4.2.1 Test problem I: no-slip and insulated walls: $c = \alpha = 0$

The first problem is the MHD flow with $V = B = 0$ on the duct walls. The flow configuration including boundary conditions is displayed in Figure 4.1. As explained in Section 4.1.1, under these boundary conditions, the boundary conditions in u^1 and u^2 become also decoupled, which allows one to generate two decoupled systems of sizes $(N-1)^2 \times (N-1)^2$ for the unknowns u^1 and u^2.

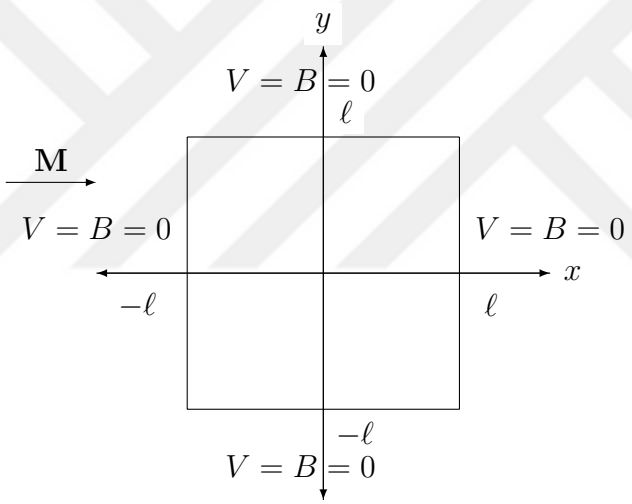


Figure 4.1: Flow configuration and the boundary conditions for Problem I.

The new finite difference equations for the modified Helmholtz equations (4.3) at the interior points are given in Equation (4.47) as

$$\begin{aligned} u^i_{m+1,n} + u^i_{m-1,n} - 4I_0(kh)u^i_{m,n} + u^i_{m,n+1} + u^i_{m,n-1} = 0 \\ m, n = 1, 2, \ldots, N-1, \quad i = 1, 2 \end{aligned} \tag{4.57}$$

with the same boundary conditions given in Equation (4.22) for the SFD scheme,

which are:

$$\begin{aligned}
u^1_{0,n} &= \frac{x_0}{2k}e^{kx_0}, \quad \text{at } x_0 = -\ell \quad \text{and} \quad u^1_{N,n} = \frac{x_N}{2k}e^{kx_N}, \quad \text{at } x_N = \ell \\
u^1_{m,0} &= \frac{x_m}{2k}e^{kx_m}, \quad \text{at } y_0 = -\ell \quad \text{and} \quad u^1_{m,N} = \frac{x_m}{2k}e^{kx_m}, \quad \text{at } y_N = \ell \\
u^2_{0,n} &= -\frac{x_0}{2k}e^{-kx_0}, \quad \text{at } x_0 = -\ell \quad \text{and} \quad u^2_{N,n} = -\frac{x_N}{2k}e^{-kx_N}, \quad \text{at } x_N = \ell \\
u^2_{m,0} &= -\frac{x_m}{2k}e^{-kx_m}, \quad \text{at } y_0 = -\ell \quad \text{and} \quad u^2_{m,N} = -\frac{x_m}{2k}e^{-kx_m}, \quad \text{at } y_N = \ell
\end{aligned} \tag{4.58}$$

for $m, n = 1, 2, ..., N-1$. When these boundary conditions are inserted into Equation (4.57), the following systems of linear equations in u^1 and u^2

$$Cu^1 = d_1 \qquad \text{and} \qquad Cu^2 = d_2 \tag{4.59}$$

are obtained as in Section 4.1.1. The only difference between the systems in Equation (4.59) and the systems in Equation (4.23) occurs in the diagonal entries of the coefficient matrix C. That is, the block tridiagonal coefficient matrix C is of size $(N-1)^2 \times (N-1)^2$ and is given by

$$C = \begin{bmatrix}
C_1 & I & & & & \\
I & C_1 & I & & \mathbf{0} & \\
 & I & C_1 & I & & \\
 & & \ddots & \ddots & \ddots & \\
 & \mathbf{0} & & I & C_1 & I \\
 & & & & I & C_1
\end{bmatrix}$$

where I is the identity matrix of size $(N-1) \times (N-1)$ and C_1 is the tridiagonal

matrix of size $(N-1)\times(N-1)$ given by

$$C_1 = \begin{bmatrix} -4I_0(kh) & 1 & 0 & 0 & \cdots & 0 \\ 1 & -4I_0(kh) & 1 & 0 & \cdots & 0 \\ 0 & 1 & -4I_0(kh) & 1 & & \\ & & \ddots & \ddots & \ddots & \\ \vdots & & & 1 & -4I_0(kh) & 1 \\ 0 & \cdots & & 0 & 1 & -4I_0(kh) \end{bmatrix}.$$

On the other hand, the unknown vectors for u^1 and u^2 are of size $(N-1)^2$, and have the same ordering as given in Equation (4.24) in Section 4.1.1. Similarly, the right hand side vectors d_1 and d_2 are the same with b_1 and b_2 given in Equation (4.25), that is $d_1 = b_1$ and $d_2 = b_2$.

4.2.2 Test problem II: Variably conducting side walls with no-slip velocity condition: $c \in (0,\infty)$ at $y \pm \ell$, $\alpha = 0$

The MHD flow is considered in a duct with insulated Hartmann walls (the walls perpendicular to the applied magnetic field) and variably conducting side walls (walls tangential to the applied magnetic field), while the no-slip velocity condition is assumed on all duct walls (see Figure 4.2). In this manner, it is intended to explore the absolute effect of the conductivity parameter $c \in (0,\infty)$ on V and B at various Hartmann numbers.

In this case, we have the same NFD equations given in Equation (4.47) as

$$\begin{aligned} u^i_{m+1,n} + u^i_{m-1,n} - 4I_0(kh)u^i_{m,n} + u^i_{m,n+1} + u^i_{m,n-1} = 0 \\ m = 1,2,...,N-1, \quad n = 0,1,2,\ldots,N, \quad i = 1,2\,. \end{aligned} \tag{4.60}$$

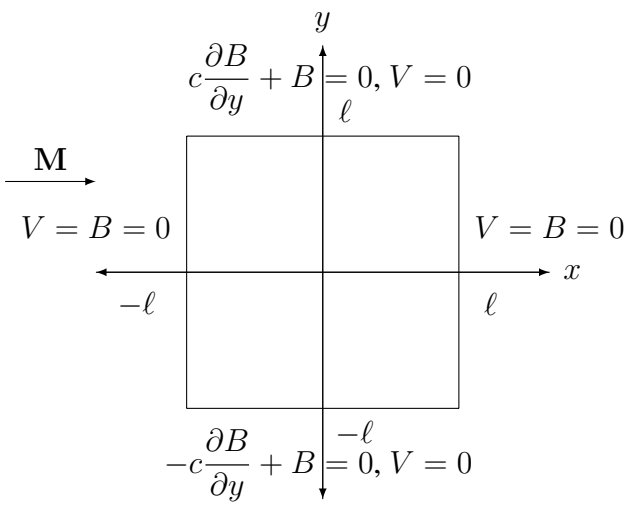


Figure 4.2: Flow configuration and the boundary conditions for Problem II.

The boundary conditions for the no-slip velocity ($V = 0$) at $x = \pm\ell$ are

$$\begin{aligned} u^1_{0,n}e^{-kx_0} + u^2_{0,n}e^{kx_0} &= 0 \quad \text{at } x = x_0 = -\ell, \quad n = 0, 1, ..., N \\ u^1_{N,n}e^{-kx_N} + u^2_{N,n}e^{kx_N} &= 0 \quad \text{at } x = x_N = \ell, \quad n = 0, 1, ..., N \end{aligned} \tag{4.61}$$

and at $y = \pm\ell$ are

$$\begin{aligned} u^1_{m,0}e^{-kx_m} + u^2_{m,0}e^{kx_m} &= 0 \quad \text{at } y = y_0 = -\ell, \quad m = 1, 2, ..., N-1 \\ u^1_{m,N}e^{-kx_m} + u^2_{m,N}e^{kx_m} &= 0 \quad \text{at } y = y_N = \ell, \quad m = 1, 2, ..., N-1. \end{aligned} \tag{4.62}$$

On the other hand, the boundary conditions for B along the insulated walls ($B = 0$, $x = \pm\ell$) are

$$\begin{aligned} u^1_{0,n}e^{-kx_0} - u^2_{0,n}e^{kx_0} &= \frac{x_0}{k} \quad \text{at } x = x_0 = -\ell, \quad n = 0, 1, ..., N \\ u^1_{N,n}e^{-kx_N} - u^2_{N,n}e^{kx_N} &= \frac{x_N}{k} \quad \text{at } x = x_N = \ell, \quad n = 0, 1, ..., N \end{aligned} \tag{4.63}$$

while along the variably conducting walls ($\pm c\frac{\partial B}{\partial y} + B = 0, y = \pm\ell$) they are obtained as

$$\begin{aligned} &(u^1_{m,1}e^{-kx_m} - u^2_{m,1}e^{kx_m}) - 2\sinh(\frac{h}{c})\left(u^1_{m,0}e^{-kx_m} - u^2_{m,0}e^{kx_m} - \frac{x_m}{k}\right) \\ &- (u^1_{m,-1}e^{-kx_m} - u^2_{m,-1}e^{kx_m}) = 0 \quad \text{at } y = y_0 = -\ell, \quad m = 1, 2, ..., N-1 \\ \\ &(u^1_{m,N+1}e^{-kx_m} - u^2_{m,N+1}e^{kx_m}) + 2\sinh(\frac{h}{c})\left(u^1_{m,N}e^{-kx_m} - u^2_{m,N}e^{kx_m} - \frac{x_m}{k}\right) \\ &- (u^1_{m,N-1}e^{-kx_m} - u^2_{m,N-1}e^{kx_m}) = 0 \quad \text{at } y = y_N = \ell, \quad m = 1, 2, ..., N-1. \end{aligned} \tag{4.64}$$

From Equations (4.61) and (4.63), we have boundary conditions at $x = \pm\ell$ as

$$\begin{aligned} u^1_{0,n} &= e^{kx_0}\frac{x_0}{2k} \quad \text{at } x_0 = -\ell \quad \text{and} \quad u^1_{N,n} = e^{kx_N}\frac{x_N}{2k} \quad \text{at } x_N = \ell \\ u^2_{0,n} &= -e^{-kx_0}\frac{x_0}{2k} \quad \text{at } x_0 = -\ell \quad \text{and} \quad u^2_{N,n} = -e^{-kx_N}\frac{x_N}{2k} \quad \text{at } x_N = \ell\,. \end{aligned} \tag{4.65}$$

As we use the new finite difference method derived from the standard central difference method for the derivative boundary conditions, we have ghost points $u^i_{m,-1}$ and $u^i_{m,N+1}$ with $i = 1, 2$ and $m = 1, 2, ..., N-1$. To eliminate them in Equation (4.64), we use the new finite difference formula (4.60) with $n = 0$ and $n = N$, $m = 1, 2, ..., N-1$, that is,

$$\begin{aligned} u^i_{m,-1} &= -u^i_{m+1,0} - u^i_{m-1,0} + 4I_0(kh)u^i_{m,0} - u^i_{m,1} \\ u^i_{m,N+1} &= -u^i_{m+1,N} - u^i_{m-1,N} + 4I_0(kh)u^i_{m,N} - u^i_{m,N-1}\,. \end{aligned} \quad \text{at } i = 1, 2$$

After the substitution of these into Equation (4.64), the finite difference equations for the boundary conditions of B at $y = \pm\ell$ become

$$\begin{aligned} &2u^1_{m,1}e^{-kx_m} - 2u^2_{m,1}e^{kx_m} + (-2\sinh(\frac{h}{c}) - 4I_0(kh))u^1_{m,0}e^{-kx_m} \\ &+ (2\sinh(\frac{h}{c}) + 4I_0(kh))u^2_{m,0}e^{kx_m} + e^{-kx_m}(u^1_{m+1,0} + u^1_{m-1,0}) \\ &+ e^{kx_m}(-u^2_{m+1,0} - u^2_{m-1,0}) = -2\sinh(\frac{h}{c})\frac{x_m}{k} \quad \text{at } y = y_0 = -\ell, \quad m = 1, 2, ..., N-1 \\ &- 2u^1_{m,N-1}e^{-kx_m} + 2u^2_{m,N-1}e^{kx_m} + (2\sinh(\frac{h}{c}) + 4I_0(kh))u^1_{m,N}e^{-kx_m} \\ &+ (-2\sinh(\frac{h}{c}) - 4I_0(kh))u^2_{m,N}e^{kx_m} + e^{-kx_m}(-u^1_{m+1,N} - u^1_{m-1,N}) \\ &+ e^{kx_m}(u^2_{m+1,N} + u^2_{m-1,N}) = 2\sinh(\frac{h}{c})\frac{x_m}{k} \quad \text{at } y = y_N = \ell, \quad m = 1, 2, ..., N-1. \end{aligned} \tag{4.66}$$

Finally, the new finite difference equations for the modified Helmholtz equations (4.3) at the interior points become

$$\begin{aligned} u^i_{m+1,n} + u^i_{m-1,n} - 4I_0(kh)u^i_{m,n} + u^i_{m,n+1} + u^i_{m,n-1} = 0 \\ m, n = 1, 2, ..., N-1, \quad i = 1, 2\,. \end{aligned} \tag{4.67}$$

When the boundary conditions (4.62), (4.65) and (4.66) for the values of $c \in (0, \infty)$, which are coupled in u^1 and u^2, are inserted in the difference equation (4.67), we have the system of linear equations

$$Cu = d\,. \tag{4.68}$$

The unknown vector u of size $(2N+2)(N-1)$ has the ordering as

$$u = \begin{bmatrix} \vec{u}^1 & | & \vec{u}^2 \end{bmatrix}^T \tag{4.69}$$

where $\vec{u}^1$ and $\vec{u}^2$ are subvectors of sizes $(N+1)(N-1)$ given by

$$\vec{u}^1 = \begin{bmatrix} u^1_{1,1} & u^1_{2,1} & \cdots & u^1_{N-1,1} & | & u^1_{1,2} & u^1_{2,2} & \cdots & u^1_{N-1,2} & | & \cdots & | & u^1_{1,N-1} & u^1_{2,N-1} & \cdots & u^1_{N-1,N-1} \end{bmatrix}^T,$$
$$\vec{u}^2 = \begin{bmatrix} u^2_{1,1} & u^2_{2,1} & \cdots & u^2_{N-1,1} & | & u^2_{1,2} & u^2_{2,2} & \cdots & u^2_{N-1,2} & | & \cdots & | & u^2_{1,N-1} & u^2_{2,N-1} & \cdots & u^2_{N-1,N-1} \end{bmatrix}^T.$$

The right hand side vector d of size $(2N+2)(N-1)$ is given by

$$d = \begin{bmatrix} d_1 & | & d_2 \end{bmatrix}^T \tag{4.70}$$

where d_1 and d_2 are subvectors of sizes $(N+1)(N-1)$

$$d_1 = \begin{bmatrix} d_{1,1} & | & d_{1,2} & | & d_{1,2} & | & \cdots & | & d_{1,2} & | & d_{1,2} & | & d_{1,1} \end{bmatrix}^T,$$
$$d_2 = \begin{bmatrix} d_{2,1} & | & d_{2,2} & | & d_{2,2} & | & \cdots & | & d_{2,2} & | & d_{2,2} & | & d_{2,1} \end{bmatrix}^T.$$

The subvectors $d_{1,1}$, $d_{1,2}$, $d_{2,1}$, and $d_{2,2}$ of sizes $(N-1)$ are given by

$$\begin{aligned}
d_{1,1} &= \begin{bmatrix} (-2\sinh(\frac{h}{c})\frac{x_1}{k} - \frac{x_0}{2k}(e^{-kh}+e^{kh})) & -2\sinh(\frac{h}{c})\frac{x_2}{k} & \cdots & -2\sinh(\frac{h}{c})\frac{x_{N-2}}{k} & (-2\sinh(\frac{h}{c})\frac{x_{N-1}}{k} - \frac{x_N}{2k}(e^{-kh}+e^{kh})) \end{bmatrix}^T \\
d_{1,2} &= \begin{bmatrix} -\frac{x_0}{2k}e^{kx_0} & 0 & \cdots & 0 & -\frac{x_N}{2k}e^{kx_N} \end{bmatrix}^T \\
d_{2,1} &= \begin{bmatrix} 0 & 0 & \cdots & 0 & 0 \end{bmatrix}^T \\
d_{2,2} &= \begin{bmatrix} \frac{x_0}{2k}e^{-kx_0} & 0 & \cdots & 0 & \frac{x_N}{2k}e^{-kx_N} \end{bmatrix}^T.
\end{aligned} \tag{4.71}$$

Under the ordering of unknown vector u, the coefficient matrix C of size $(2N+2)(N-1)\times(2N+2)(N-1)$ can be written in terms of block matrices C_i, $i = 1,2,3,4$ of sizes $(N+1)(N-1)\times(N+1)(N-1)$ as follows:

$$C = \begin{bmatrix} C_1 & C_2 \\ C_3 & C_4 \end{bmatrix}. \tag{4.72}$$

Here, C_1 is equal to

$$C_1 = \begin{bmatrix} C_{1,1} & C_{1,2} & & & & \\ I & C_{1,3} & I & & \mathbf{0} & \\ & I & C_{1,3} & I & & \\ & & \ddots & \ddots & \ddots & \\ & \mathbf{0} & & I & C_{1,3} & I \\ & & & & C_{1,2} & C_{1,1} \end{bmatrix} \tag{4.73}$$

where I is the identity matrix of size $(N-1)\times(N-1)$ and $C_{1,1}$, $C_{1,2}$, and $C_{1,3}$ are submatrices of sizes $(N-1)\times(N-1)$ with

$$C_{1,1}=\begin{cases}(-2\sinh(\frac{h}{c})-4I_0(kh))e^{-kx_i} & \text{if } i=j\\ e^{-kx_i} & \text{if } \mid i-j\mid=1\\ 0 & \text{otherwise ,}\end{cases} \tag{4.74}$$

and

$$C_{1,2}=\begin{cases}2e^{-kx_i} & \text{if } i=j\\ 0 & \text{otherwise ,}\end{cases} \tag{4.75}$$

and

$$C_{1,3}=\begin{cases}-4I_0(kh) & \text{if } i=j\\ 1 & \text{if } \mid i-j\mid=1\\ 0 & \text{otherwise .}\end{cases} \tag{4.76}$$

The second block tridiagonal matrix C_2 is

$$C_2=\begin{bmatrix}C_{2,1} & C_{2,2} & & 0\\ & & 0 & \\ 0 & & C_{2,2} & C_{2,1}\end{bmatrix} \tag{4.77}$$

where $C_{2,1}$ and $C_{2,2}$ are also tridiagonal matrices of sizes $(N-1)\times(N-1)$ with

$$C_{2,1}=\begin{cases}(2\sinh(\frac{h}{c})+4I_0(kh))e^{kx_i} & \text{if } i=j\\ -e^{kx_i} & \text{if } \mid i-j\mid=1\\ 0 & \text{otherwise ,}\end{cases} \tag{4.78}$$

and

$$C_{2,2}=\begin{cases}-2e^{kx_i} & \text{if } i=j\\ 0 & \text{otherwise .}\end{cases} \tag{4.79}$$

The third matrix C_3 has the form

$$C_3 = \begin{bmatrix} C_{3,1} & & 0 \\ & 0 & \\ 0 & & C_{3,1} \end{bmatrix} \tag{4.80}$$

where $C_{3,1}$ is a submatrix of size $(N-1)\times(N-1)$ which is given by

$$C_{3,1} = \begin{cases} e^{-kx_i} & \text{if } i = j \\ 0 & \text{otherwise .} \end{cases} \tag{4.81}$$

Finally, the block tridiagonal matrix C_4 has the form

$$C_4 = \begin{bmatrix} C_{4,1} & & & & \\ I & C_{4,2} & I & & 0 \\ & I & C_{4,2} & I & \\ & & \ddots & \ddots & \ddots \\ & 0 & & I & C_{4,2} & I \\ & & & & & C_{4,1} \end{bmatrix} \tag{4.82}$$

where $C_{4,1}$ and $C_{4,2}$ are the submatrices of sizes $(N-1)\times(N-1)$ with the following entries:

$$C_{4,1} = \begin{cases} e^{kx_i} & \text{if } i = j \\ 0 & \text{otherwise ,} \end{cases} \tag{4.83}$$

and

$$C_{4,2} = \begin{cases} -4I_0(kh) & \text{if } i = j \\ 1 & \text{if } \mid i-j \mid = 1 \\ 0 & \text{otherwise .} \end{cases} \tag{4.84}$$

As mentioned, the system (4.68) is obtained for the non-zero and finite conductivity parameter, that is $c \in (0,\infty)$. The case when the walls are all insulated (i.e. $c = 0$) was considered in Problem I. On the other hand, when the side duct walls are perfectly conducting, that is $c = \infty$ and $\pm\dfrac{\partial B}{\partial y} = 0$ at $y = \pm\ell$, the matrix-vector form of the problem is obtained from the system (4.68) by computing the coefficients of the

matrices $C_{1,1}$ in Equation (4.73) and $C_{2,1}$ in Equation (4.77) as $c \to \infty$. That is, in coefficient matrix C only the matrices $C_{1,1}$ and $C_{2,1}$ change, and they reduce to

$$C_{1,1} = \begin{cases} -4I_0(kh)e^{-kx_i} & \text{if } i = j \\ e^{-kx_i} & \text{if } \mid i-j \mid = 1 \\ 0 & \text{otherwise ,} \end{cases} \tag{4.85}$$

and

$$C_{2,1} = \begin{cases} 4I_0(kh)e^{kx_i} & \text{if } i = j \\ -e^{kx_i} & \text{if } \mid i-j \mid = 1 \\ 0 & \text{otherwise} \end{cases} . \tag{4.86}$$

Similarly, the right-hand side vector is also obtained from the vector d given in Equation (4.70) by computing the related entries as $c \to \infty$. That is, only the $d_{1,1}$ subvector of d defined in Equation (4.71) alters and it reduces to

$$d_{1,1} = \left[-\frac{x_0}{2k}(e^{-kh} + e^{kh}) \quad 0 \quad \cdots \quad 0 \quad -\frac{x_N}{2k}(e^{-kh} + e^{kh}) \right]^T$$

for the case when the side walls are perfectly conducting.

4.2.3 Test Problem III: Insulated duct with slippery side walls: $c = 0$, $\alpha \neq 0$ at $y = \pm\ell$

This section focuses on developing the matrix-vector form of the NFD equations for the MHD duct flow in the presence of slippery duct walls. In order to investigate the absolute influence of the slip length on the velocity and the induced magnetic field, the MHD flow is considered in a duct with the side walls taken as slippery while all the walls are thought to be electrically insulated (see Figure 4.3).

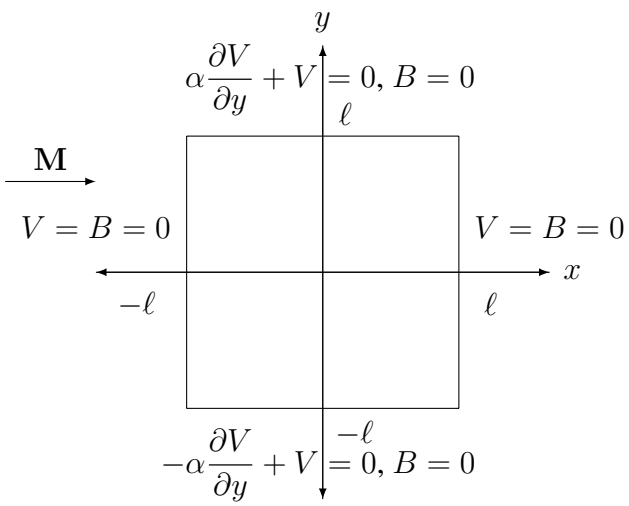


Figure 4.3: Flow configuration and the boundary conditions for Problem III.

The new finite difference equations for the modified Helmholtz equations (4.3) is the same with Equation (4.47) as well and it is given as

$$\begin{gathered} u^i_{m+1,n}+u^i_{m-1,n}-4I_0(kh)u^i_{m,n}+u^i_{m,n+1}+u^i_{m,n-1}=0 \\ m=1,2,...,N-1, \quad n=0,1,2,\ldots,N, \quad i=1,2\,. \end{gathered} \tag{4.87}$$

In this problem, the difference equations of V and B along the Hartmann walls $x=\pm\ell$ are the same with the ones given in Equations (4.61) and (4.63) since we have $V=B=0$ at $x=\pm\ell$ as in Problem II. By combining Equations (4.61) and (4.63), one can obtain the boundary conditions along $x=\pm\ell$ in terms of u^1 and u^2 as follows:

$$\begin{aligned} u^1_{0,n}&=e^{kx_0}\frac{x_0}{2k} \quad \text{at } x_0=-\ell \quad \text{and} \quad u^1_{N,n}=e^{kx_N}\frac{x_N}{2k} \quad \text{at } x_N=\ell \\ u^2_{0,n}&=-e^{-kx_0}\frac{x_0}{2k} \quad \text{at } x_0=-\ell \quad \text{and} \quad u^2_{N,n}=-e^{-kx_N}\frac{x_N}{2k} \quad \text{at } x_N=\ell\,. \end{aligned} \tag{4.88}$$

On the other hand, due to slip velocity condition ($\pm\alpha\dfrac{\partial V}{\partial y}+V=0$) at $y=\pm\ell$, the

NFD equations for V along these boundaries become (see Equation (4.54))

$$
\begin{aligned}
&(u^1_{m,1}e^{-kx_m} + u^2_{m,1}e^{kx_m}) - 2\sinh(\frac{h}{\alpha})(u^1_{m,0}e^{-kx_m} + u^2_{m,0}e^{kx_m}) \\
&- (u^1_{m,-1}e^{-kx_m} + u^2_{m,-1}e^{kx_m}) = 0 \quad \text{at } y = y_0 = -\ell, \quad m = 1, 2, ..., N-1 \\
&(u^1_{m,N+1}e^{-kx_m} + u^2_{m,N+1}e^{kx_m}) + 2\sinh(\frac{h}{\alpha})\left(u^1_{m,N}e^{-kx_m} + u^2_{m,N}e^{kx_m}\right) \\
&- (u^1_{m,N-1}e^{-kx_m} + u^2_{m,N-1}e^{kx_m}) = 0 \quad \text{at } y = y_N = \ell, \quad m = 1, 2, ..., N-1.
\end{aligned}
\tag{4.89}
$$

Finally, the boundary conditions for ($B = 0$) along the side walls $y = \pm\ell$ become

$$
\begin{aligned}
u^1_{m,0}e^{-kx_m} - u^2_{m,0}e^{kx_m} &= \frac{x_m}{k} \quad \text{at } y = y_0 = -\ell, \quad m = 1, 2, ..., N-1 \\
u^1_{m,N}e^{-kx_m} - u^2_{m,N}e^{kx_m} &= \frac{x_m}{k} \quad \text{at } y = y_N = \ell, \quad m = 1, 2, ..., N-1.
\end{aligned}
\tag{4.90}
$$

The ghost points $u^i_{m,-1}$ and $u^i_{m,N+1}$ ($i = 1, 2$ and $m = 1, 2, ..., N-1$) occurring in Equation (4.89) are eliminated by the use of NFD formula (4.87) with $n = 0$ and $n = N$, $m = 1, 2, ..., N-1$. That is,

$$
\begin{aligned}
u^i_{m,-1} &= -u^i_{m+1,0} - u^i_{m-1,0} + 4I_0(kh)u^i_{m,0} - u^i_{m,1} \\
u^i_{m,N+1} &= -u^i_{m+1,N} - u^i_{m-1,N} + 4I_0(kh)u^i_{m,N} - u^i_{m,N-1}\,.
\end{aligned}
\qquad \text{at } i = 1, 2
$$

After the substitution of these into Equation (4.89), the finite difference equations for the velocity boundary condition at $y = \pm\ell$ become

$$
\begin{aligned}
&2u^1_{m,1}e^{-kx_m} + 2u^2_{m,1}e^{kx_m} + (-2\sinh(\frac{h}{\alpha}) - 4I_0(kh))u^1_{m,0}e^{-kx_m} \\
&+ (-2\sinh(\frac{h}{\alpha}) - 4I_0(kh))u^2_{m,0}e^{kx_m} + e^{-kx_m}(u^1_{m+1,0} + u^1_{m-1,0}) \\
&+ e^{kx_m}(u^2_{m+1,0} + u^2_{m-1,0}) = 0 \quad \text{at } y = y_0 = -\ell, \quad m = 1, 2, ..., N-1 \\
&- 2u^1_{m,N-1}e^{-kx_m} - 2u^2_{m,N-1}e^{kx_m} + (2\sinh(\frac{h}{\alpha}) + 4I_0(kh))u^1_{m,N}e^{-kx_m} \\
&+ (2\sinh(\frac{h}{\alpha}) + 4I_0(kh))u^2_{m,N}e^{kx_m} + e^{-kx_m}(-u^1_{m+1,N} - u^1_{m-1,N}) \\
&+ e^{kx_m}(-u^2_{m+1,N} - u^2_{m-1,N}) = 0 \quad \text{at } y = y_N = \ell, \quad m = 1, 2, ..., N-1.
\end{aligned}
\tag{4.91}
$$

Finally, the new finite difference equations for the modified Helmholtz equations at the interior points become

$$
\begin{aligned}
u^i_{m+1,n} + u^i_{m-1,n} - 4I_0(kh)u^i_{m,n} + u^i_{m,n+1} + u^i_{m,n-1} &= 0 \\
m, n = 1, 2, ..., N-1, \quad i = 1, 2\,.&
\end{aligned}
\tag{4.92}
$$

The insertion of these boundary conditions in Equation (4.92), one can end up with a system of linear equations as

$$Cu = d\,. \tag{4.93}$$

The unknown vector u and d of sizes $(2N+2)(N-1)$ have the same ordering as given in Equations (4.69) and (4.70). However, due to the insulated walls ($B = 0$, $c = 0$), only the subvectors $d_{1,1}$ and $d_{2,2}$ of the vector d change and they become

$$d_{1,1} = \left[\frac{x_0}{2k}(-e^{-kh} + e^{kh}) \quad 0 \quad \cdots \quad 0 \quad \frac{x_N}{2k}(e^{-kh} - e^{kh})\right]^T$$
$$d_{2,1} = \left[\frac{x_1}{k} \quad \frac{x_2}{k} \quad \cdots \quad \frac{x_{N-2}}{k} \quad \frac{x_{N-1}}{k}\right]^T .$$

The coefficient matrix C of size $(2N+2)(N-1) \times (2N+2)(N-1)$ is in the same form with the one given in Equation (4.68), however, due to slip velocity conditions at side walls, the submatrices $C_{1,1}$, $C_{2,1}$, $C_{2,2}$ and $C_{4,1}$ of sizes $(N-1) \times (N-1)$ are different when compared with the ones in Problem II. That is, these submatrices are given as follows:

$$C_{1,1} = \begin{cases} (-2\sinh(\dfrac{h}{\alpha}) - 4I_0(kh))e^{-kx_i} & \text{if } i = j \\ e^{-kx_i} & \text{if } \mid i-j \mid = 1 \\ 0 & \text{otherwise ,} \end{cases} \tag{4.94}$$

$$C_{2,1} = \begin{cases} (-2\sinh(\dfrac{h}{\alpha}) - 4I_0(kh))e^{kx_i} & \text{if } i = j \\ e^{kx_i} & \text{if } \mid i-j \mid = 1 \\ 0 & \text{otherwise ,} \end{cases} \tag{4.95}$$

$$C_{2,2} = \begin{cases} 2e^{kx_i} & \text{if } i = j \\ 0 & \text{otherwise ,} \end{cases} \tag{4.96}$$

and

$$C_{4,1} = \begin{cases} -e^{kx_i} & \text{if } i = j \\ 0 & \text{otherwise .} \end{cases} \tag{4.97}$$

To conclude, in all test problems when the resulting linear systems are solved, the unknown values of u^1 and u^2 are obtained at both the interior and/or boundary grid points. Then, by using back substitutions (4.6) the solutions are obtained for the original variables velocity V and induced magnetic field B.

4.3 Numerical results for two-dimensional MHD duct flow

The numerical calculations are performed for three MHD duct flow problems described by using different types of boundary conditions as mentioned in previous Section 4.2. The flow is driven in the direction of an infinite channel axis with a rectangular cross-section subject to a uniform constant horizontally applied magnetic field. The computational domain is determined as a square duct taking $\ell_x = \ell_y = \ell = 1$ in all test problems. The flow behavior under the influence of variably conducting walls with no-slip or slip velocity conditions are examined for numerous values of Hartmann number, $5 \leq M \leq 100$.

4.3.1 Test Problem I: no-slip and insulated walls: $c = \alpha = 0$

The MHD flow in a duct with no-slip and insulated walls, which is regarded as the benchmark for the MHD duct flow and has the analytical solution by Shercliff [2], is solved by SFD and NFD methods. The validity of the numerical algorithms for SFD and NFD is evaluated quantitatively by means of relative errors and volumetric flow rates. The relative errors between the exact and approximate V and B values obtained by NFD and SFD schemes are tabulated in Table 4.1 at different numbers of subintervals N when $M = 100$. It is observed that the NFD method achieves significantly more precise results than the SFD scheme at each N as in the one-dimensional MHD

Table 4.1: Relative errors for SFD and NFD at $M = 100$ in Problem I

		SFD		NFD	
N	h	e_V	e_B	e_V	e_B
40	0.0500	3.5389e+06	3.7518e+06	20.3921	21.5122
80	0.0250	113.4969	120.1656	1.4397	1.4889
100	0.0200	18.9969	20.0905	0.7535	0.7738
200	0.0100	0.8496	0.8750	0.1428	0.1443
240	0.0083	0.5046	0.5162	0.0964	0.0972
320	0.00625	0.2443	0.2480	0.0527	0.0530
400	0.0050	0.1461	0.1478	0.0333	0.0335

problem. That is, the relative error is around 10^{-2} when $N = 320$ while it is around 10^{-1} in SFD scheme. A finer mesh is required in both methods at high $M = 100$ for smaller errors.

Furthermore, the numerical results in terms of volumetric flow rate,

$$Q = \int_{\Omega} V d\Omega, \qquad \Omega = \{(x, y) \mid -1 < x, y < 1\} \tag{4.98}$$

obtained by SFD and NFD schemes namely Q^{sfd} and Q^{nfd}, are compared with the analytical ones, Q^{exact}, determined from the theoretical solution given in Shercliff [2] in Table 4.2 at various M. The well agreement of the numerical results, especially the ones obtained by NFD scheme, with the exact ones is observed at each M by using enough number of subintervals N. It is also noted that the flow rate decreases as the intensity of the magnetic field increases.

Table 4.2: Volumetric flow rate for Problem I

M	N	Q^{exact}	Q^{sfd}	Q^{nfd}
5	80	0.3926	0.3927	0.3926
10	100	0.2607	0.2612	0.2608
25	120	0.1270	0.1298	0.1278
50	280	0.0689	0.0711	0.0695
100	400	0.0362	0.0412	0.0374

The choice of the number of subintervals N at $M = 100$ is determined in accordance with tests on the distributions of maximum values V^{max} and B^{max}, and also the variations of the mean bulk velocity, ($V^{mb} = \frac{1}{A(\Omega)} \int_{\Omega} V d\Omega$, where $A(\Omega)$ is the area of computational domain Ω), and mean bulk induced magnetic field, ($B^{mb} = \frac{1}{A(\Omega)} \int_{\Omega} B d\Omega$), with respect to the number of subintervals N. That is, Figure 4.4 displays the variations of the exact, SFD and NFD maximum velocity and induced magnetic field values with respect to N along the horizontal centerline $y = 0$, whereas the variations of mean bulk V and B versus N are shown in Figure 4.5. The findings shown in these figures display that when $N \approx 240$ in NFD and $N \approx 360$ in SFD, sufficient convergence to the exact values is attained, and higher values of N no longer produce a discernible change in the maximum and mean bulk values. As a result, $N \leq 240$ in the NFD scheme and $N \leq 360$ in the SFD scheme are used at Hartmann

values $M \leq 100$ to discretize the computational domain for the calculations that follow in this problem. As in the one-dimensional MHD flow in Chapter 3, the SFD scheme requires a finer mesh when compared to the one used in the NFD scheme in two-dimension as well.

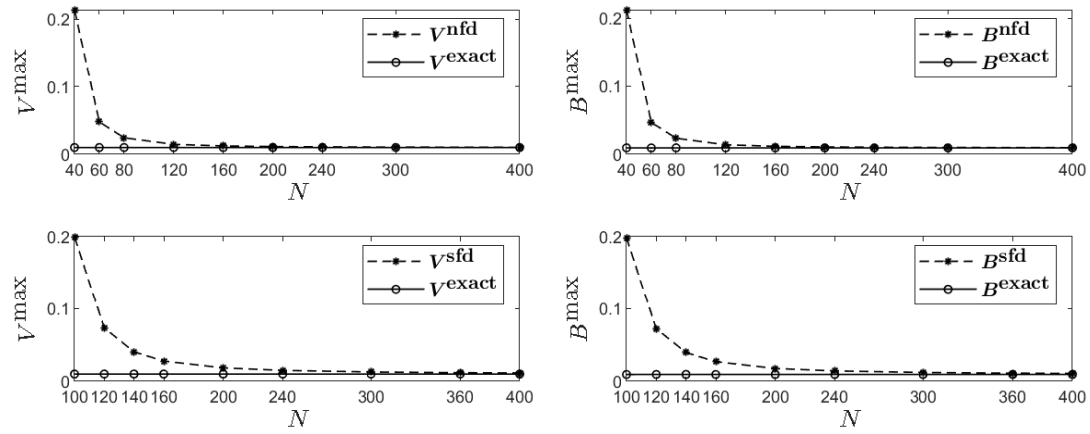


Figure 4.4: Grid dependency test for Problem I: $\alpha = c = 0$, $M = 100$ along $y = 0$.

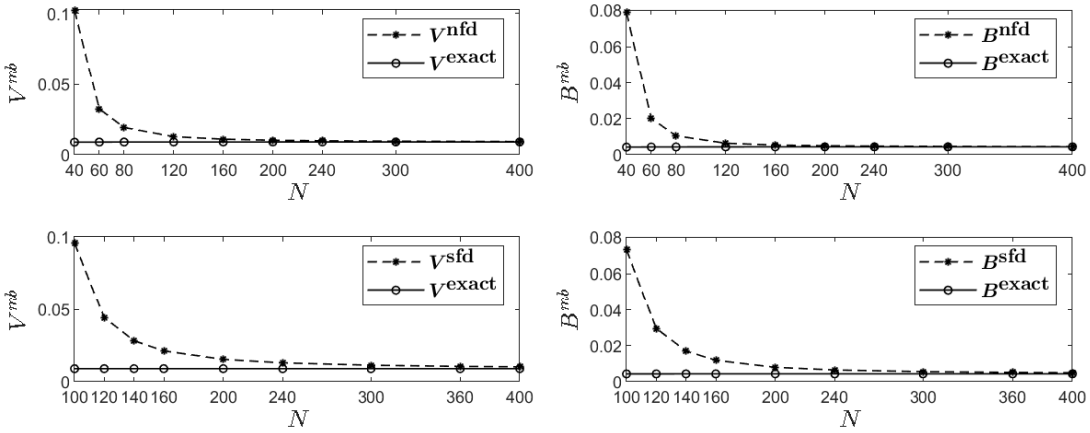
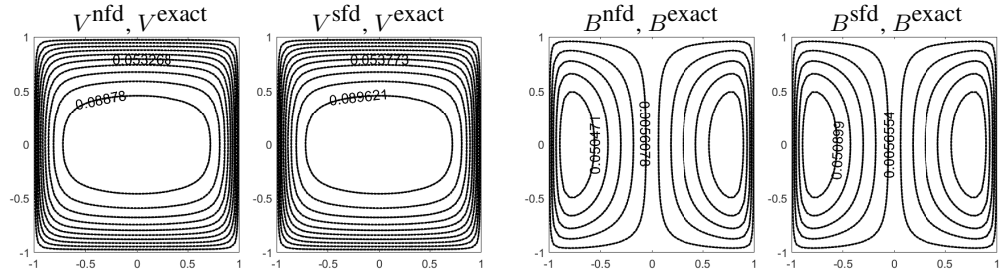
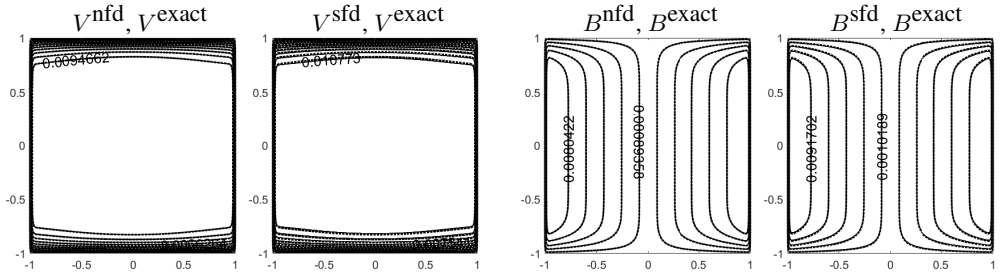


Figure 4.5: Grid dependency test for Problem I: $\alpha = c = 0$, $M = 100$.

A qualitative comparison between the numerical results obtained by SFD and NFD schemes with the exact ones in terms of equivelocity and induced magnetic field contours is demonstrated in Figure 4.6 for $M = 10$, $N = 40$ and $M = 100$, $N = 360$. The NFD scheme produces better results than the SFD scheme when the same grid is used in both methods at each $M = 10,\ 100$. The flow becomes stagnant at the center of the duct and boundary layers are formed along the vertical walls in the profiles of both V and B as M increases.

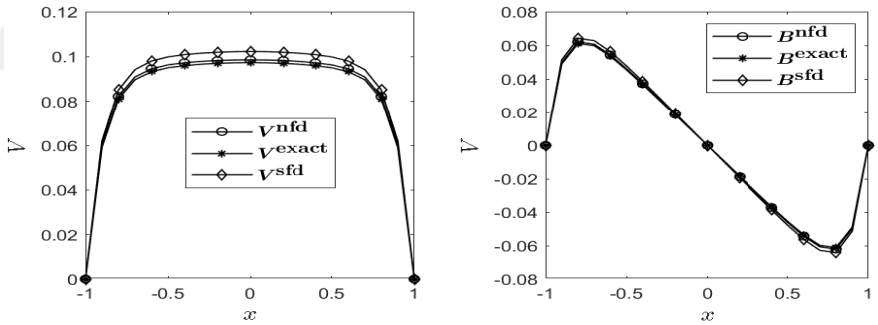


a) $M = 10$, $N = 40$

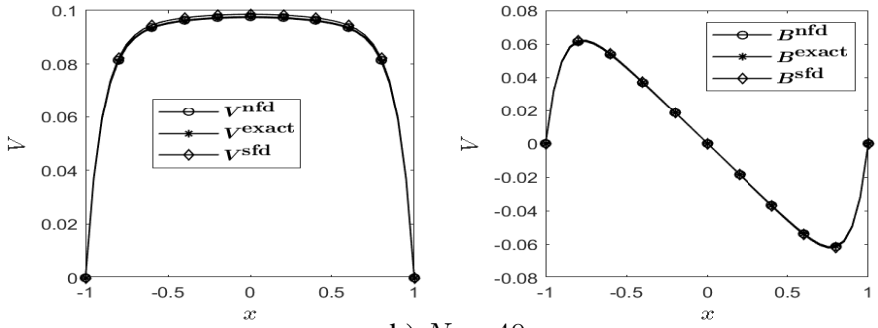


b) $M = 100$, $N = 360$

Figure 4.6: Problem I: Comparison of the numerical solutions by SFD (solid) and NFD (solid) with exact solution (dotted) at $M = 10,\ 100$.



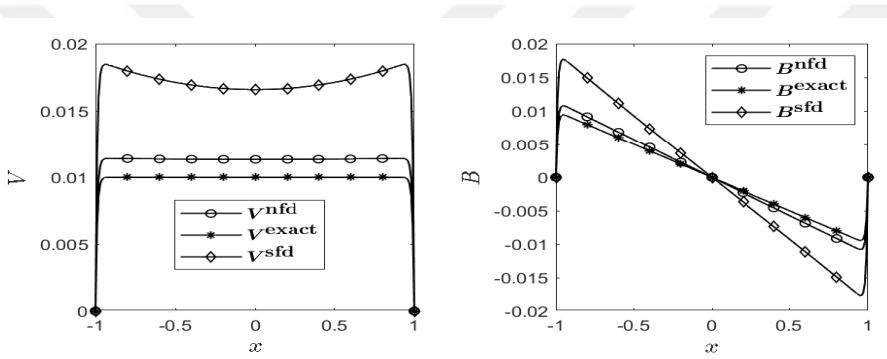
a) $N = 20$



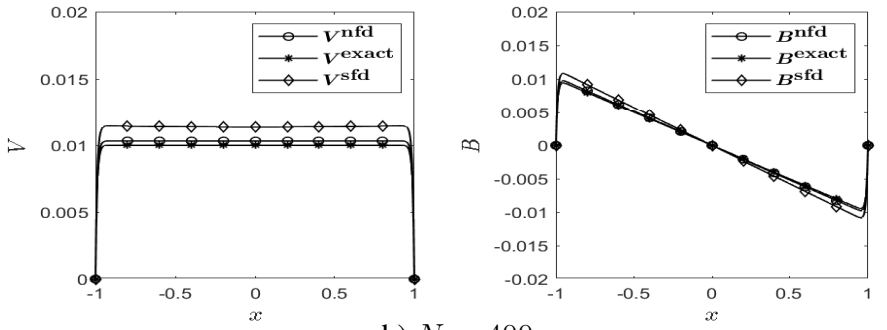
b) $N = 40$

Figure 4.7: Problem I: Variations of the velocity and induced magnetic field along $y = 0$ at $M = 10$.

In Figures 4.7 and 4.8, the velocity and induced magnetic field profiles are drawn along the horizontal centerline $y = 0$ to validate the numerical results produced by the SFD and NFD against the analytical solutions when $M = 10$, $N = 20, 40$, and $M = 100$, $N = 200, 400$. At small $M = 10$, both NFD and SFD results agree well with the exact ones when an appropriate mesh (i.e. one needs to take $N = 40$ for SFD while even $N = 20$ is enough for the NFD scheme) is taken. On the other hand, at high $M = 100$, although both of the methods experience deviations from the exact solution along the horizontal centerline $y = 0$, especially for the velocity the NFD scheme gives much better results and it requires a coarser mesh in each case when compared to SFD method. As a result, in the subsequent calculations and the test problems only the numerical results obtained by using the NFD scheme are provided.



a) $N = 200$



b) $N = 400$

Figure 4.8: Problem I: Variations of the velocity and induced magnetic field along $y = 0$ at $M = 100$.

Finally, to investigate the effect of the Hartmann number on the V and B, a number of simulations for M values ranging from $M = 5$ to $M = 100$ are performed, and the findings are visualized in Figure 4.9. The magnitudes of the velocity and the induced magnetic both decrease with an increase in M, which is the well-known flattening tendency of the MHD flow, and it happens when the strength of the magnetic field that

is being applied externally increases by bigger values of M as observed in Chapter 3 for one-dimensional MHD flow.

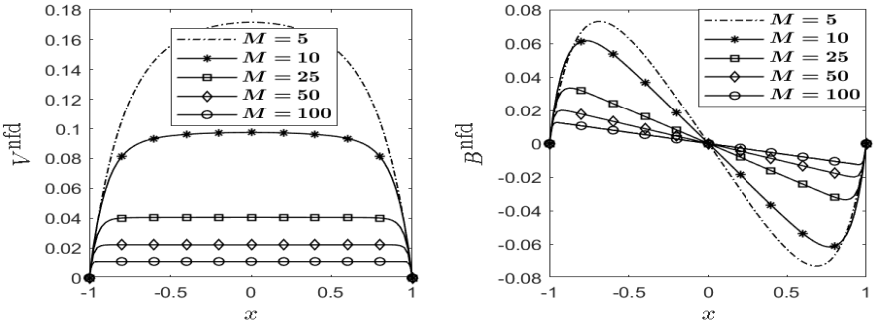


Figure 4.9: Problem I: Effect of M on V and B along $y = 0$ by using NFD scheme with $N = 80$ for $5 \leq M \leq 50$, and $N = 240$ for $M = 100$.

4.3.2 Test Problem II: Variably conducting side walls with no-slip velocity condition: $c \in (0, \infty)$ at $y = \pm 1$, $\alpha = 0$

In this problem, numerical simulations utilizing NFD scheme are carried out for $5 \leq M \leq 50$ to explore the effect of the conductivity parameter $c \in (0, \infty)$ on V and B at various Hartmann values. The number of subintervals N is chosen depending on the grid dependency test, which is performed using different grid sizes in terms of $V^{\max}$ and $B^{\max}$ along the horizontal centerline $y = 0$ at a moderate $M = 35$ and with the conductivity of $c = 2$. Figure 4.10 shows that $N = 128$ is enough since the maximum V and B values do not significantly change as N increases further to $N = 256$. Therefore, in this problem, the domain is discretized by utilizing $N = 128$ subintervals for each Hartmann number.

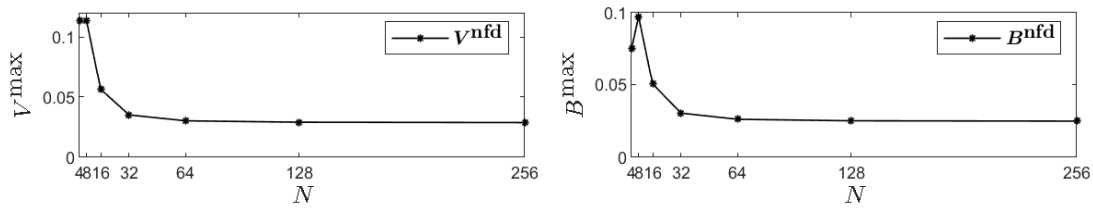
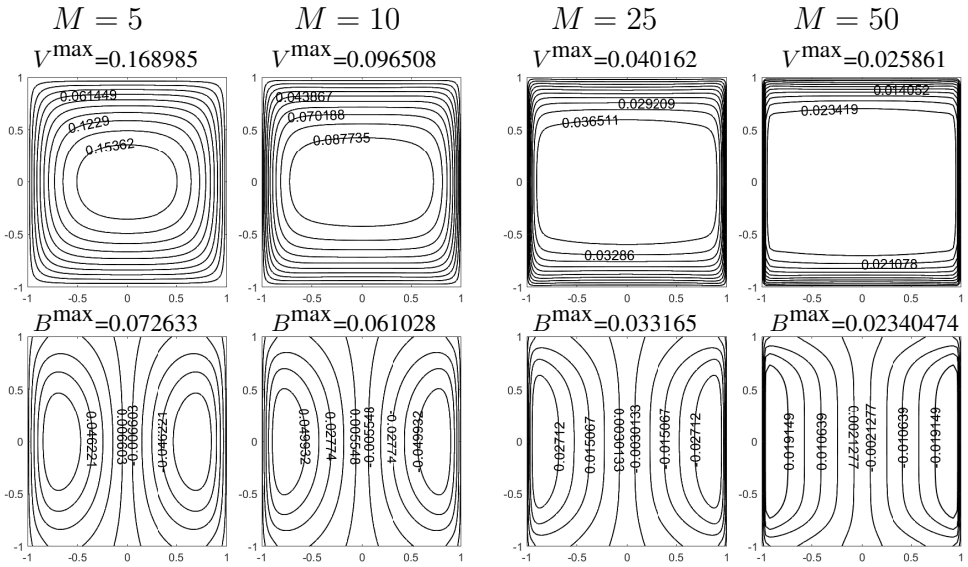


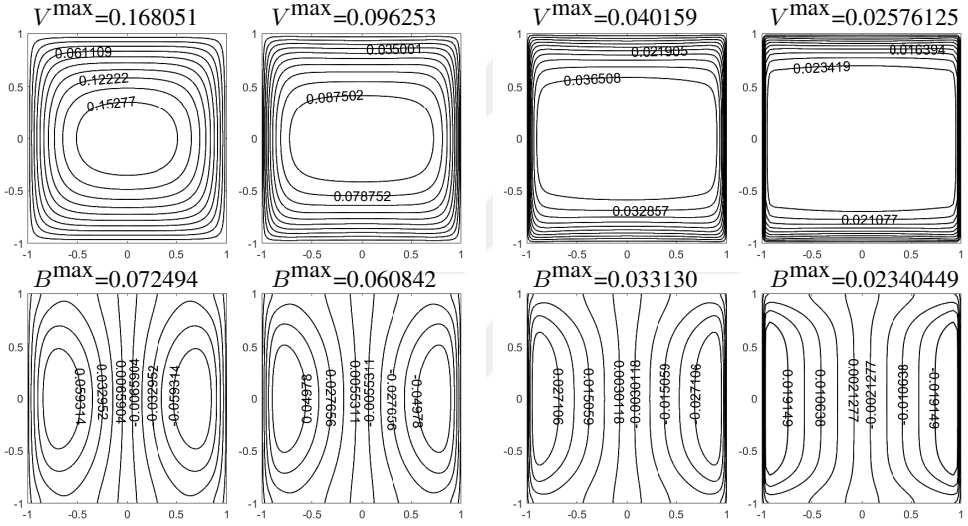
Figure 4.10: Grid dependency test for Problem II: $\alpha = 0$, $c = 2$, $M = 35$ along $y = 0$.

Figure 4.11 illustrates equivelocity and the induced magnetic field lines with increasing values of conductivity parameter c at the side walls $y = \pm 1$ for various Hartmann numbers, $M = 5,\ 10,\ 25,\ 50$. The maximum values of the velocity and the induced magnetic field throughout the duct are also shown in this figure. It is observed that an increase in the conductivity parameter c results in a slight decrease in the magnitudes of both the velocity and the induced magnetic field at each Hartmann number through the whole duct, which agrees with the results obtained in the work of [28]. Additionally, the induced magnetic field lines tend to strike the variably conducting side walls more perpendicularly as c increases. When the side walls become perfectly conducting, that is $c = \infty$, the magnetic field lines become fully perpendicular to the side walls [5]. On the other hand, as M increases both V and B decrease in magnitude as previously mentioned, and the flow becomes uniform at the center of the duct, while the core of the vortices in B are elongated vertically forming a boundary layer along the vertical Hartmann walls.

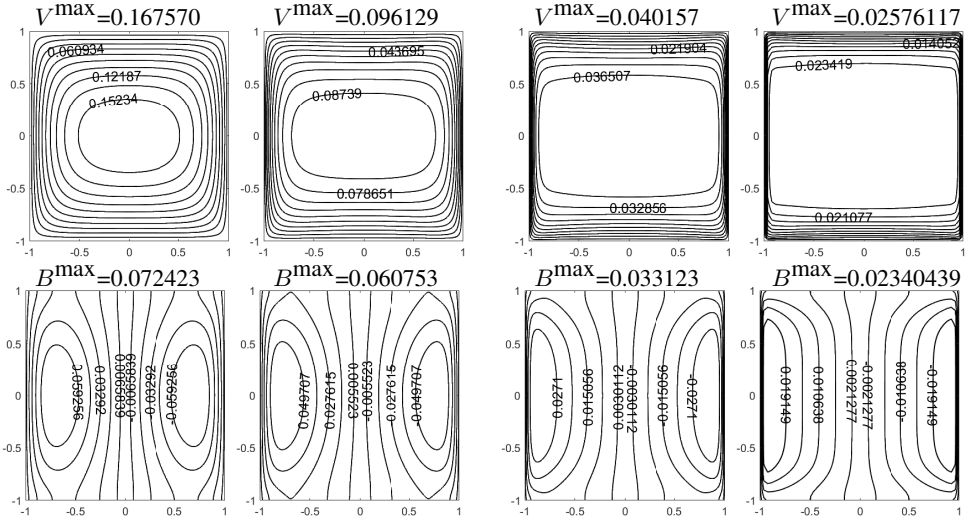
The impacts of the conductivity parameter $c\ (= 0,\ 0.1,\ 0.5,\ 1,\ 5,\ \infty)$ and Hartmann number $M = 10,\ 35$ on the variations of the velocity and the induced magnetic field are displayed along the horizontal centerline $y = 0$ in Figure 4.12 and along the line $y \approx 0.9844$ (which is close to conducting upper side wall $y = 1$) in Figure 4.13. It is observed that the conductivity parameter c has almost no effect on the velocity and induced magnetic field profiles along the centerline $y = 0$ as expected since the line $y = 0$ is far from the conductivity effect along $y = \pm 1$. On the other hand, the velocity shows an M-line profile along the line $y \approx 0.9844$. Then, an increase in c improves the velocity magnitude in the region close to vertical walls, while it reduces the velocity at the central region along the line $y \approx 0.9844$. The M-shaped is more pronounced at $M = 35$ following the stronger increase in V close to vertical walls as c increases. On the other hand, the B values are increased in magnitude as c increases, but the increase rate decreases at higher M due to the suppressing effect of M on the conductivity parameter.



a) $c = 0.5$

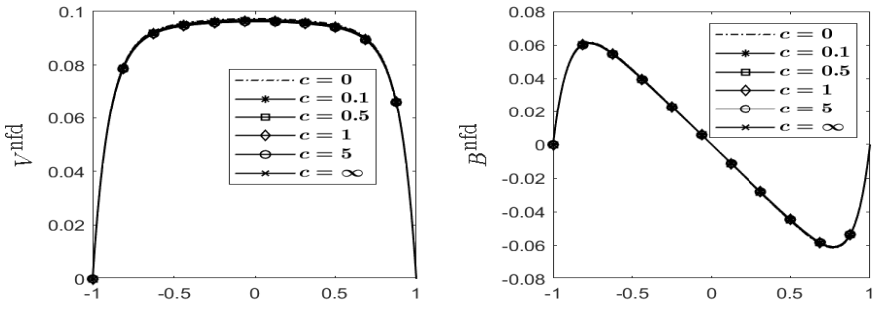


b) $c = 2$

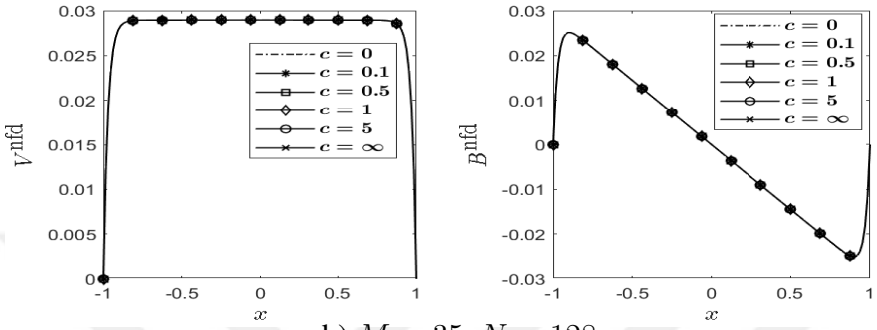


c) $c = \infty$

Figure 4.11: Problem II: Effects of M and c on velocity and induced magnetic field, $N = 128$.

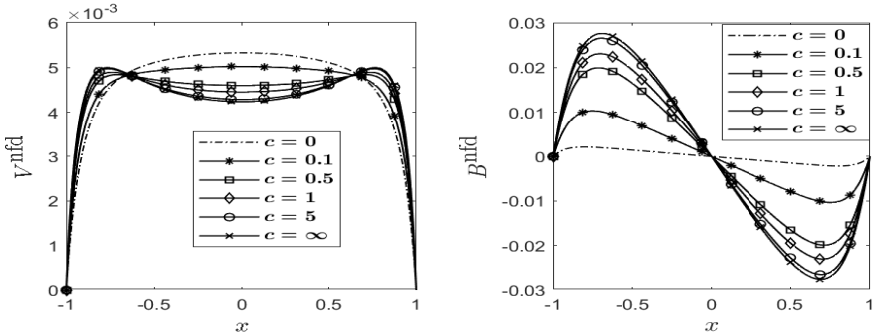


a) $M = 10$, $N = 128$

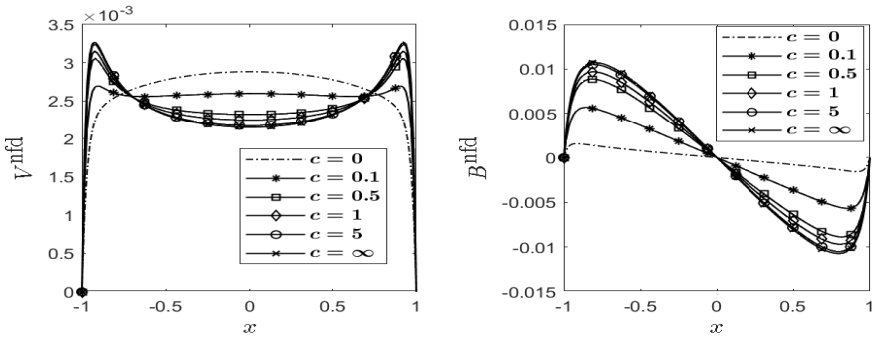


b) $M = 35$, $N = 128$

Figure 4.12: Problem II: Effects of c and M on the distributions of V and B along $y = 0$.



a) $M = 10$, $N = 128$



b) $M = 35$, $N = 128$

Figure 4.13: Problem II: Effects of c and M on the distributions of V and B along $y = 0.9844$.

4.3.3 Test Problem III: Insulated duct with slippery side walls: $\alpha \neq 0$ at $y = \pm 1$, $c = 0$

Finally, we solve the MHD flow in an insulated duct with slipping side walls at $y = \pm 1$ in order to investigate the pure effect of the slip length on the flow and induced magnetic field. The square duct is discretized by using $N = 128$ subintervals, as in Problem II. The choice of N is determined according to the tests (see Figure 4.14) using different numbers of N to evaluate $V^{\max}$ and $B^{\max}$ along $y = 0$ line for the case $M = 35$ and $\alpha = 0.4$ at $y = \pm 1$.

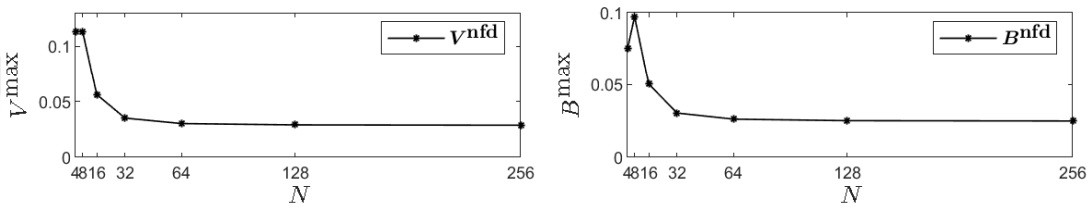


Figure 4.14: Grid dependency test for Test Problem III: $M = 35$, $\alpha = 0.4$ along $y = 0$.

The equivelocity and induced magnetic field lines are drawn in Figure 4.15 and 4.16, respectively, to see the effects of the slip length $\alpha = 0.02,\ 0.04,\ 0.2,\ 0.4$ on the flow and magnetic fields at $M = 5, 10, 25, 50$. An increase in α results in an increase in the magnitude of V at each M as observed in the work of Arslan [28]. The vortex formed in the equivelocity profile at $\alpha = 0.02,\ 0.04,\ 0.2$ splits into two symmetrical vertices close to sliding side walls when $\alpha = 0.4$ and at moderate values of $M = 25$ and $M = 50$. As a result, the strong influence of slip $\alpha = 0.4$ reduces the thickness of the boundary layers created along the horizontal walls at large M, and then they finally vanish at higher M when $\alpha = 0.4$. Contrarily, the slip length has almost no impact on the profile of induced magnetic field lines, except for a slight increase in the magnitude of B at a fixed M.

Figure 4.17 shows the effect of the slipping length ($\alpha = 0.02,\ 0.04,\ 0.1,\ 0.2,\ 0.4$) on the variation of the velocity and the induced magnetic field along the horizontal centerline $y = 0$ at $M = 10,\ 35$. It is observed that as α increases, there is no

significant change in the variations of V and B along the horizontal centerline $y = 0$ at each $M = 10,\ 35$ as expected, since $y = 0$ line is not in the region where the slip effect is dominant.

On the other hand, Figure 4.18 shows the impact of the slipping length α on the variations of the velocity and the induced magnetic field along $y \approx 0.9844$ which is close to the slippery upper wall $y = 1$ for $M = 10,\ 35$. Thus, the effect of α is more pronounced along $y \approx 0.9844$. In other words, both the velocity and induced magnetic increase rapidly in magnitude as α increases.

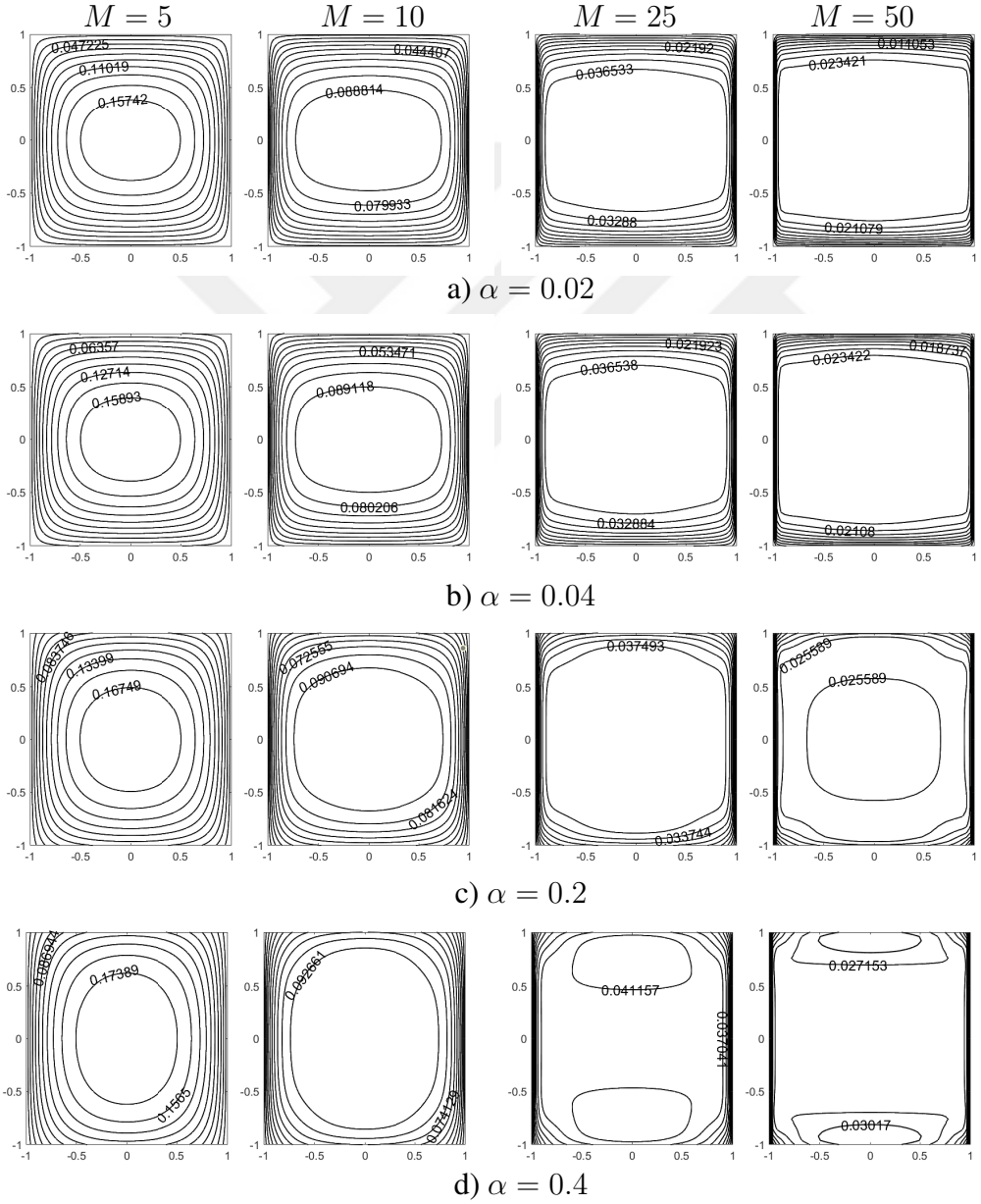


Figure 4.15: Problem III: Effects of M and α on velocity, $N = 128$.

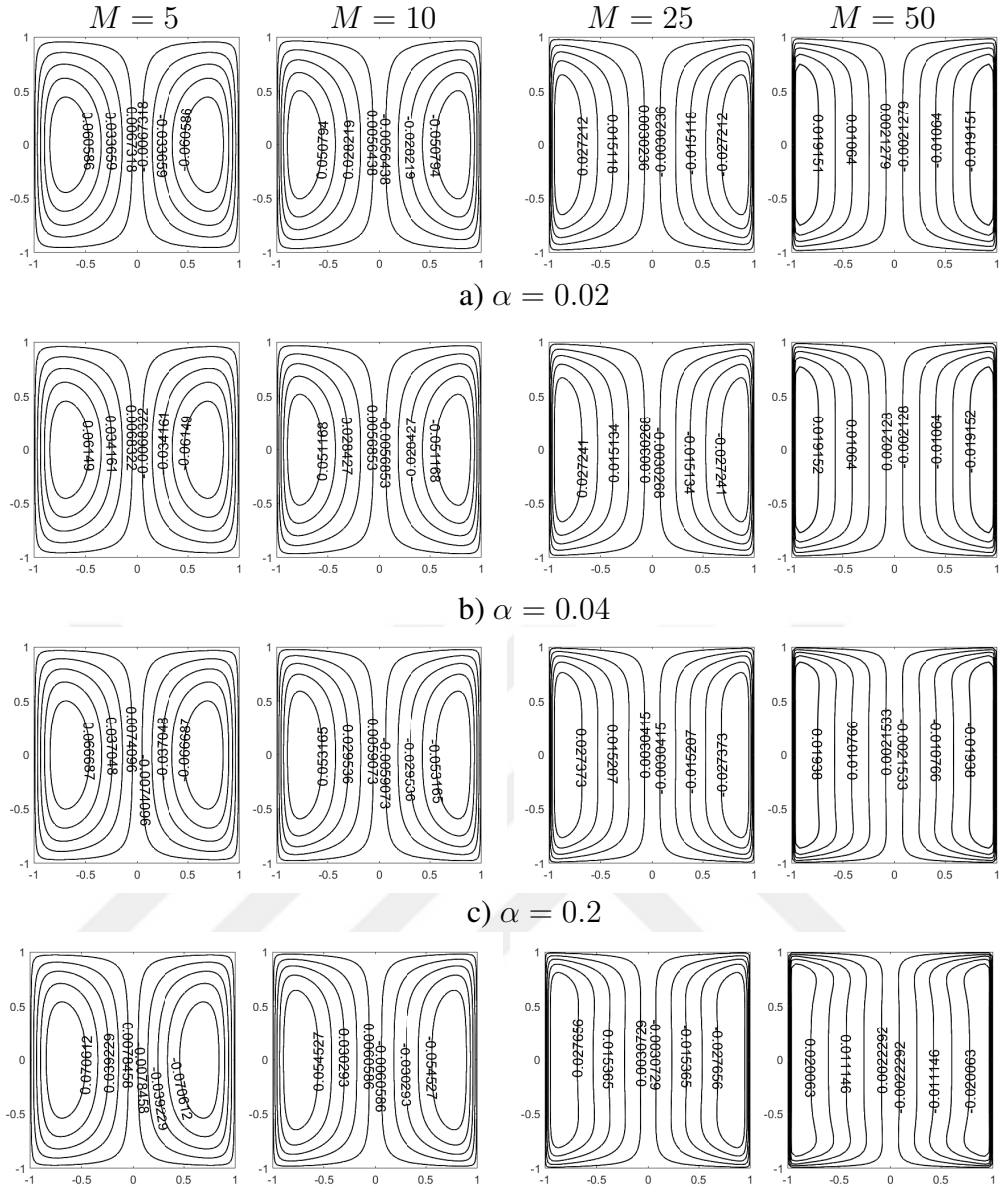
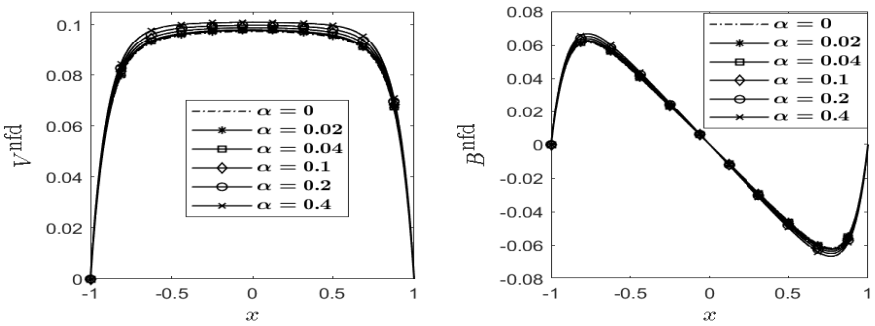
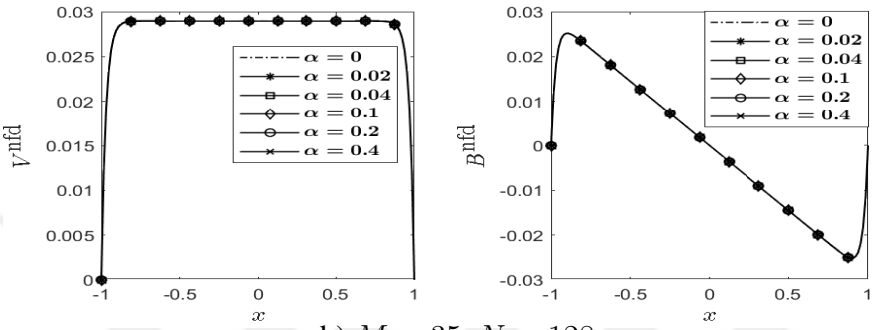


Figure 4.16: Problem III: Effects of M and α on induced magnetic field, $N = 128$.

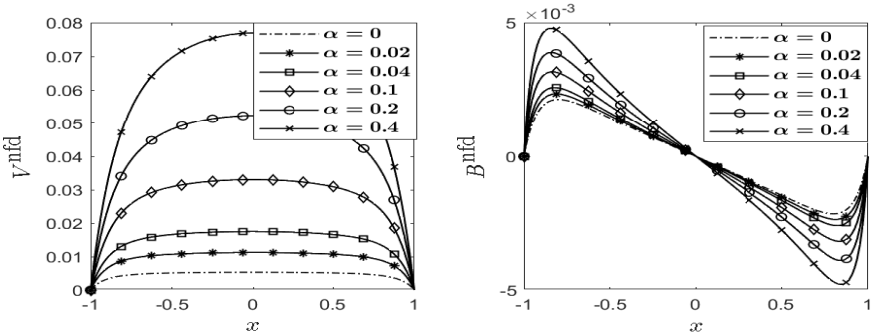


a) $M = 10$, $N = 128$

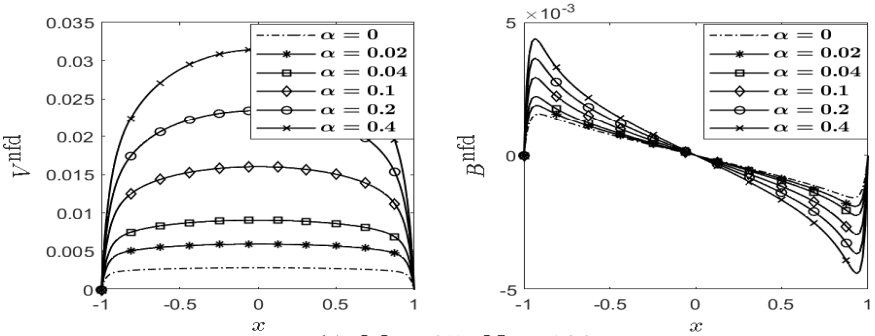


b) $M = 35$, $N = 128$

Figure 4.17: Problem III: Effects of α and M on the distributions of V and B along $y = 0$.



a) $M = 10$, $N = 128$



b) $M = 35$, $N = 128$

Figure 4.18: Problem III: Effects of α and M on the distributions of V and B along $y = 0.9844$.

CHAPTER 5

CONCLUSION

The present thesis compares the use of two finite difference methods, namely standard and new finite difference approaches, to solve the problems of one- and two-dimensional MHD flows driven by a constant pressure gradient between two infinite parallel plates (namely, MHD Hartmann flow) and through infinite channels/pipes with rectangular cross-sections (namely, MHD duct flow), respectively. The equations that govern the MHD flow problems are basically convection-diffusion type equations coupled in velocity and induced magnetic field. It is challenging to solve these problems in their original coupled form, especially in two dimensions. To overcome not only this difficulty but also to be able to derive NFD formulas, they are decoupled via suitable transformations into two modified Helmholtz equations. In order to approximate second-order derivatives in one- and two-dimensional modified Helmholtz equations, and the first-order derivatives in mixed-type boundary conditions, which include electrically insulated and variably conducting plates under no-slip or slip velocity conditions, the NFD formulas are first derived. Then, the numerical simulations using both the SFD and NFD schemes are performed for various values of the Hartmann number M to examine the combined effects of the conductivity parameter c and the slip length α on the velocity and the induced magnetic field.

The numerical findings obtained from SFD and NFD approaches are compared with the analytical solutions in both one-dimensional MHD Hartmann flow and the two-dimensional MHD flow in a duct with insulated and no-slip walls. The NFD scheme has been found to provide numerical results that are noticeably more accurate than those of the SFD method in each problem, even with a coarse mesh. Then, the SFD

and NFD solutions to these MHD flow problems subject to different boundary conditions are investigated for a range of slip length and conductivity parameter. The numerical results, which are common in both the one-dimensional MHD Hartmann flow and two-dimensional MHD duct flow, can be summarized as follows:

- The magnitudes of the velocity V and the induced magnetic field B drop as the intensity of the magnetic field increases by larger values of M, which matches the well-known flattening tendency of the MHD flow.

- The values of V and B through the computational domain are observed to climb for each Hartmann number as the slip length α increases, but the rate of rise is low for larger Hartmann numbers due to the damping effect of the magnetic field's strength.

- In contrast to the effect of slip length, the conductivity parameter c has the opposite influence on the values of V and B across the whole computational domain. That is, a rise in the conductivity parameter causes a reduction in V and B magnitudes throughout the whole computational domain. However, especially in the case of one-dimensional MHD flow, the amount of the decrease in values of B is very small or negligible.

- On the other hand, when the distribution of the induced magnetic field in the MHD duct flow is examined along a line near duct walls with variable conductivity, it is found that the magnitude of B along this line increases in response to an increase in the conductivity parameter. As c rises, the values of B, however, vary anti-symmetrically with respect to the vertical centerline $x = 0$. This means that the value of B is rising on $-1 \leq x \leq 0$ and falling on $0 \leq x \leq 1$. Thus, the magnitude of B throughout the computational domain is not greatly influenced by a change in the conductivity parameter as described in the preceding paragraph because the amount of this drop and rise balances each other.

- Additionally, as c rises, the induced magnetic field lines tend to strike the conducting boundaries perpendicularly, which shows that at high values of c the boundaries become almost perfectly conducting.

To sum up, the present study develops a novel finite difference method that, in comparison to the results produced by the standard finite difference scheme, offers significantly more precise solutions to the MHD flow problems with mixed-type boundary conditions in velocity and induced magnetic field. However, for two-dimensional MHD flow, the results were either obtained in a rectangular duct with variable conductivity and no-slip walls or insulated and slipping walls up to moderate values of Hartmann number. Consequently, this study can be expanded to include the NFD scheme solutions of the MHD flow in circular or triangular ducts with variable conducting walls that also exhibit slip. Additionally, after applying the mixed-type velocity and induced magnetic field boundary conditions, the discretized NFD system can be reconfigured in such a way that the coefficient matrix becomes symmetric, which might make it possible to achieve results even at higher Hartmann number values.

REFERENCES

[1] L. Dragoş, *Magneto-Fluid dynamics*. England: Abacus Press, 1975.

[2] J. Shercliff, "Steady motion of conducting fluids in pipes under transverse fields," *Proceedings of the Cambridge Philosophical Society*, vol. 49, pp. 136–144, 1953.

[3] L. A. Lambe, R. Luczak, and J. W. Nehrbass, "A new finite difference method for the Helmholtz equation using symbolic computation," *International Journal of Computational Engineering Science*, vol. 4, no. 1, pp. 121–144, 2003.

[4] G. Li and Y. S. Wong, "Exact finite difference schemes for solving Helmholtz equation at any wavenumber," *International Journal of Numerical Analysis and Modeling*, vol. 2, no. 1, pp. 91–108, 2011.

[5] U. Müller and L. Bühler, *Magnetofluiddynamics in Channels and Containers*. Springer-Verlag Berlin Heidelberg, 2001.

[6] S. Smolentsev, "MHD duct flows under hydrodynamic "slip" condition," *Theoretical and Computational Fluid Dynamics*, vol. 23, pp. 557–570, 2009.

[7] E. Ligere, I. Dzenite, and A. Matvejevs, "Analytical solution of a problem on MHD flow in a rectangular duct," in *Recent Advances in Mathematics: Proceedings of the 2015 International Conference on Pure Mathematics, Applied Mathematics and Computational Methods*, (Zakynthos Island, Greece), 2015.

[8] E. Ligere, I. Dzenite, and A. Matvejevs, "MHD flow in the duct with perfectly conducting Hartmann walls and slip condition on side walls," in *Proceedings of the* 10^{th} *PAMIR InternationalConference-Fundamentals and Applied MHD*, (Cagliari, Italy), 2016.

[9] E. Ligere, I. Dzenite, and A. Matvejevs, "Analytical solution of the problem on MHD flow in duct with perfectly conducting Hartmann walls and slip condition on conducting side walls," in *Proceedings of the* 16^{th} *International Scien-*

tific Conference-Engineering for Rural Development, vol. 16, (Jelgava, Latvia), pp. 1301–1305, 2017.

[10] B. Singh and J. Lal, "Finite element method in MHD channel flow problems," *International Journal for Numerical Methods in Engineering*, vol. 18, no. 2, pp. 1104–1111, 1982.

[11] B. Singh and J. Lal, "Finite element method of MHD channel flow with arbitrary wall conductivity," *J. Math. Phys. Sci.*, vol. 18, pp. 501–516, 1984.

[12] L. Gardner and G. Gardner, "A two-dimensional Bi-cubic B-spline finite element used in a study of MHD duct flow," *Computers Methods in Applied Mechanics and Engineering*, vol. 124, no. 4, pp. 365–375, 1995.

[13] M. Tezer-Sezgin and S. Köksal, "Finite element method for solving MHD flow in a rectangular duct," *International Journal for Numerical Methods in Engineering*, vol. 28, no. 2, pp. 445–459, 1989.

[14] K. Barrett, "Duct flow with a transverse magnetic field at high Hartmann numbers," *International Journal for Numerical Methods in Engineering*, vol. 50, no. 8, pp. 1893–1906, 2001.

[15] Z. Demendy and T. Nagy, "A new algorithm for solution of equations of MHD channel flows at moderate Hartmann numbers," *Acta Mechanica*, vol. 123, pp. 135–149, 1997.

[16] A. Nesliturk and M. Tezer-Sezgin, "The finite element method for MHD flow at high Hartmann numbers," *Computers Methods in Applied Mechanics and Engineering*, vol. 194, no. 9-11, pp. 1201–1224, 2005.

[17] A. Nesliturk and M. Tezer-Sezgin, "Finite element method solution of electrically driven magnetohydrodynamic flow," *Journal of Computational and Applied Mathematics*, vol. 192, no. 2, pp. 339–352, 2006.

[18] C. Bozkaya, *"Boundary element method solution of initial and boundary value problems in fluid dynamics and magnetohydrodynamics"*. PhD thesis, METU, June 2008.

[19] C. Bozkaya, "Effect of boundary conditions on magnetohydrodynamics duct flow," *Journal of Coupled Systems and Multiscale Dynamics*, vol. 5, no. 2, pp. 168–176, 2017.

[20] P. Senel and M. Tezer-Sezgin, "MHD flow in a circular pipe with arbitrarily conducting slipping walls," *Journal of Physics: Conference Series*, vol. 1141, p. 012033, 2018.

[21] P. Senel and M. Tezer-Sezgin, "DRBEM solution to MHD flow in ducts with thin slipping side walls and separated by conducting thick Hartmann walls," *Computers and Mathematics with Applications*, vol. 78, no. 9, pp. 3165 – 3174, 2019.

[22] C. Aydin and M. Tezer-Sezgin, "DRBEM solution of the Cauchy MHD duct flow with a slipping perturbed boundary," *Engineering Analysis with Boundary Elements*, vol. 93, pp. 94 – 104, 2018.

[23] C. Bozkaya and O. Turk, "Chebyshev spectral collocation method for MHD duct flow under slip condition," *Applied Mathematics and Mechanics*, vol. 22, no. 2, pp. 118–129, 2022.

[24] B. Singh and J. Lal, "MHD axial flow in a triangular pipe under transverse magnetic field," *Indian Journal of Technology*, vol. 9, pp. 101–115, 1978.

[25] B. Singh and J. Lal, "MHD axial flow in a triangular pipe under transverse magnetic field parallel to a side of the triangle," *Indian Journal of Technology*, vol. 17, pp. 184–189, 1979.

[26] M. Chutia and P. N. Deka, "Numerical solution for coupled MHD flow equations in a square duct in the presence of strong inclined magnetic field," *International Journal of Advanced Research in Physical Science (IJARPS)*, vol. 2, no. 9, pp. 20–29, 2015.

[27] K. R. Raslan and K. K. Ali, "Numerical study of MHD-duct flow using the two-dimensional finite difference method," *Applied Mathematics & Information Sciences*, vol. 14, pp. 693–697, 2020.

[28] S. Arslan, "Finite difference method solution of magnetohydrodynamic flow in channels with electrically conducting and slipping walls," Master's thesis, METU, may 2018.

[29] S. Arslan and M. Tezer-Sezgin, "Exact and FDM solutions of 1D MHD flow between parallel electrically conducting and slipping plates," *Advances in Computational Mathematics*, vol. 45, pp. 1923–1938, 2019.

[30] S. Arslan and M. Tezer-Sezgin, "FDM solution of MHD flow in a rectangular duct with slipping and partly insulated partly conducting side walls," vol. 1391, 2019.

[31] S. Britt, E. Turkel, and S. Tsynkov, "A high order compact time/space finite difference scheme for the wave equation with variable speed of sound," *Journal of Scientific Computing*, vol. 76, pp. 777–811, 2018.

[32] I. Singer and E. Turkel, "High-order finite difference methods for the Helmholtz equation," *Computer Methods in Applied Mechanics and Engineering*, vol. 163, pp. 343–358, 1998.

[33] A. Kahana, F. Smith, E. Turkel, and S. Tsynkov, "A high order compact time/space finite difference scheme for the 2D and 3D wave equation with a damping layer," *Journal of Computational Physics*, vol. 460, p. 111161, 2022.

[34] I. Harari and E. Turkel, "Accurate finite difference methods for time-harmonic wave propagation," *Journal of Computational Physics*, vol. 119, no. 2, pp. 252–270, 1995.

[35] I. Singer and E. Turkel, "Sixth-order accurate finite difference schemes for the Helmholtz equation," *Journal of Computational Acoustics*, vol. 14, no. 3, pp. 339–351, 2006.

[36] G. Sutmann, "Compact finite difference schemes of sixth-order for the Helmholtz equation," *Journal of Computational and Applied Mathematics*, vol. 203, pp. 15–31, 2007.

[37] M. Nabavi, M. K. Siddiqui, and J. Dargahi, "A new 9-point sixth-order accurate compact finite-difference method for the Helmholtz equation," *Journal of Sound and Vibration*, vol. 307, pp. 972–982, 2007.

[38] X. Li, “On solving boundary value problems of modified Helmholtz equations by plane wave functions,” *Journal of Computational and Applied Mathematics*, vol. 195, no. 1-2, pp. 66–82, 2006.

[39] M. Abramowitz and I. A. Stegun, *Handbook of Mathematical Functions with Formulas, Graphs and Mathematical Tables*. National Bureau of Standards, Applied Mathematics Series 55, 10 ed., 1972.